UNIUNEA EUROPEANĂ
GUVERNUL ROMÂNIEI MINISTERUL MUNCII, FAMILIEI ŞI PROTECŢIEI SOCIALE AMPOSDRU
Fondul Social European POS DRU 2007-2013
Instrumente Structurale 2007-2013
MINISTERUL EDUCAŢIEI CERCETĂRII TINERETULUI ŞI SPORTULUI
OIPOSDRU
UNIVERSITATEA ALEXANDRU IOAN CUZA IAŞI

Proiect cofinanţat din Fondul Social European prin Programul Operaţional Sectorial Dezvoltarea Resurselor Umane 2007-2013
Investeşte în oameni!

Center of training and analysis in risk's engineering

International Journal of Risk Theory

Vol. 1, 2011

Alexandru Myller Publishing
Iaşi

Center of training and analysis in risk's engineering

International Journal of Risk Theory

Vol 1

Alexandru Myller
Publishing
Iaşi, 2011

Center of training and analysis in risk's engineering
International Journal of Risk Theory
ISSN: 2248 – 1672
ISSN-L: 2248 – 1672

Executive Editors:

Ennio CORTELLINI
e-mail: cortellini@uaic.ro; ennio.cortellini@tin.it
Ioan TOFAN
e-mail: ioantofan@yahoo.it; tofan@uaic.ro
Dănuţ RUSU
e-mail: drusu@uaic.ro

ALEXANDRU MYLLER PUBLISHING
Bd. CAROL I, No.11, Iaşi, Romania, tel. 0232-201225 / fax. 0232-201060
e-mail: ijrt@uaic.ro

Content

MARS - A COMPETITIVE PWR BASED COMPLETELY ON PASSIVE SAFETY SYSTEMS

Gianfranco CARUSO*, Maurizio CUMO*, Antonio NAVIGLIO*

* *"SAPIENZA" University of Rome - DIAEE, Corso Vittorio Emanuele II, 244 – 00186 Rome, ITALY,*
E-mail: gianfranco.caruso@uniroma1.it; maurizio.cumo@uniroma1.it; antonio.naviglio@uniroma1.it;

Key Features of the MARS Project

The MARS nuclear power plant is a cheap, simple, extremely safe PWR plant incorporating all main well-proven features of a "traditional" PWR plant.
A production plant is made of medium-power modules: each reactor module may produce up to some 1000 MWth; the design here presented refers to a size of 600 MWth. The whole design is strongly simplified, thanks to safety characteristics based on simple, almost completely static and exclusively passive-type emergency systems. The probability of core integrity failure is a vanishing event (according to rigorous PRA evaluations, core damage probability in the range of 1E-7 event/year).
The core cooling system includes one loop only, with recirculation-type steam generator; during normal operation, the primary coolant is pumped in the reactor vessel and in the primary loop, while, in emergency conditions, the coolant flow in the core is completely guaranteed through an independent cooling system, transferring heat to the external atmosphere with natural circulation and relying on only static components and one non-static, passive component (check valves, 400% redundant on two independent cooling trains).

In the design here presented, the MARS core (600 MWth) is of quite traditional design and includes 89 fuel assemblies, 17x17 pin array. 84 fuel assemblies have an irradiation period of 54 months, while 5 assemblies have a 72-months irradiation cycle. The refueling strategy is based on 1/3 core reloading, so the refueling operation will occur every (18+1) months. The safety margins are huge, also because of the total absence, in the MARS reactor, of fast thermal-hydraulic accidental transients. The nuclear design is based on traditional geometries and materials. At the CEA, Saclay, an innovative MARS nuclear design has been studied, incorporating the features of advanced French nuclear fuel and allowing quite higher irradiation cycles, together with simplification in primary coolant chemical control system and improved proliferation-resistance characteristics (BU achieved higher than 60.000 MWd/t).

The MARS reactor plant is equipped with a secondary pressurized containment filled with cold water, enveloping the full primary coolant pressure boundary. Deterministically, this does eliminate any loss of primary coolant. A containment building is foreseen to face external events in accordance with the strictest European regulations (aircraft impact). This containment building is able to withstand any internal pressurization, also in the incredible event of a complete loss of the core coolant pressure boundary.

LOCAs, ATWSs and LOFAs are eliminated in the MARS concept, making the plant an incredibly reliable, safe, easy-to-manage nuclear power plant.
The requirements of the radwaste system are quite limited, and the doses to operation and maintenance personnel are the lowest, thanks – among other – to the few components physically in contact with the primary coolant (only 7 components).

In spite of the exeptional safety and radiological protection features, the investment and operation costs for a MARS power production station are quite low.
This is a consequence of the huge plant simplification (drastic reduction of the number of systems and components, drastic reduction of components relevant to safety, reduction of concrete volumes) and of a design fully oriented to pre-fabrication and easy assembling/disassembling, that make the construction time incomparably short, limit the cost of all components, allow easy component substitution in case of failure instead of local repair.

The plant lifetime is 70-100 years, with the possibility of removal of components that could act as bottlenecks in the lifetime of the plant (as the reactor vessel itself).
Decommissioning of the MARS nuclear power plant is indeed quite an easy and fast job.
The total direct investment cost, including contingencies, has been evaluated with accuracy and is of 1650 US$/kWe (referred to a 3-reactor-module, 450 MWe station).
The cost of electric energy produced is equal to 0.035 US$/kWh (value that falls below 0.02 US$ after the first 20 years assumed for the debt service period). Further cost reduction may be achieved in the phase of final design.

The MARS NPP is a targeted solution for utilities requiring:

- Medium size NPP;
- Incomparably high safety and reliability, i.e., due to the closeness of the plant to highly inhabited towns (essential if the plant has to be used also for desalination purposes);
- Cheap electric production;
- Easy operation and maintenance;
- Fast plant construction;
- Possibility of multi - purpose production (electricity / heat / desalinated water).

Utilization of Passive Systems in the MARS NPP

The original idea behind the extensive use of passive safety systems in the MARS NPP was based on:

- simplification of the design, also to make it cheaper to build, operate and maintain;
- increase in the real safety of the plant through systems which were intrinsically simple and reliable, based on the action of ‘natural’ laws;
- improvement in the perception of safety of the plant for the same reasons.

A passive design strives to ensure that the three major safety functions can be carried out in a passive or quasi-passive manner. These functions are:

- reactor shut down in any plant condition;

- decay heat removal;
- fission product containment.

Passive safety emphasizes the use of natural forces (gravity, self-correcting neutronic feedback, thermal dilatation) and de-emphasizes systems which require large amounts of electricity (pumps) or energy, rapid automatic response, complex logic.

The design of the MARS (Multipurpose Advanced "inherently" Safe Reactor) plant started in 1983 at the Department of Nuclear Engineering and Energy Conversion of the University of Rome "La Sapienza", with the aim at proposing a new concept of fission-type nuclear plant to be used for a wide range of applications, including desalination and district heating.
The possibility of utilization of the plant in high-density population areas or in developing areas was the main reason for the search for improved safety requirements: the plant had to be simple, with an easy-to-understand and incontrovertible capacity to avoid any radiological hazard to the population. Typically, the safety approach had to be clearly understandable, on deterministic bases. The design was focused on a nuclear power generation capacity of 600 MWth, corresponding to about 170 MWe in the case of only electrical production, with a modular solution to satisfy progressively increasing power requirements (then power may vary, but very high power levels are not compatible with performance characteristics of some main passive safety systems).
The design was carried out using a step-by-step approach, which addressed all major issues regarding plant safety, performance and cost.
In particular, in order to make the MARS plant economically competitive with other nuclear plant solutions and with fossil-fueled thermal power plants, it was necessary to adopt a somewhat extreme simplification criterion in the design approach. This simplified design involves mainly in-shop construction with only a "few" operations of easy assembling and simple substitution of all mechanical components for maintenance purposes, and easy removal for the final, complete decommissioning.

In May 1994 the preliminary design was completed, the preliminary safety report was submitted by ENEA, (the Italian State Agency for Energy, Environment and Innovation) to the Italian Nuclear Safety Authority, ANPA**,** for comments. Quite a lot of experimental tests on innovative components were performed.
The MARS nuclear power plant (NPP) design widely uses the well-proven technology and the operation experience of Westinghouse PWRs, but also incorporates several innovative features that hugely improve the safety performance, while keeping the cost of KWh competitive with traditional large power plants. Extensive use of passive safety, in depth plant simplification and decommissioning oriented design were the main guidelines for the design development.

The MARS NPP is designed to produce electric energy and/or industrial heat. The most efficient utilization of such kind of plant is definitively co-generation. Typical destinations of heat produced in a MARS NPP are low temperature utilizations of hot water or low pressure steam; among these, the following utilizations were analysed:

- water desalination using low temperature processes (as thermo-compression or multiple

effects);
- district heating;
- food industry (conservation industry).

System Configuration

The MARS reactor is moderated and cooled by pressurized light water (PWR). The reference rated core thermal power, here referred to, is 600 MW. In case of only electric energy production, 150 MWe of gross power (146 MWe net power) are produced in a 600 MWth plant, with 25% gross efficiency (24.5% net efficiency).
In case of co-generation, the electric energy production strongly depends on the thermodynamic requirements of the produced hot water or steam. Co-generation cycles have been designed for the production of electric power ranging between 80 and 100 MWe and of hot water or steam at a temperature around 100°C.

The original MARS design incorporated only well proven nuclear reactor technologies, in order to make it easier plant licensing: major innovations concerned ECCS and some auxiliary systems. So, nuclear reactor characteristics here described are quite similar to well-known PWRs (primary loop type, core geometry and materials, reactor control type, etc.).

The MARS design here described is characterized by the following innovative solutions, representing completely passive safety features:

- an innovative, passive-type, quasi-static emergency core cooling system, based only on natural circulation of cooling fluids and using external air as ultimate heat sink;
- an innovative, additional, passive-type scram system based on a two-metals core temperature sensor and operated by gravity (proposed as optional);
- full enclosure of the primary-coolant boundary in a pressurized containment filled with low enthalpy water (primary loop jacket). The absence of common mode failures, thanks to a special design, limits to irrelevant values the probability of loss of primary coolant.

As said the fuel is low-enrichment uranium dioxide (in the fuel loading strategy here described, the loading U235 enrichment is 2.8%); the core includes 89 “standard” PWR fuel assemblies. The assemblies are zircalloy-cladded with rod array 17x17, including 264 fuel rods and 25 positions for zircalloy guide tubes for control rods (black, Ag-In-Cd; grey, stainless steel) or for burnable poisons (borosilicate). Fuel rod pitch is 1.26 cm. Fuel rod active length is 260 cm.
Light water flows in a single cooling loop. The average core coolant temperature is 234 °C. Reactor internals are AISI 304 made. Reactor vessel internal diameter is 3000 mm; the overall height of the assembled vessel is 11091 mm. The average fuel burn-up per cycle (3 irradiation cycles; 5 assemblies are irradiated for 4 cycles) is about 11,300 MWd/t. An alternative core design foresees a full core irradiation of 60,000 MWd/t.

The Innovative Safety Core Cooling System

The primary cooling system (Fig. 1) includes one loop only, with 25" I.D. pipes, one vertical-axis U-tube steam generator and one canned rotor pump directly connected to the steam generator outlet nozzle. Connected to the reactor vessel is the Safety Core Cooling System (SCCS). A vapour-bubble pressurizer controls the pressure inside the primary cooling system. On/off valves (primary loop Main Isolation System, MIS) are installed in the primary cooling loop, in order to isolate, if necessary, the Steam Generator and the primary pump (i.e., in the event of a SG tube rupture).
The primary cooling system and the Safety Core Cooling System are inside a pressurized containment, filled with water at the same pressure as the primary coolant, but at a lower temperature (70 °C), called CPP (pressurized Containment for Primary loop Protection – Fig. 2) which allows the reduction (even the elimination) of primary stresses on the primary coolant boundary and provides an intrinsic defence to loss of coolant.The cooling of MARS core in emergency conditions is provided by the Safety Core Cooling System (SCCS – Fig. 3) is designed to transfer the core decay heat directly from the reactor pressure vessel to the external air, without the intervention of any energized system or component. The system operating principle relies on water density differences, due to temperature differences between two vertical fluid columns, causing the fluid circulation.

The presence of multiple circuits (Primary Safety Cooling loop, PSC; Intermediate Safety Cooling loop, ISC; and pool and condenser loop (Third Safety Cooling loop, or TSC)) in a cascade functional operation chain provides redundant barriers between activated reactor coolant and external environment.The SCCS includes two trains; each train may remove 100% of the core decay power. In an accidental event causing the reduction of the core coolant flow (such as station black-out or primary pump trip), its activation is automatic (without any intervention either by the operator or by the control and supervision system, because the PSC interception valves are kept in closed position by the forces due the primary coolant flow and start opening when this flow decreases under a set-point value); the operation of the system is completely passive.
The SCCS operation relies on the operation of special check valves able to automatically open, without any operator intervention and without the needs of energized systems, when the operating conditions require additional core cooling. These valves have a completely innovative design (Fig. 4). They are kept in closed position by means of the pressure difference between the reactor vessel inlet and outlet (that is roughly proportional to the square of the coolant flow-rate); when the flow-rate through the core goes to zero, the pressure difference decreases and when it is no longer sufficient to sustain the weight of the valve plug, this falls, and a complete flow area is opened, with a very low hydraulic resistance. Two valves, each one 100% capacity, are inserted in each SCCS train and, to increase the system availability to values that make its failure incredible, the additional two valves (in each loop, the second valve is of traditional design) are different in typology and mechanical construction.

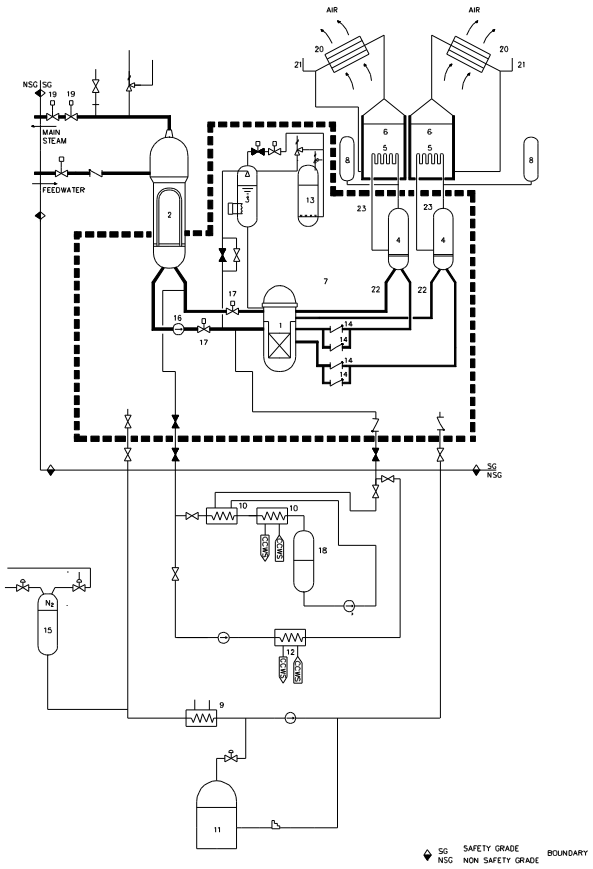

Legend

1. reactor
2. steam generator
3. pressurizer
4. heat-exchanger (reactor coolant/ intermediate coolant)
5. heat-exchanger (intermediate coolant/ final heat sink coolant)
6. water reservoir
7. pressurized containment for primary loop protection (CPP)
8. intermediate loop pressurizer
9. heat-exchanger (primary containment water cooling system)
10. chemical and volumetric control system heat-exchangers
11. water storage tank
12. residual heat removal system heat-exchanger
13. pressurizer relief tank
14. safety core cooling system check valve
15. primary containment pressure control system pressurizer
16. main coolant pump
17. primary loop on/off valve
18. VCS tank
19. steam line on/off valve
20. ultimate heat sink condenser
21. communication path with the atmosphere
22. safety core cooling system primary loop
23. safety core cooling system intermediate loop

Figure 1 – MARS primary cooling system

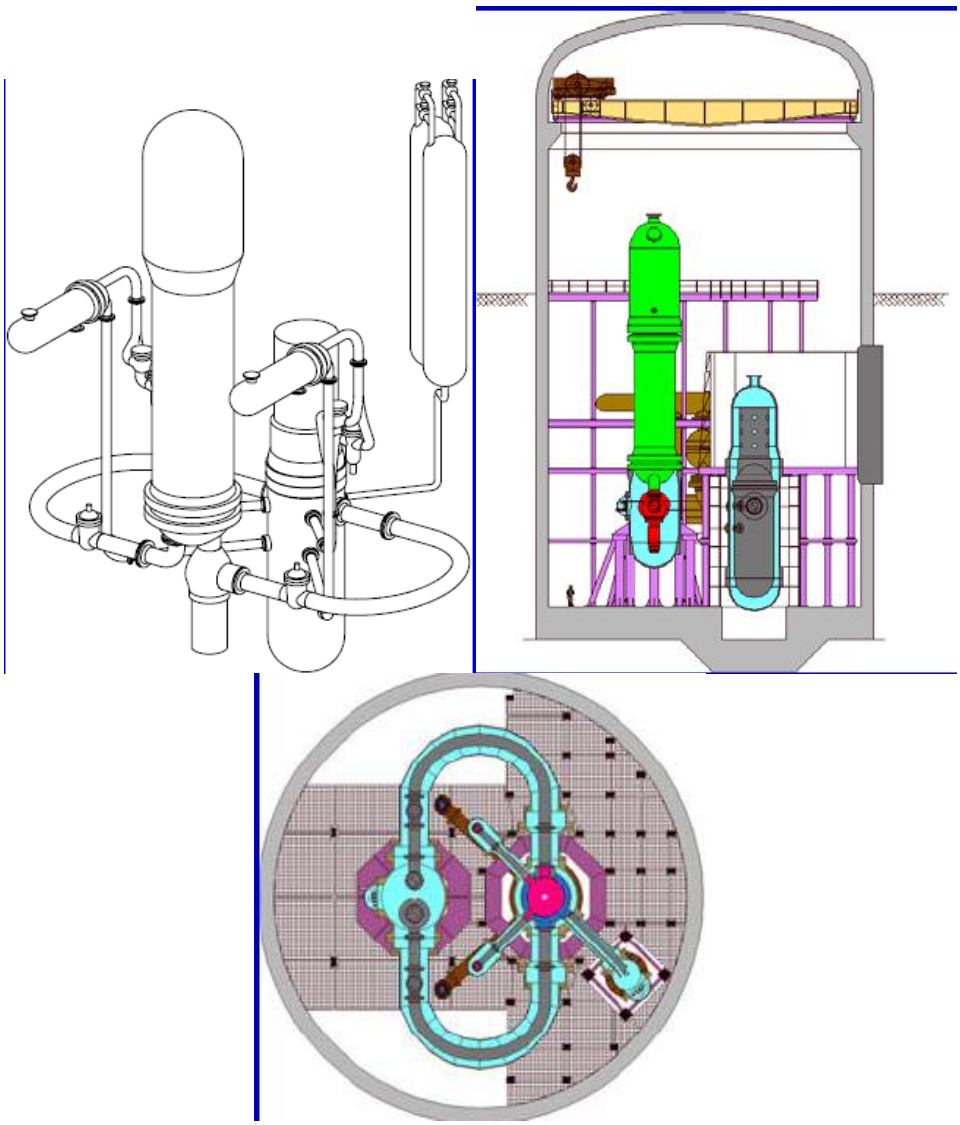

Figure 2 – Pressurized containment for primary loop protection (CPP)

When any of the four check valves is opened, the flow in the PSC, after a short transient phase, is assured by a difference in level of about 7 m between the vessel outlet nozzle and the primary heat exchanger and by the difference between inlet and outlet vessel temperatures.

A horizontal-axis U-tube heat exchanger (Fig. 5) transfers heat from the PSC to the ISC. Pressure in the ISC loop is slightly higher than 75 bar (controlled by a dedicated pressurizer); this value guarantees sub-cooled water conditions of the fluid during any accidental situation or transient; the difference in level for natural circulation in the ISC loop is of about 10 m.

A second heat exchanger transfers the heat from the ISC circuit to the water of a reservoir. The steam produced in the reservoir is mixed with air initially present in the dome over the pool; pressure in the dome rises and this causes a flow of the air-steam mixture towards a small connection path with the atmosphere. Between the pool dome and the connection path with the atmosphere an inclined-tube heat exchanger is placed, where steam is partially condensed thanks to the action of external air drawn by a chimney.

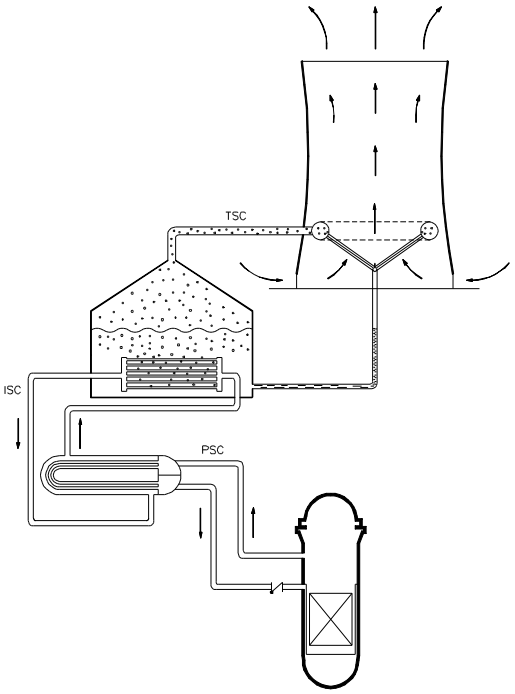

Figure 3 – Scheme of the safety core cooling system SCCS

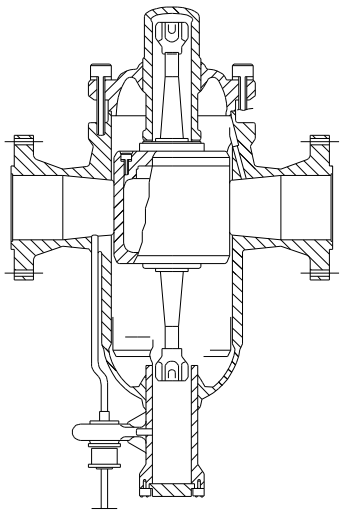

Figure 4 – SCCS special check valve

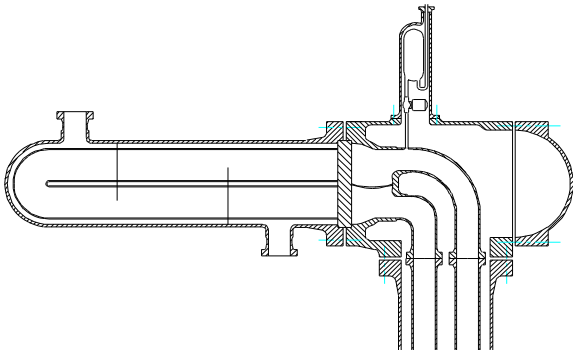

Figure 5 – SCCS primary heat exchanger

The above mentioned choices introduced some constraints to the plant design; in particular the first limit, imposed by the functional requirements of the special emergency core cooling system, regards the rated thermal power, that cannot exceed approximately 1000 thermal MW, and in the solution herein described has been chosen equal to 600 MWth. Another characterizing parameter is the pressure in the primary system, chosen equal to 75 bar, which is different from the pressure values usually adopted in PWRs for the production of electric power (150-170 bar). This choice, that leads to a loss in thermodynamic efficiency of the plant because of the limitation of the higher isotherm in the steam cycle, has nevertheless allowed the adoption of the pressurized Containment for Primary loop Protection (CPP, the pressurized boundary that envelopes the primary cooling system and the emergency core cooling system), substantially eliminating the possibility of any type of loss-of-coolant accidents, including control rod ejection accident.
The inclusion of the primary coolant system (average operating temperature: 234 °C) inside the low-enthalpy-water-filled pressurized containment (CPP, at the temperature of 70 °C) requires thermal insulation to reduce heat losses from the primary coolant system. An insulating system has been designed on the external side of the whole primary coolant boundary (only the lower head of the reactor vessel is thermally insulated in the internal part), through matrices of stainless steel wiring, that cause the presence of semi-stagnant water and can resist to high pressure and to fast pressure gradients, with acceptable shape modifications. This system limits heat losses to about 0.3% of the reactor thermal power.

The Experimental Facility NICOLE to Test the Innovative Safety Core Cooling System

To experimentally analyze the transient performance of the MARS emergency decay heat removal system, the experimental facility NICOLE (Naturally Induced circulation COoling Loop for Emergency) was designed and built.

The NICOLE plant essentially includes:

- a heat generator, which simulates the PSC/ISC heat exchanger;
- a pool (heat sink), which simulates the ISC/TSC heat exchanger;
- a water circulating loop, which includes a hot leg, a cold leg and which simulates the intermediate circulating loop of MARS emergency decay heat removal system.

The heat generator is a steel cylinder, having a 1.7 m diameter and a 2.6 m height. It is shown in the Fig. 6. A volume of diathermic oil (up to 6 m3) simulates the primary fluid in the PSC/ISC heat exchanger. The oil inventory can be varied to simulate different primary fluid thermal capacities.
Thermal power (up to 50 kW) is generated by 8 electrical heaters immersed in the oil volume. Oil has been used being its vapour pressure extremely low even at high temperatures (up to 200 °C).
The heat generator includes two 20 mm OD tube bundles, to transfer heat to the water circulating loop. Each tube bundle can be isolated by a check valve, to vary the heat transfer surface of the heat exchanger. A variable speed mixer allows to vary the oil heat transfer coefficient and to maintain the oil temperature uniform.
NICOLE pool is shown in the Fig. 7. In the pool a volume of water (up to 2.8 m3) simulates the TSC pool fluid in the MARS emergency decay heat removal system. Pool water inventory can be varied to modify its thermal capacity.
A heat exchanger, realized with a ½" BWG tubes bundle, is immersed in the water pool. The number of operating tubes can be varied by isolation valves, to allow variations of the heat transfer surface. The initial pool water temperature can be varied through electrical heaters that are immersed in the pool water.

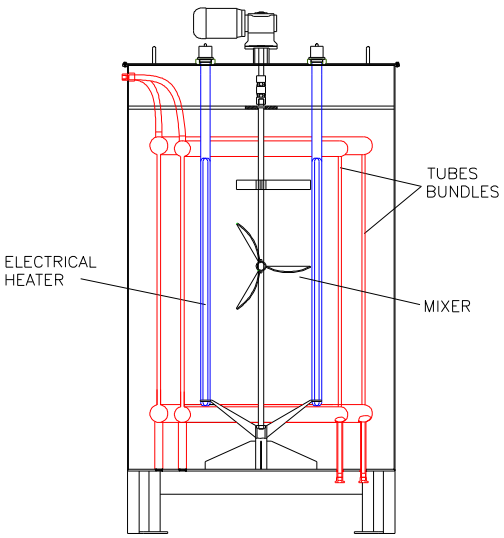

Figure 6 – Heat generator of the NICOLE experimental plant

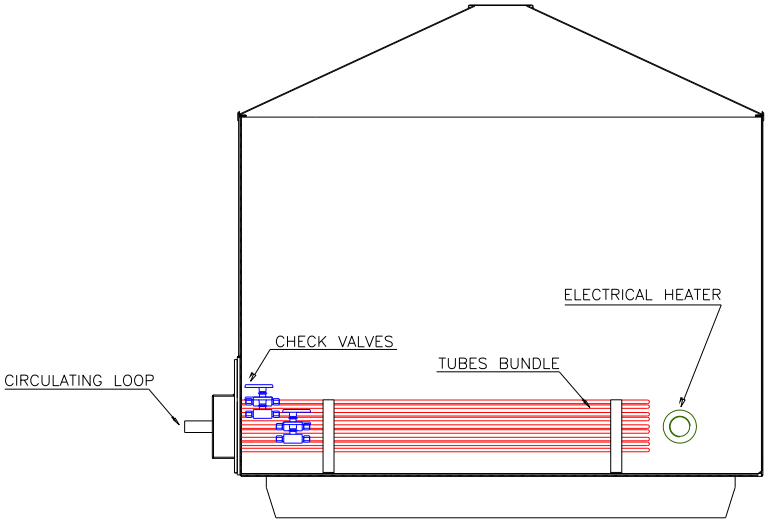

Figure 7 – Pool of the NICOLE experimental plant

The circulating loop is realized by 1" OD steel tubes. It includes a hot leg, connecting the heat generator tubes bundles outlet with the pool tubes bundle inlet and a cold leg, between the pool HX outlet with the heat generator tube bundles inlet. A regulation valve is located on the cold leg, to impose further pressure drops in the loop and to simulate, in this way, different circulating loop configurations. A nitrogen pressurizer is placed on the hot leg of the circulating loop to limit its pressure variations.
A further loop can be connected to the pool, with an air-cooled heat exchanger to condense the steam eventually produced and to maintain the liquid inventory in the pool.

NICOLE plant also includes the following auxiliary systems:

- a water charging/discharging system for the pool and the circulating loop;
- an oil charging/discharging system for the heat generator;
- a nitrogen charging/discharging system for the pressurizer;
- a compressed air circuit for the air pressure-actuated valves;
- a safety relief system on the pressurizer.

The experimental facility is instrumented with the following control instruments:

- 30 temperature transmitters;
- 5 pressure transmitters;
- 3 level transmitters;

1 mass flow transmitter.

The NICOLE plant is controlled by a computerized system, by which also transient conditions in the power generation or circulating loop pressure drops can be imposed. A simplified scheme of the experimental plant and its P&ID are shown in Figure 8.

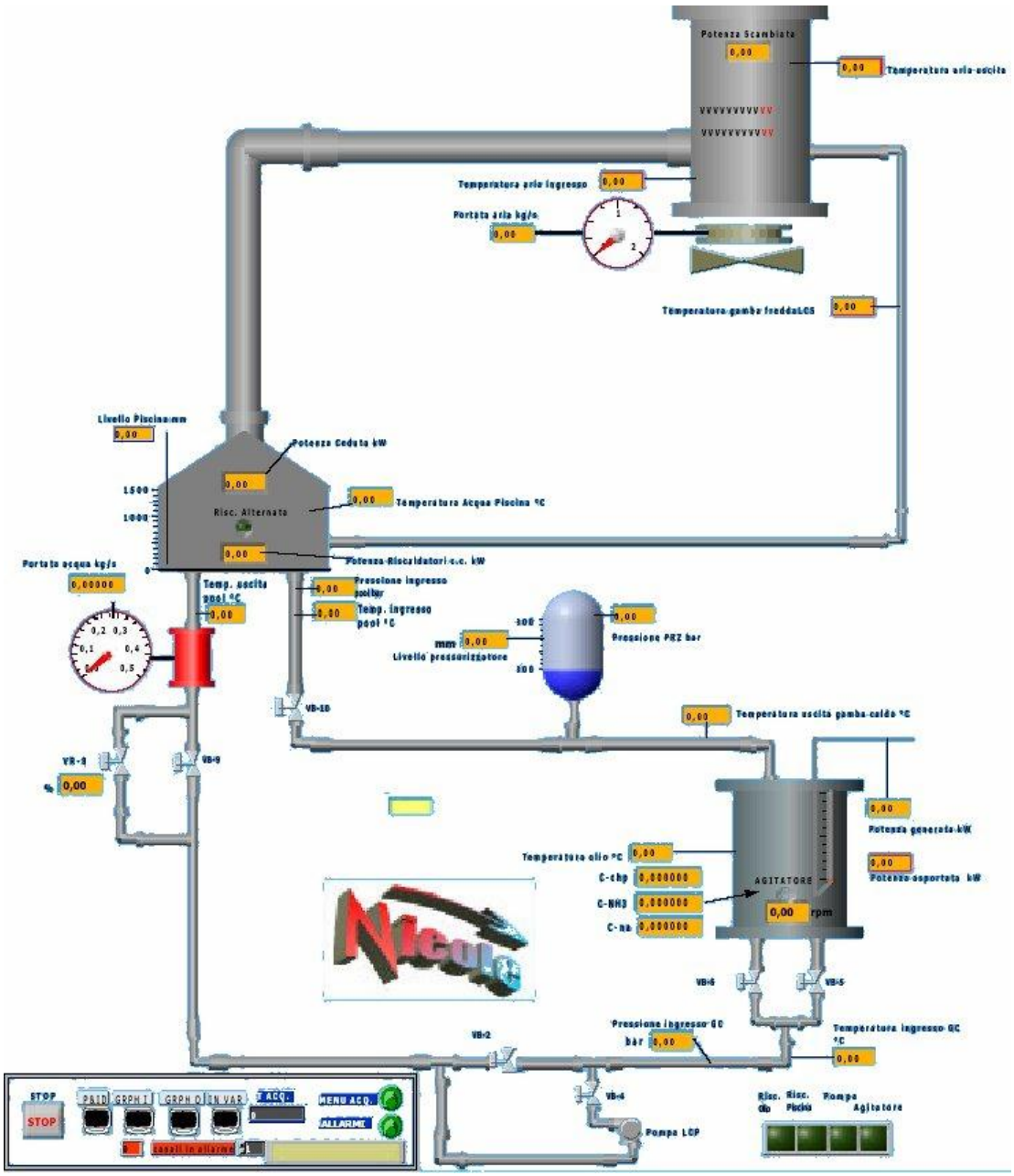

Figure 8 – Simplified scheme of the NICOLE plant

The NICOLE plant has been also conceived as a scaled model of the intermediate loop of MARS emergency decay heat removal system.

The scaling procedure that has been used is the so called “time preserving volumetric” (Ishii and Kataoka, 1984). This procedure is particularly suitable for the scaling of natural circulation systems, because it allows to reproduce, through the employment of a scaled model, both the transient temporal evolution and the fluids temperature and pressure profiles.

With reference to the application of time preserving volumetric procedure, the parameters of the intermediate loop of MARS emergency decay heat removal system are:

H = vertical height of the emergency system intermediate loop = 10 m;

P = thermal power transferred in the PSC/ISC heat exchanger and in the ISC/TSC heat exchanger = 6 MW (decay heat= 1% of full power);

A = hot leg and cold leg flow area = 9.86×10-2 m^2 (16" tubes);
V = pool water volume = 290 m^3;
$(US)_{PSC/ISC}$ = 3.7×105 W/K;
$(US)_{ISC/TSC}$ = 3.49×105 W/K;
$\sum_j \left[\left(\frac{f_m \times L}{D_h} \right)_j + K_j \right]$ = equivalent friction factor of the intermediate loop = 56.5.

Where:
L = component length in the fluid flow direction [m];
D_h = component hydraulic diameter [m];
f_m = Moody friction factor [-];
K = concentrated friction factor [-];
S = heat transfer surface area [m^2];
U = global heat transfer coefficient [W/m^2K];

The experimental plant parameters are:

H = plant vertical height = 9 m;
P = thermal power to be generated by electrical heaters in the heat generator = 20 kW;
A = flow area of hot leg and cold leg = 6.93×10-4 m^2;
V = pool water volume = 1 m^3;
$(US)_{GC}$ = 1.25×103 W/K;
$(US)_{POOL}$ = 1.17×103 W/K;

$\sum_j \left[\left(\frac{f_m \times L}{D_h} \right)_j + K_j \right]$ = equivalent friction factor = 58.7.

Therefore, using 20 mm ID tubes for the hot leg and for the cold leg (at the moment they are realized through 1" tubes OD) and a 520 mm water level in the pool, NICOLE plant can be considered as a scaled model, by a scaling factor of approximately 1/300, of the intermediate loop of MARS emergency decay heat removal system.

Simulation Analysis

The experimental plant NICOLE has been preliminary tested in more than 30 experiments in transient conditions. The aim of these tests was to verify the plant functionality and operability and the accuracy of the control and data acquisition systems. The experimental data were also used to validate the RELAP5 nodalization, by which it has been possible to simulate with high accuracy different transients during the pre-test phases.

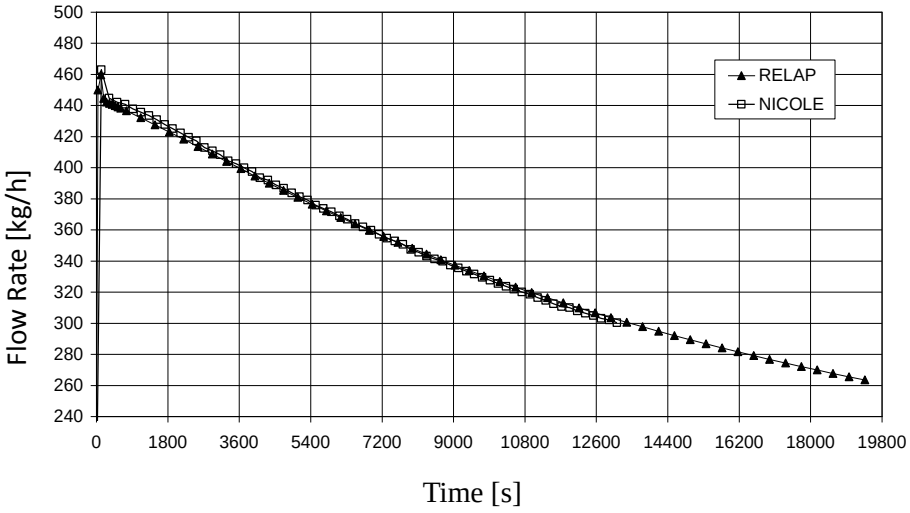

Figure 9 – Flow rate in a natural circulation test. Experimental data and RELAP results comparison

In Fig. 9, a typical comparison between the experimental data from the NICOLE plant and the RELAP5 results is shown. This example refers to the flow rate in natural circulation during a cooling phase of the system.

Experimental Analysis on the Natural Draft – Dry Cooling Tower

The goal of the experimentation is to investigate a dry cooling tower system in order to find the most efficient technical solutions to remove the core residual heat decay in passive safety conditions. The investigation regards the following points:

- the influence of the heat exchanger arrangement: vertical and horizontal;
- the shape of the tower which depends on the angle inclination;
- the effects of the wind.

The experimental apparatus includes (see the picture in Figure 10):

- two different arrangements of the electrical heaters which simulate the heat exchanger;
- the general hyperboloidal shape of the tower reproduced by two conical pieces coupled in order to make up the throat. There are three different angle solutions for the lower cone: for each of them there are three or four different upper cones;
- an air fan to create the wind conditions.

The instrumentation used to perform the experimental analysis is:

- an air velocity transducer to measure the air velocity at the inlet just behind the heaters and at the throat;
- hot wire anemometers to measure the air temperature at the outlet;
- thermoresistences to measure the external air temperature and the temperature at the throat;
- a voltmeter/amperometer for measuring the values of the power given to the heaters.

The efficiency was evaluated by introducing a thermal parameter and a geometrical parameter. The thermal parameter is defined as the ratio between the inlet-outlet temperature difference

over the external temperature, $Ft = \Delta T/T_e$;

Figure 10 – The experimental apparatus

The geometrical parameter is defined as the ratio between the throat diameter and the outlet diameter of the upper cone $Fg = D_t/D_o$.

The tests were performed at four different electrical heaters temperature (130°, 110°, 90° and 70°C) for each configuration (cone shapes). Then the power, the mass flow rate and the thermal heat transfer coefficient were measured in function of the thermal and the geometrical factor. By observing the results at the different heaters temperatures and in several ambient temperatures, it seems that a configuration that best performs the heat exchange does exist (in Figure 11 the mass flow rate is plotted versus of the geometrical factor, for a fixed throat diameter and at the heaters temperature of 110°C). This trend also appears bym the CFD analysis (Fig. 12).

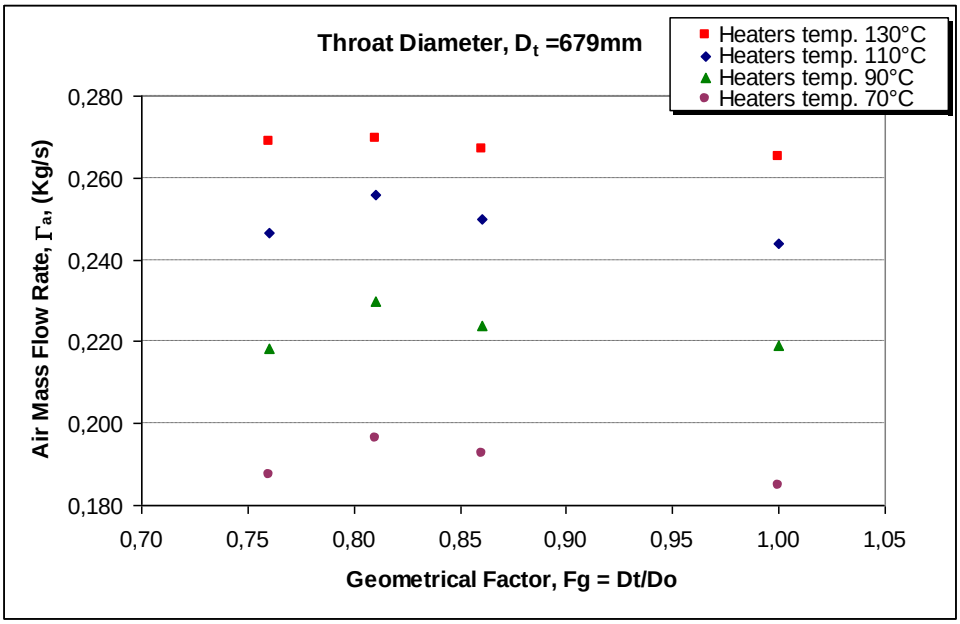

Figure 11 – Mass flow rate versus of the geometrical parameter

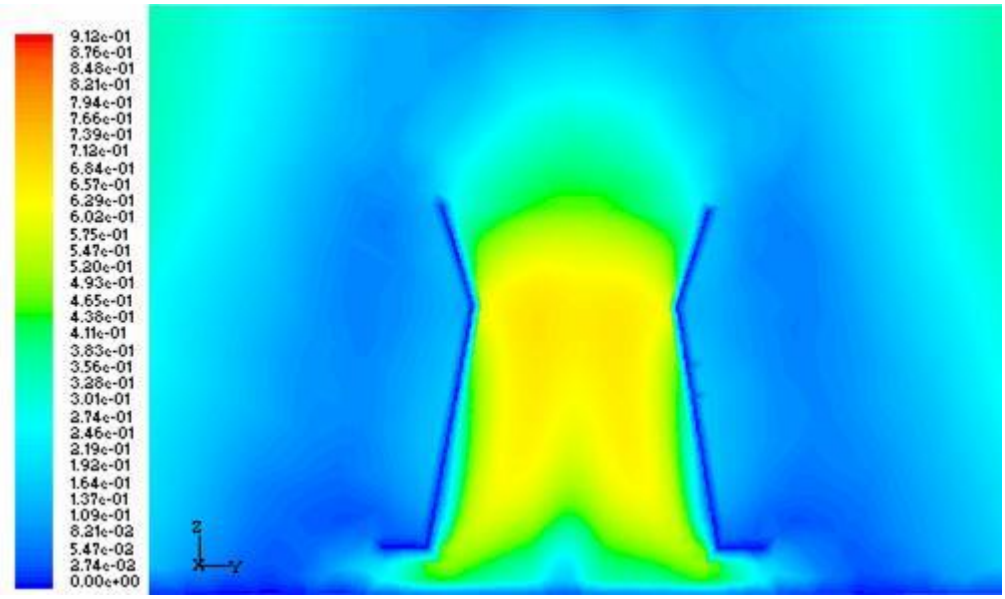

Figure 12 –The axial contours of the velocity magnitude by a CFD analysis for the tower with a throat diameter of 679 mm and outlet diameter of 888 mm at the electrical heaters temperature of 130°C

Back-Up Temperature-Actuated Scram System (ATSS)

General description

The core of the MARS reactor is optionally equipped with two different control rod systems. The first one, active type, is quite similar to classic PWR control rod systems; the second one, passive type, causes the control rods insertion into the core when the core coolant temperature reaches a selectable set value.

The overall number of fuel assemblies is 89 and the core diameter is 228 cm, compatible with the dimensions of the reactor vessel hypothesized during the preliminary design of the plant.

The core includes three zones with different enrichment (1/3 core strategy loading). The control rod clusters are distributed according to Fig. 13. They are grouped as follows:

4 blue clusters (belonging to the active system);
8 red clusters (belonging to the active system);
8 green clusters (belonging to the active system);
16 purple clusters (belonging to the active system);
9 yellow clusters (belonging to the passive system).

The new scram system (ATSS) was conceived and designed to provide an automatic and safe shutdown of the reactor (scram) as soon as the fluid temperature in the core rises above a selected set point.

This special scram system also eliminates the occurrence of ATWS accidents.

The reactivity control by the ATSS is obtained through the action of control rod clusters with the same geometrical and physical characteristics as the traditional scram system. The innovative features of the ATSS are in the type of actuator selected. Each ATSS control rod cluster is controlled by a special actuator, based on a simple physical principle: the thermal expansion of a rod, due to the variation of temperature of the core coolant, which leads to the disconnection of hooks holding the control rod cluster.

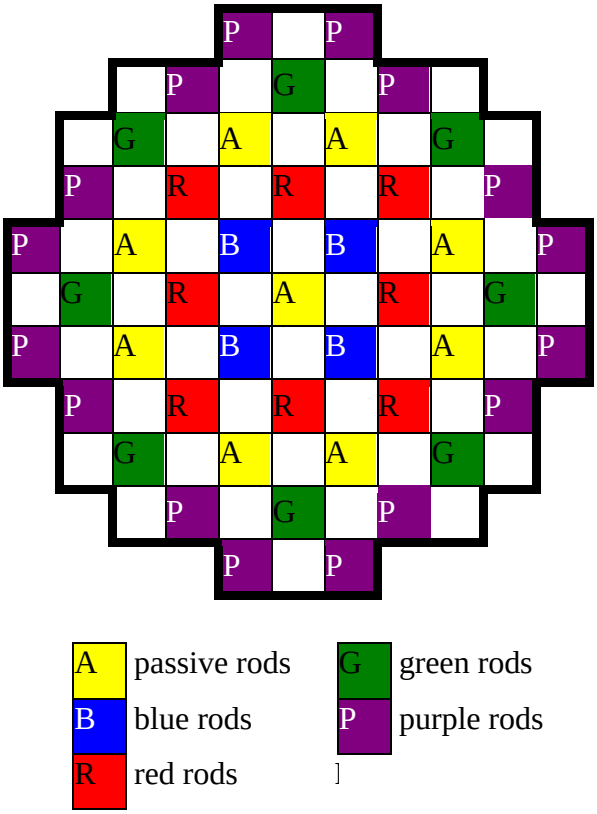

Figure 13 - Control rod cluster distribution

From a mechanical point of view, the ATSS actuation principle is based on two rods made with materials with very different thermal expansion coefficients, which are connected in the lower extremities. If the upper extremity of rod B is fixed on the structure of the reactor vessel internals and that of rod A is maintained free, when a temperature variation in the core occurs, the A upper edge will exhibit a displacement referred to the B edge. This displacement is used to cause the hook disconnection (Fig. 14).

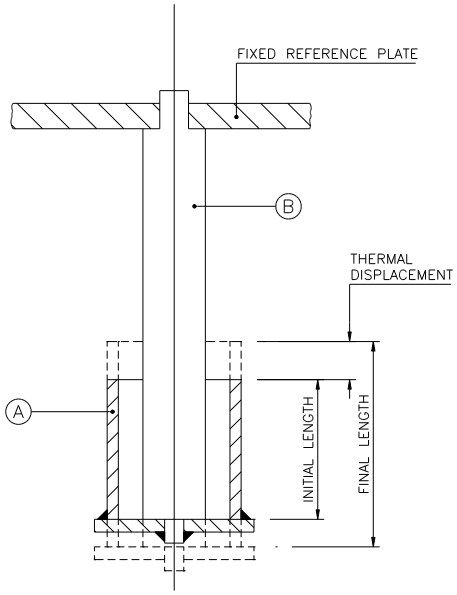

Figure 14 - Operation scheme of ATSS

The ATSS two-metal sensor is manufactured using a concentric, internal rod (rod B) connected to a 9.6 O.D. mm hollow rod (with the dimensions of a fuel rod). This allows the insertion of the mechanism into the fuel element. The sensor is inserted into the center of a fuel assembly which hosts the control rod cluster.
The differential expansion is transmitted to the upper extremity, where the control rod disconnection device is placed: the mechanical force developed in the sensor itself directly releases the hook sustaining the ATSS control rod cluster (Fig. 15).

In the preliminary design, the ATSS sensor is made of two coaxial cylinders:

- the internal cylinder is made of INVAR (Fe 63.5%, Ni 36%, Mg+C bal.): $\alpha_1 = 4.5 \cdot 10^{-6}\ °C^{-1}$;
- the external hollow cylinder is made of AISI 316: $\alpha_2 = 17 \cdot 10^{-6}\ °C^{-1}$.

If L is the total length of the two cylinders, the corresponding differential displacement Δl is:

$$\Delta l = \Delta l_1 - \Delta l_2 = \alpha_1 \cdot L_1 \cdot \Delta T - \alpha_2 \cdot L_2 \cdot \Delta T = (\alpha_1 L_1 - \alpha_2 L_2) \cdot \Delta T$$

For instance, with $L_1 = L_2 \approx 5$m, an increase $\Delta T = 30°C$ leads to a displacement of about 1.6 mm (Fig. 16). Even taking into account the compression due to friction forces, the expected "output" differential displacement is about 1.2 mm. Detailed calculations through specific computer programs have been performed to analyze the time response of the new device and its geometrical and thermo-mechanical behaviour, with particular reference to the force to be developed on the hook.
Actually, new analyses based on different materials are being performed to obtain greater displacement in less than 2 seconds (assuming a similar increase of the average temperature in the core as in the preliminary design). Two special alloys have been identified: AISI 72, characterized by an expansion coefficient of about $27 \cdot 10^{-6}\ °C^{-1}$, and Alloy 39, with $\alpha_1 = 3.2 \cdot 10^{-6}\ °C^{-1}$. Coupling these two materials, an effective expansion of about 2.9 mm in 2 seconds can be obtained.

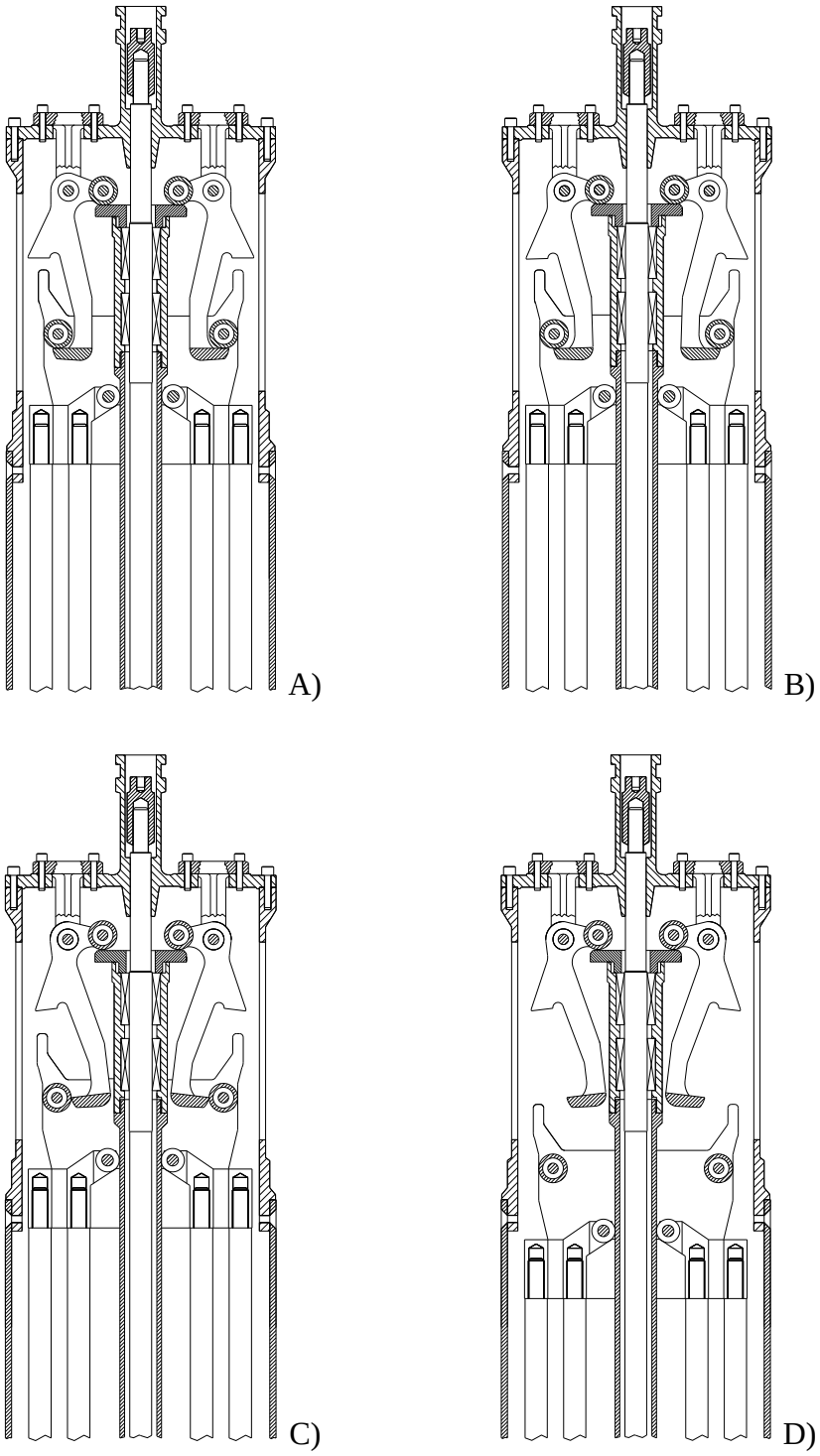

Figure 15 - ATSS operation sequence

Other experimental activities

In the specific case of the MARS reactor plant, the experimental activities regard only the performance demonstration of fluid circuits and of a few innovative mechanical components. In fact, this nuclear plant is based on consolidated, well proven, traditional engineered solutions for all the “nuclear” system. The innovative parts of the MARS design regard the

performance of hydraulic circuits whose operation is based on simple physical laws, according to plant solutions which are very well consolidated and well proven in generalized engineering applications.

Since the safety behavior of the MARS nuclear plant and, in particular, of its emergency cooling system, is easy-to-understand and may be conceptually shown through easy experimental tests, an experimental activity has been nevertheless carried out.

In the following, some of additional experimental tests carried out are briefly summarized.

An experimental facility (called MORIS) was built at the ENEA research centre of Casaccia, to simulate the general thermal-hydraulic behavior of the MARS primary cooling system and of the emergency core cooling system (see Fig. 16, Palazzi et al., 1988). The tests were successful.

In the same laboratories, the innovative check valve developed and designed for application in parallel with a traditional-type clapet valve in each line of the two parallel trains of the primary loop of the safety core cooling system (SCCS) was successfully tested, in the experimental facility CIVAP (see Figs 17 and 18, Ferrari et al., 1997), in an important scale and with clean and dirty water.

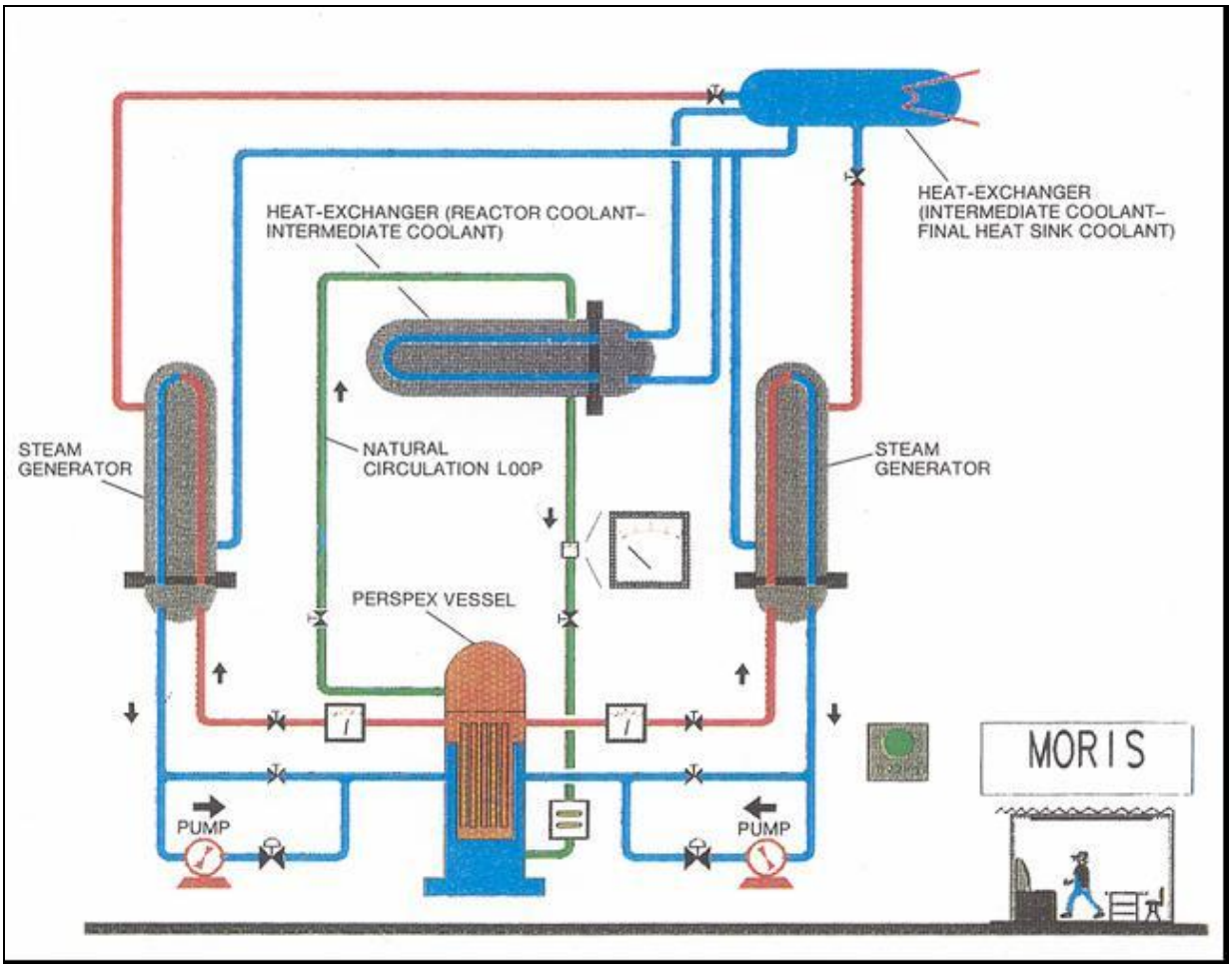

Figure 16 - Simplified scheme of the MORIS Experimental Facility

Figure 17 - CIVAP Experimental Facility

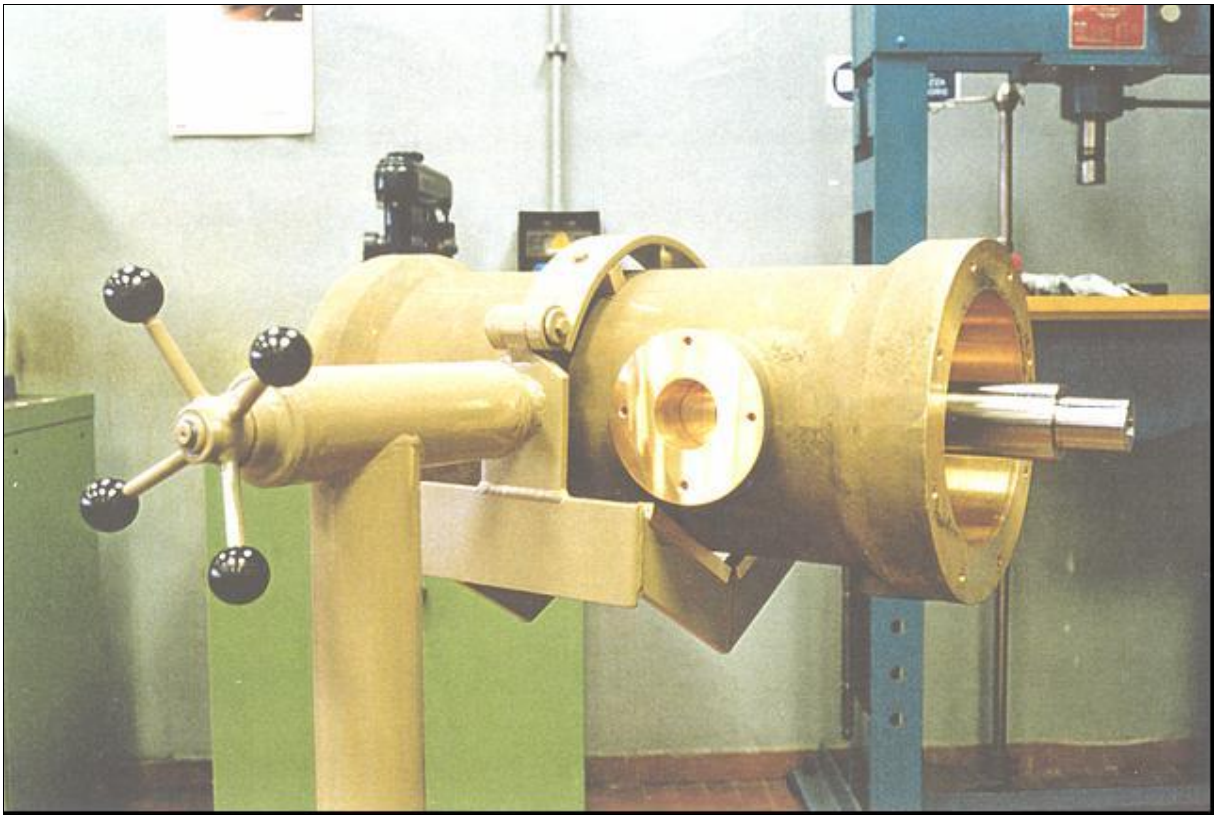

Figure 18 - Innovative MARS SCCS check valve during assembling before testing

Among the additional experimental activities carried out at the University of Rome "La Sapienza", in the laboratories of the "Nuclear engineering and energy conversion" Department,

concerning thermal-hydraulic phenomena and components, we mention:

- natural circulation in steady state and in transient conditions, simulating the operation conditions of the SCCS;
- boiling in pools with water at atmospheric pressure, with inclined tubes, simulating the pool heat exchangers of the SCCS;
- condensation of steam with low and high concentration of non-condensable gases inside inclined tubes, simulating the atmospheric condenser of the SCCS.

The tests have shown a very good performance and a very high reliability of the components and systems of the MARS nuclear plant.

REFERENCES

[1] *Generation IV Roadmap*, Generation IV International Forum.
[2] *SNE TP - Strategic Research Agenda* (http://www.snetp.eu/www/snetp/images/stories/Docs-AboutSNETP/sra2009.pdf).
[3] B. Farrar, J.C. Lefevre, S. Kubo, C.H. Mitchell, Y. Yoshinari, S. Itooka, *Fast reactor decay heat removal; approach to the safety system design in Japan and Europe*, Nuclear Engineering and design 193 (1999).
[4] M. Matsuura, M. Hatori, M. Ikeda, *Design and modification of steam generator safety system of FBR MONJU*, Nuclear Engineering and Design, Volume 237, Issues 12–13, July 2007, Pages 1419-1428.
[5] G.L.Fiorini, A.Vasile, *European Commission-7th Framework Programme: The Collaborative Project on European Sodium Fast Reactor (CP ESFR)*, Nuclear Engineering and Design, Volume 241, Issue 9, September 2011, Pages 3461-3469.
[6] A. Vasile & al., *The Collaborative Project for a European Sodium Fast Reactor CP ESFR*, ICAPP 2011.
[7] Y. Chikazawa, S. Kotake, S. Sawada, *Comparison of advanced fast reactor pool and loop configurations from the viewpoint of construction cost*, Nuclear Engineering and Design, Volume 241, Issue 1, January 2011, Pages 378-385.

A PROPOSAL FOR SIMPLIFICATION AND COST REDUCTION OF SFRs

Antonio NAVIGLIO[*], Damiano VITALE DI MAIO[*], Fabio GIANNETTI[*], Gianfranco CARUSO[*], Gabriele D'AMICO[*]

[*] *"SAPIENZA" University of Rome - DIAEE, Corso Vittorio Emanuele II, 244 – 00186 Rome, ITALY,*
E-mail: antonio.naviglio@uniroma1.it; damiano.vitaledimaio@uniroma1.it;
fabio.giannetti@uniroma1.it; gianfranco.caruso@uniroma1.it

ABSTRACT

The present work is aimed at describing an innovative plant solution able to greatly simplify and to make a fast neutron Sodium cooled nuclear reactor plant cheaper, without impairing safety. An innovative system has been developed, aimed at eliminating the intermediate sodium loop. It is based on a special heat exchanger that "joins" the intermediate heat exchanger, typical SFRs component, to the steam generator. The presence of an intermediate loop in Sodium Fast Reactors (SFR) is due to the high reactivity features of sodium with air or water. Thanks to this circuit a reaction between primary sodium (radioactive) and water/steam, within the energy conversion system, is prevented and, at the same time, the following presence of reaction product in the primary circuit, with the safety implication it would have, is avoided. Moreover, the plant solution proposed allows maintaining a physical double separation between primary sodium and water/steam, but avoiding any moving component within the fluid between primary sodium and water/steam.

The research leading to these results has received funding from the European Community's Seventh R&TD Framework Programme (FP7/2007-2011) under grant agreement n° 232658.

1 INTRODUCTION ON SODIUM FAST REACTORS (SFRs)

1.1 Key aspects of SFRs relevant for the new design

1.1.1 Selection of sodium in Nuclear Power Plants

The use of Sodium in a Fast Neutron Nuclear Power Plant (NPP) is linked with several aspects that have to be considered. Sodium is characterized by special features that make it very attractive to be used for removal of thermal power produced within the core of a nuclear reactor:

- An excellent thermal conductivity of liquid sodium implies a very high heat transfer capability even at modest liquid velocities (high power density in fuel is possible);
- A high volumetric expansion coefficient of liquid sodium, that is useful to reach the condition of natural circulation of the coolant with modest temperature difference (cool ability of fuel is easier to be achieved in accidental conditions);
- A high boiling temperature at low pressure allows high energy conversion efficiency at quite low operation pressures.

At the same time, sodium physical-chemical characteristics have also negative effects:

- An excellent thermal conductivity has thermal-mechanical implications in fast temperature variations (thermal shock risks);

- A limited heat capacity implies higher temperature difference between inlet and outlet for given power and flow;
- A melting point at operating pressure (near atmospheric) higher than the room temperature requires a special heating system in order to avoid coolant freezing;
- A high chemical reactivity of sodium with air and water strongly affects safety and therefore has several implications on plant system and component design, as well as on plant operation and maintenance activities and costs.

1.2 SFRs schemes

Solutions adopted in design of nuclear reactor systems using sodium as primary coolant, have always been aimed at preventing any possible contact between the primary coolant (active sodium) and the energy conversion fluid (water), as well as between active sodium and the environment. Usually, three independent circuits have been used to reach this purpose: the active primary coolant flows within the first loop including the nuclear reactor and an intermediate heat exchanger (IHX); the secondary coolant (sodium) flows within an intermediate loop including the secondary side of the IHX and the primary side of steam generators (SG) where the working fluid (water) vaporizes and is super-heated before reaching the steam turbine.

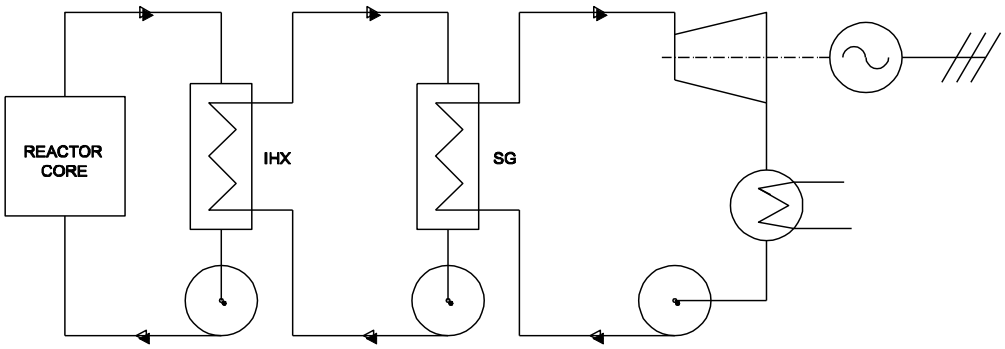

Figure 1. Scheme of a classical solution for SFRs

The intermediate loop is necessary to prevent a possible interaction between the primary active sodium and high pressure water/steam in case of a separating barrier failure: sodium-water reaction products and water itself would enter into the primary coolant boundary, destructive phenomena could occur owing to the high energy generation due to water/sodium reaction, with possible release of radioactivity in the reactor building. Components of the primary circuit are generally arranged according to two different schemes:

- loop solution, characterized by:
  - limited primary vessel size and primary sodium amount in it;
  - pumps and intermediate heat exchanger easy to maintain;
  - long piping extension and large number of connections;
  - on the whole, it is not a compact solution.
- pool solution:
  - compactness of the whole system;
  - primary sodium presence only within the primary tank;

- system easy to fill and drain;
- higher thermal inertia due to the larger amount of primary sodium in the reactor tank;
- particles within sodium may be deposited in low speed zones.

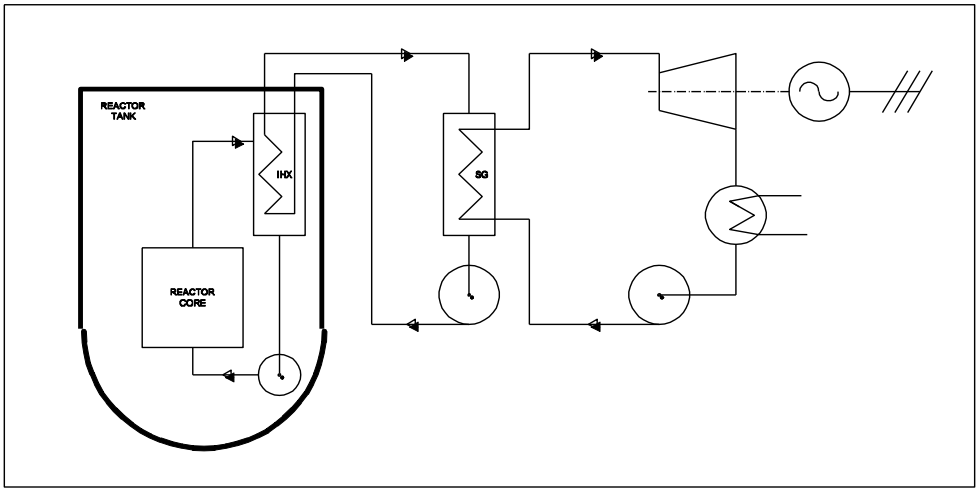

Figure 2. Scheme of a pool type Sodium Fast Reactor

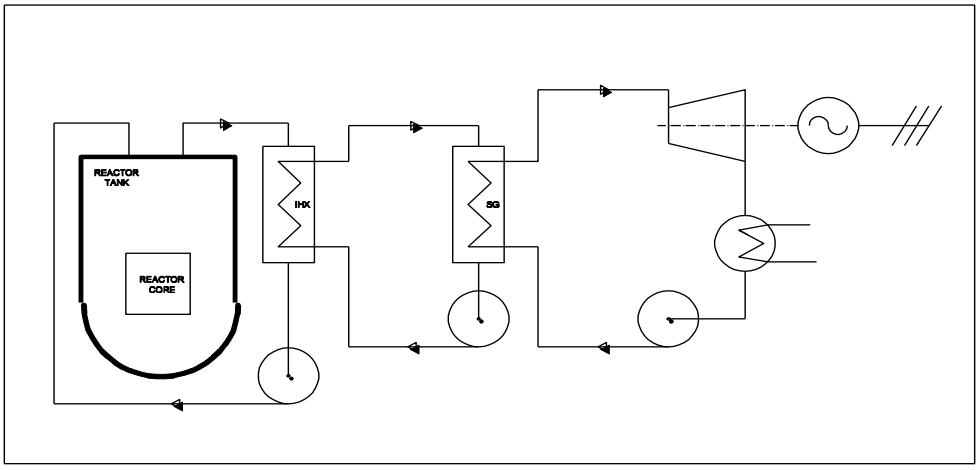

Figure 3. Scheme of a loop type Sodium Fast Reactor

1.2.1 Schemes of three typical SFRs projects (Superphénix, Monju, BN 600)

Different countries have chosen different solutions and reactors of both types have been built. Three reactors are briefly analyzed below and their main characteristics are reported in the table.

Table 1. Characteristics of three SFRs

Reactor (country)	**Reactor power MW_{th} (MW_e)**	**First criticality**	**Final shut-down**	**Operational period (years)**
Superphénix (France)	3000 (1240)	1985	1997	12
BN-600 (Russia)	1470 (600)	1980	(2020)	31
MONJU (Japan)	714 (280)	1994	-	17

1.2.2 Superphénix

The Superphénix NPP was based on a reactor that has been operating in France up to 1997. It was characterized by a pool configuration and each circuit (primary, secondary and tertiary) was made up of 4 parallel loops. The whole system included 4 SGs, 4 primary pumps and 8 IHXs. The primary sodium (about 2500 tons) flowed through the core between 395 °C and 545 °C. The primary sodium flowed within the shell side of the IHX where it released heat to the secondary sodium. Thanks to once-through SGs, steam at 487°C and 177 bar was produced.

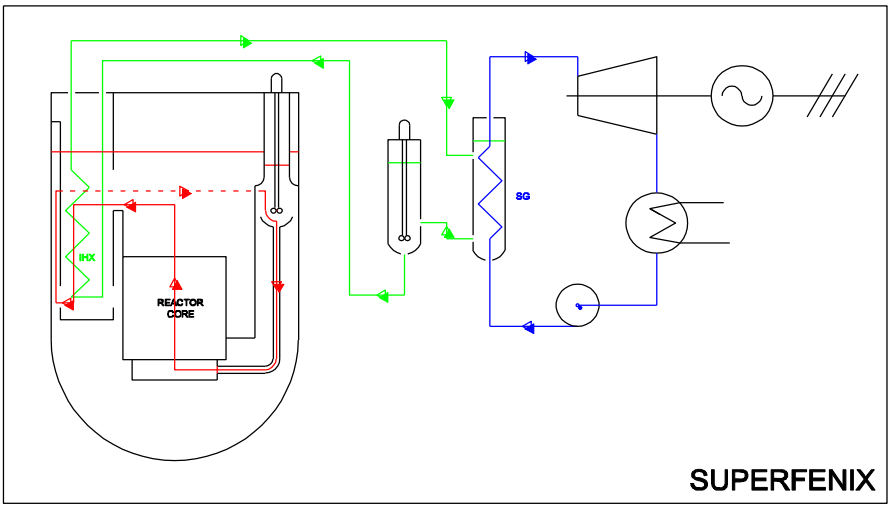

Figure 4. Scheme of the Superphénix reactor

1.2.3 BN-600

The BN-600 reactor is a pool type, it was built in Russia, and it is still operative. Each circuit of the system (primary, secondary and tertiary) is characterized by 3 parallel loops. Primary sodium flows through the core, passing from 365 °C to 535 °C before reaching the IHX where the secondary sodium reaches 510 °C and produces steam at 500 °C and 132 bar.

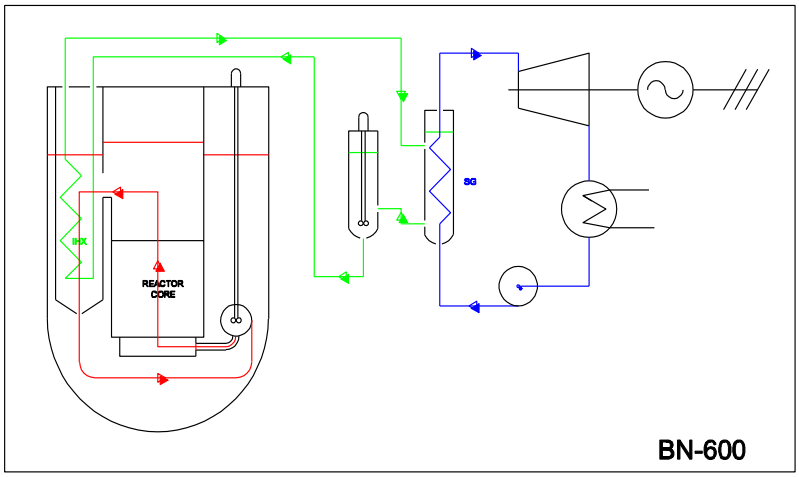

Figure 5. Scheme of the BN-600 reactor

1.2.4 Monju

Unlike the previously described solutions, the Monju reactor is a loop type, choice mainly due to seismic considerations, for easier accessibility of the components and to use the experience gained with the experimental reactor Joyo. The reactor was built in Japan and is still in operation.

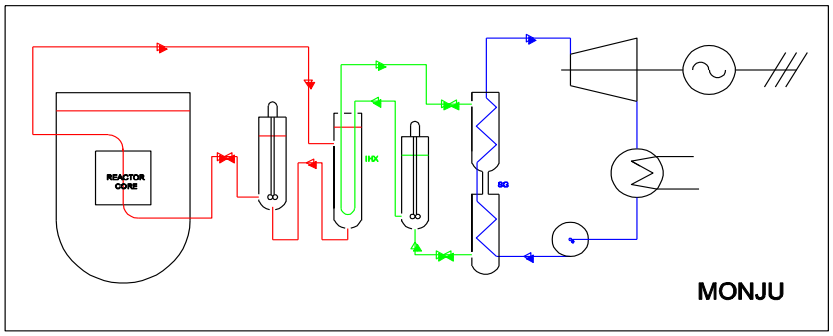

Figure 6. Scheme of the Monju reactor

1.3 *Main aspects concerning Sodium as coolant*

In order to design a NPP with sodium as primary coolant, the high chemical reactivity, the incompressibility of liquid sodium as well as the high thermal expansion coefficient have to be taken into account. The system foresees an inert argon volume to cover free sodium surfaces to prevent exothermic reactions between sodium and air/water. At the same time the free sodium level within the component, with argon above, is used for expansion purposes. The system components and pipes are traced with electrical heaters to always maintain sodium in liquid state. The main problems connected with the use of sodium as coolant are analyzed in the following sections.

1.3.1 Sodium–water reactions

The main problem is due to the highly exothermic reaction between sodium and water (SWR)[1]. Sodium reacts with water/steam generating sodium hydroxide, hydrogen and heat accordingly with equation [1]:

$$Na + H_2O \rightarrow NaOH + \frac{1}{2}H_2 + 140\frac{kJ}{mol}$$

[1] The SWR is a complex process where reactions take place in two different steps. Concerning safety analysis, the first step of reaction is the most important one because it generates heat, hydrogen and rapid pressure increase:

1. The first step is characterized by a high rate and release of gaseous hydrogen and heat:

$$Na + H_2O \rightarrow NaOH + \frac{1}{2}H_2 + 140\frac{kJ}{mol}$$

2. The second step is characterized by the reaction of products of the first step and additional sodium, according to these equations:

$$2Na + NaOH \rightarrow Na_2O + NaH$$

$$Na + \frac{1}{2}H_2 \rightarrow NaH$$

Then, the total reaction may be represented as:

$$4Na + H_2O \rightarrow 2NaH + Na_2O$$

The reactions between sodium and water/steam have major implications in the design, material selection and protection system of sodium-heated SGs. These components are the most critical ones for successful operation of a sodium cooled fast reactor power plant. The implications in the SG design that have to be taken into account are high temperatures at reaction front, failure propagation to adjacent tubes, material erosion and high pressure within the sodium side of the SG. This reaction occurred several times during the operation of some reactors; some examples are reported below:

- Phénix: 30 kg of water injected within the sodium bulk.
- PFR: failure of a superheater tube due to bundle vibrations.
- BN 350 and BN 600: the worst event took place in January 1981, with 40 kg of water injected within the sodium.

The lessons learned from these accidents are:

1. In terms of protection:
   - need of high reliability and rapidity of the hydrogen detection system;
   - automatic shutdown accompanied by rapid depressurization on the steam side;
   - modularization on design of a casing around the SG, capable of confining even the most violent SWR;
   - existence of safety membranes to limit any pressure increase.

2. In terms of prevention:
   - better thermo-mechanical design;
   - more suitable materials;
   - extreme quality in manufacturing (100% inspection, non-extended welds, etc.);
   - precautions in use (prevention of spurious thermal shocks, circuit well protected during drainages, etc.).

Superphénix did not have any SWR: nevertheless, the short reactor lifetime did not allow validating the SG solution. Several minor problems were verified in plant operation and maintenance. Since 1991, the BN-600 and BN-350 reactors have had no further SWRs.

1.3.2 Sodium–air reactions

Liquid sodium reacts with air and oxidation reaction can occur in a runaway manner, leading to sodium fire [2]:

$$2Na + O_2 \rightarrow Na_2O_2 + 519\frac{kJ}{mole}$$

$$2Na + \frac{1}{2}O_2 \rightarrow Na_2O + 435\frac{kJ}{mole}$$

The ignition temperature of sodium is 220°C in damp air, 200°C in dry air and as low as 120°C in stirred liquid pool. Sodium burning is accompanied by production of dense sodium oxide

fumes even if the produced heat is much less than conventional hydrocarbon fires. The system must be leak-tight to prevent sodium leaks. The piping/components must be equipped with leak-detection devices in order to limit the effects of fire.

1.3.3 Sodium leaks

Concerning the core cooling and integrity, primary coolant leaks are less hazardous in SFRs than in others reactors, because sodium is only slightly pressurized. Anyway, several sodium leaks took place on reactors, sometimes leading to sodium fires. The most serious sodium leak occurred at Monju (approximately 640 kg of Na) which resulted in reactor shutdown during more than 12 years. The leaks' amounts are very different, from less than one gram (detected during inspection) to massive events (BN-600, 2 leaks greater than 300 kg and one involving 1000 kg).

These sodium leaks can have very different origins:

- Construction defects or problems due to design;
- Material problems, such as 321 steel stress cracking;
- Thermal crazing leading to through cracks;
- Corrosion following air intake into the circuits;
- Operator error (for example, during thawing of the circuit and the corresponding expansion of the sodium).

Lessons have been learnt from these incidents in terms of design, circuit operating procedures, leak detection and protection from sodium fires.

The two latter points have led to the following:

- Diversified, redundant detection instrumentation ;
- Need for rapid drainage of sodium circuits;
- Sectoring around the sodium areas to limit the quantity of air available in the event of a possible fire;
- Insulation protection of the concrete floors and walls, covered with a metal plate;
- Possibility of inert gas blanketing of the areas involved.

1.4 Cost aspects and Generation IV requirements

The Generation IV reactors are designed according to stringent specifications, in particular regarding sustainability, economics, safety and reliability, proliferation resistance and physical protection. Most of the designs under development are generally not expected to be available for commercial construction before 2030. The GIF (Generation IV International Forum) provided the criteria for identifying and selecting six nuclear energy systems to further develop. Some of these criteria, especially those related with economic and safety aspects, are summarized below [3]:

"[...]

Economics: Generation IV nuclear energy systems will have a clear life-cycle cost advantage over other energy sources.
Economics: Generation IV nuclear energy systems will have a level of financial risk comparable to other energy projects.
Safety and Reliability: Generation IV nuclear energy system operations will excel in safety and reliability.
Safety and Reliability: Generation IV nuclear energy systems will have a very low likelihood and degree of reactor core damage.
Safety and Reliability: Generation IV nuclear energy systems will eliminate the need for offsite emergency response.
[…]"

2. THE "CANDLE"CONCEPT: INTERMEDIATE SODIUM LOOP NOT NECESSARY

Core cooling in a nuclear reactor is the most important function of the whole power plant, together with a safe shutdown. Since a small interference in the core cooling could lead to a significant drifting in the reactor behavior, the primary coolant must operate under very well-known and controlled conditions (i.e. high purity, no coolant path obstructions, no cavitations phenomena, etc…).
In SFRs, a risk linked to the possibility that a SWR occurs and reaction products can circulate within the primary loop exists. Since a water/steam tube rupture can lead to a chemical exothermic reaction and the products are explosive (H_2), caustic and corrosive (NaOH), and can obstruct the fuel sub-channels within the core, prevention of any contamination of the primary coolant is of primary importance. For this purpose, as already anticipated in the paper, an intermediate circuit, between primary sodium and the tertiary circuit (water/steam as working fluid), is always adopted.
The use of an intermediate heat exchanger (IHX) in plant solutions already built implies the presence of another hydraulic loop (possibly, multiple), which complicates the overall design, increases the plant costs and adds other maintenance issues; thus its elimination, or drastic simplification, would be extremely advantageous from the standpoint of efficiency, costs and safety.
The innovative solution, here presented and called "candle", is based on a double barrier separation between the water and the primary sodium, replacing the conventional intermediate sodium loop with a simple heat transfer system, working in absence of moving fluids. Thanks to this solution all the secondary sodium auxiliary systems (pumps, valves, dump vessels, etc…) are no longer necessary. The merging of the IHX with the SG allows achieving all the above mentioned objectives concerning reliability, economics and safety.

2.1 Introduction on the "candle" concept

The candle is the key-component of the proposed innovation in SFR design; it has been foreseen with a very simple configuration, as shown below (Figure 7).

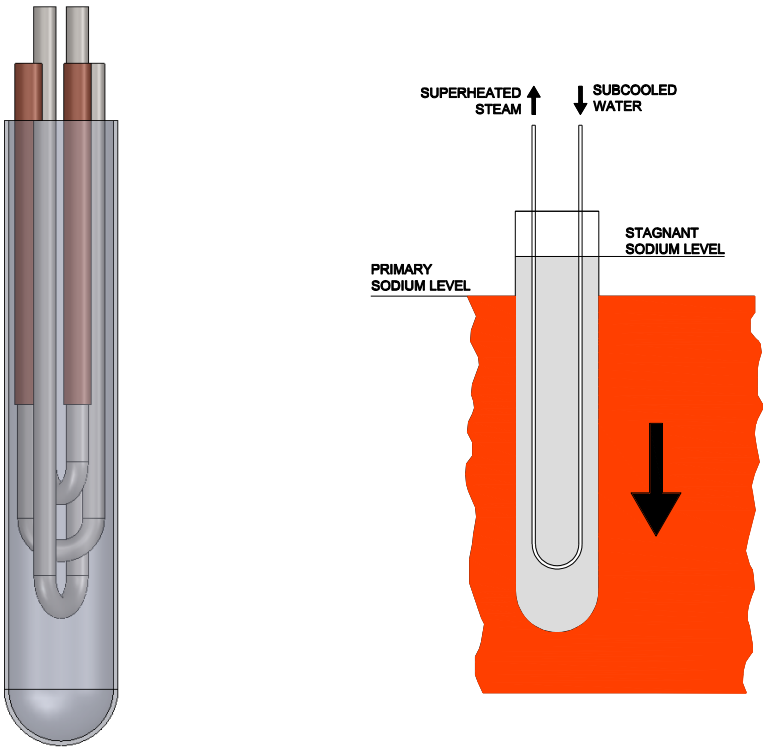

Figure 7. The "Candle" concept and its working scheme

The candle consists of a small diameter vessel, containing three "U-bend" tubes (arranged in angles of 120°); the straight vessel has an easy–to-manufacture geometry and it presents no irregularity, while the inner tubes are foreseen with a relatively large U-bend, in order to achieve a relevant manufacturing easiness, and to have very low stresses. The structural material for the vessel and the tubes is assumed to be stainless steel (having a high corrosion resistance with sodium and mechanical strength). The candle is submerged in primary sodium, and it is filled with a coupling fluid, which thermally connects the primary sodium and the water flowing within the tubes.

The primary sodium, outside the candle vessel, flows downward transferring heat. The filling fluid has been chosen taking into account its thermal-physical properties since it has the purpose of transferring heat from the core coolant (primary sodium) to the working fluid (water) mainly by conduction. In the reference case, sodium has been chosen as filling fluid.

2.2 Advantages of the concept and critical points to focus

Thanks to the innovative proposed concept, the overall NSSS size is greatly reduced. In Figure 8 and Figure 9, it can be seen that the presence of the candle inside the system greatly reduces the number of components and systems required, especially avoiding any moving part within the secondary circuit.

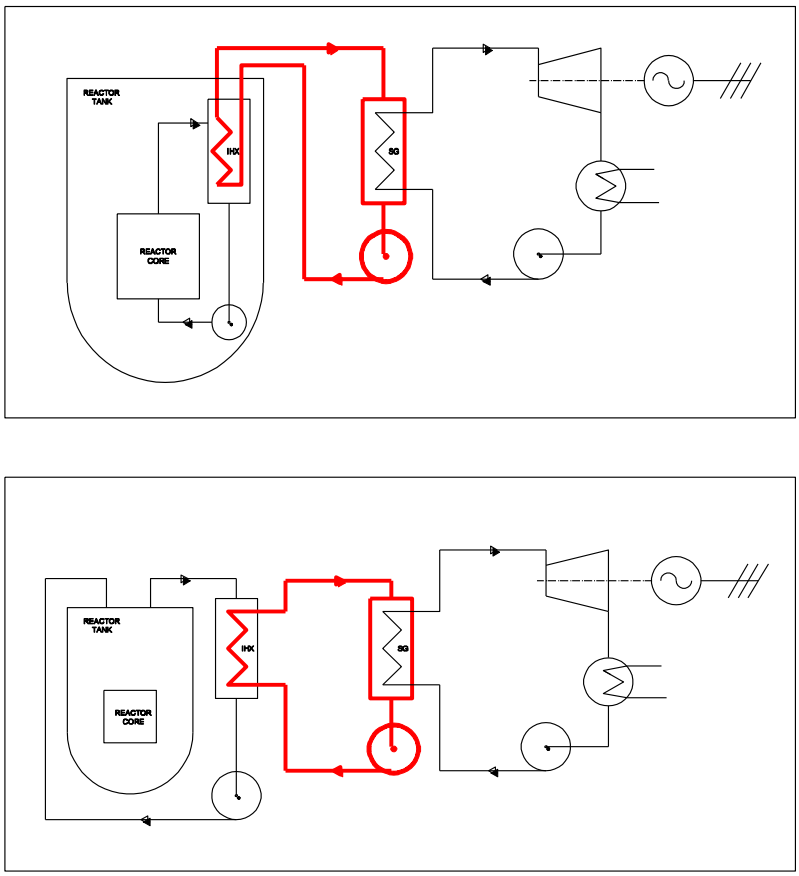

Figure 8. The pool and loop standard concept schemes (secondary circuits in red)

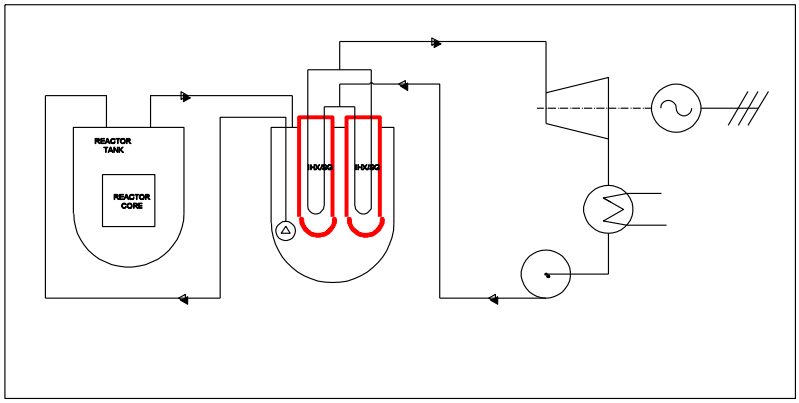

Figure 9. The "Candle" concept scheme (secondary circuit in red)

The presence of the candles implies also simpler construction processes. Such an innovative solution requires a dedicated safety analysis to verify the feasibility of the system. In particular, the heat exchanger characteristics and the problems due to the presence of impurities (eventually, generated from a sodium water interaction) in the primary coolant should be verified in the reference accident conditions to assure that:

- No consequences derive from the interaction of primary sodium and secondary stagnant coolant;

- The failure of a water/steam tube and the consequent interaction between secondary stagnant coolant and the working fluid do not compromise the integrity of adjacent tubes within the same candle;
- The failure of a tube and the consequent interaction between secondary stagnant coolant and the working fluid do not compromise the integrity of candle vessel, in order to prevent any possible interaction between water and primary sodium and the possibility that reaction products reach the primary circuit and hence the core.

3. ENGINEERING ASPECTS OF THE PROPOSED DESIGN FOR THE CANDLE

3.1 Design criteria

3.1.1 "U" tubes radius selection

The selection of the "U" tubes bend radius, within the candle vessel, is a key parameter since it affects the manufacturing costs of the steam generator and, indirectly, the minimal candle vessel diameter. The radius is a function of the tube thickness and diameter that were selected as follows:

- Tube thickness to withstand the pressure difference between the working fluid (about 185 bar) and the secondary stagnant fluid (about 3 bar). Conservative evaluation implied atmosphere pressure as reference pressure instead of the real operating pressure;
- Tube internal diameter to maintain the water/steam velocity lower than defined values having acceptable heat transfer coefficient. In any case the minimization of the total number of the candles within the system has to be considered as one of main targets.

The selection of the "U" tube radius affects the candle vessel diameter and generally an iterative process is required in order to define the optimum "U" tube diameter, the "U" tube bend radius and hence the candle vessel diameter.

3.1.2 Candle diameter selection

The choice of the candle vessel diameter has to be made taking into account the following issues:

- Minimization of the overall Candle dimensions;
- Costs minimization:
  - Use of standard commercial pipe for vessel and tubes for "U" tubes;
  - Candle vessel diameter large enough to allow a sufficient space to have a 180° "U" tube bend with a standard radius and easy manufacturing processes;
- Diameter large enough to have a sufficient heat transfer surface from primary sodium to the stagnant secondary coolant;
- Diameter large enough to allow an easy discharge of the stagnant secondary sodium (if any) in case of a sodium water reaction (failure of a tube), in order to minimize the severity of the pressure transient;
- Diameter small enough to minimize the stagnant sodium thermal resistance.

Taking into account these issues, a diameter of 0.1 m was selected in correspondence to a ¾" BWG 13 tube selected as reference for the "U" tubes.

3.1.3 Finned/not finned

In order to enhance the heat transfer performance of the steam generator, or to reduce the tube length with other parameters being equal, fins can be added in the riser tubes section. The presence of finned tubes could improve the heat transfer capability of the system but is strongly affected by the filling fluid choice in addition to the type and material of fins. In fact, if the thermal conductivity of the filling fluid, in which heat transfer is mainly based on conduction, is higher than that of the fins material, a solution based on not finned tubes is preferable.

3.1.4 Heat transfer enhancement

A common issue related with once-through steam generators is the strong reduction of the heat transfer capability of the system in the post dry-out region. The dry-out corresponds to the point in which the drying of the inner wall of the tube occurs and the heat transfer coefficient decreases because of the steam presence against the tube wall.

Once the post dry-out condition is reached, the complete vaporization of the droplets entrained into the steam flow becomes more difficult because specific power decreases, due to heat transfer occurring basically with a vapor phase. Since this issue strongly penalizes the heat transfer performance of the steam generator, and the dimensions of the candles, possible solutions have been investigated in order to minimize this effect. Each solution analyzed has been evaluated to verify: first, the feasibility and secondly, possible contras that can affect the whole system. Among the analyzed systems, taking into account problems related to the manufacturing complication of the candle and to the increase of total pressure drop within the system, the choice has regarded a special use of a standard heat transfer enhancement device; in particular, the chosen device was a “twisted tape”.

Twisted tapes are usually used in single-phase zones, where the helical flow allows to locally increasing the velocity and hence the heat transfer coefficient. The special use within the candle system concerns the use of the turbulence enhancement system from the dry-out point up to the outlet section, achieving two benefits:

1. Within the post dry-out zone (liquid deficient zone), thanks to the centrifugal force, the droplets entrained into the steam flow are forced outward against the tube wall and immediately vaporize guaranteeing a high heat transfer coefficient also within the liquid deficient zone. The heat transfer coefficient, since the liquid droplets are in saturation condition, results as high as in the nucleate boiling and the droplets can completely vaporize in a very short length.
2. Since the post dry-out region is reduced by the inclusion of the twisted-tape, the superheating zone is longer for a same tube length. Moreover, thanks to the presence of the twisted-tape, an average increase of about 1.5 times in the heat transfer coefficient is expected.

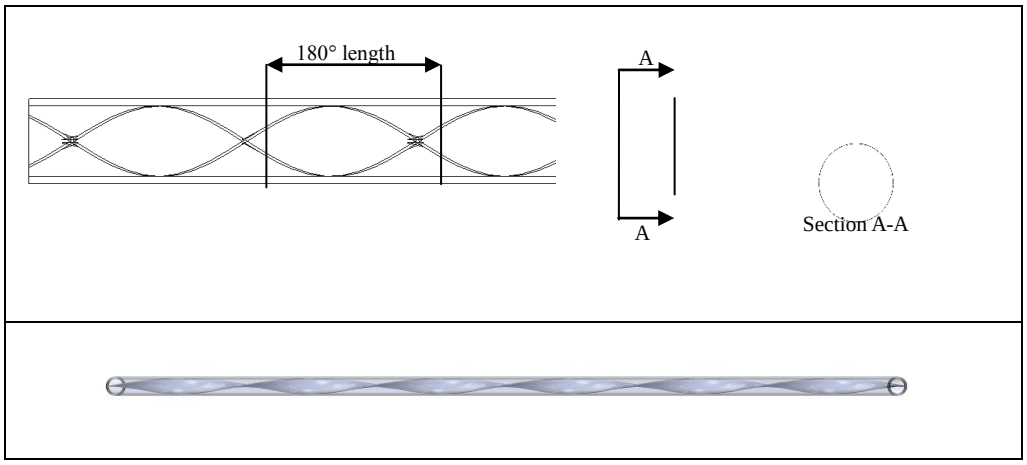

Figure 10. Scheme and main parameters of a twisted tape insert

Obviously, it is of primary importance the definition of the dry-out point from where the twisted tape has to be foreseen. In fact, the presence of twisted tape within the tube causes an increase in pressure drops especially concerning the two-phase region.
The optimum, from an engineering point of view, is that the twisted tape starts from the dry-out point and arrives up to the outlet section (see Figure11).
Since the heat transfer coefficient, in the post dry-out region, falls down, an evaluation of the improvement in the heat transfer coefficient due to the twisted tape insertion has been carried out (see Figure).

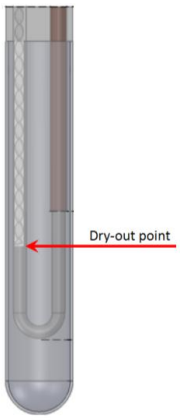

Figure11. Scheme of the candle concept with the insertion of a twisted tape above the dry-out point

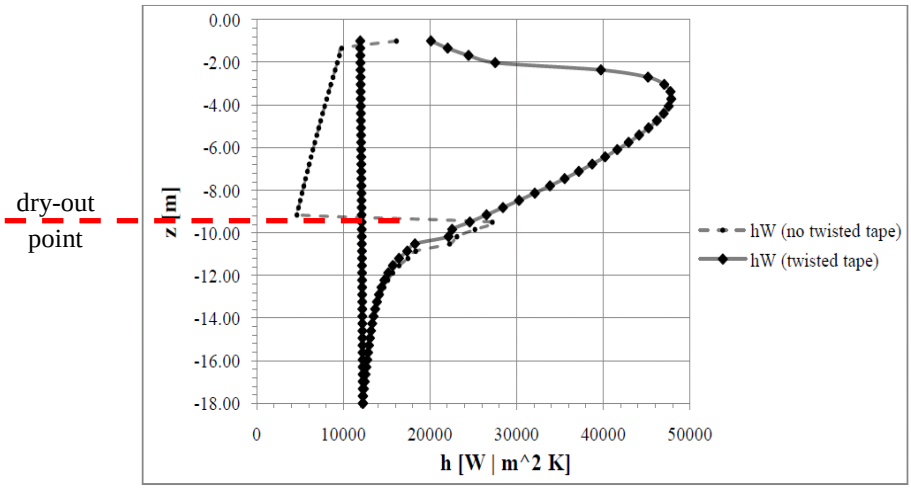

Figure 12. Evaluation of the heat transfer coefficient trend as a function of the "U" tube length

3.1.5 Insulator length

The candle heat exchanger consists of "U" tubes and, within the preheating section, the working fluid flows downward against the natural circulation direction. To maintain at acceptable values the density difference between the inlet section and the lower section of the "U" tube, the saturation condition of the working fluid has to be avoided. In order to prevent reaching the saturation point within the downcomer, an insulating layer aimed at limiting the heat transfer from primary sodium (through the stagnant fluid) to the working fluid has been foreseen around the downcomer tube. In order to optimize the performance of the heat exchanger, the length of the insulator has to be long enough to cause saturation condition of the working fluid in the bottom part of the riser section, in order to support natural circulation.

3.1.6 Choice of filling fluid

In order to choose the best filling fluid for the secondary stagnant coolant, a comparison among different liquid metals has been performed. For each material, pros and contras have been compared in order to evaluate the best solution for the filling fluid. In particular, the comparison has been based on costs, chemical and physical risks, thermal-physical properties, etc. This analysis considered Sodium, Lead, Gallium and Indium.

3.1.6.1 Best choice

Trying to find a compromise between the overall system performance and its reliability, taking into account safety aspects and issues concerning the corrosiveness of alternative liquid metals selected, the most appropriate filling fluid has been considered sodium.

For the candle, a filling fluid characterized by a high thermal conductivity is necessary, in order to reduce thermal losses within the candle and to minimize the number of required candles. From the safety point of view, an intermediate fluid equal to the primary coolant is a huge advantage: in case of an integrity failure of the candle vessel two identical fluids will be put in contact without any consequence for the plant safety. Moreover, sodium is a relatively light metal and this is an advantage both concerning structural solutions (also taking into account abnormal design loads as seismic ones) and for candle draining process.

The choice of the filling fluid has fallen on sodium, mainly for three reasons:

- The high thermal conductivity allows having high heat transfer coefficient even in stagnation conditions, where the heat transfer capability of the system is mainly based on conduction.
- The low density value of sodium implies smaller structures compared with alternative filling fluids analyzed and hence lower costs.
- Chemical behavior of fluids and criticality in material selection.

4. IN-SIGHT ON SAFETY OF A CANDLE-BASED INTEGRATED IHX/SG

4.1 The candle resistance

Preliminary studies have been carried out in order to identify the minimum candle vessel thickness to withstand loads in accident conditions, when a sodium water reaction occurs. The rough evaluation showed that the pressure transient following the SWR occurrence is strongly influenced by the time required for sodium removal from the candle volume. At present, detailed CFD analyses are being carried out in order to obtain a detailed pressure and temperature transient during the accident evolution. The pressure difference existing between the filling fluid and the working fluid implies the critical flow condition that limits the water mass flow rate and hence the quantity of water that can react with sodium per unit time. The safety margins related with maximum values of pressure and temperature can lead to modify the candle vessel diameter in order to reduce the required time to eliminate sodium form the candle volume.

4.2 The need not to involve surrounding candles

If a water tube rupture occurs within a candle, or if a water leakage from the distribution system occurs, the water could flow, from the SG upper volume, inside the candle vessel. With the purpose of avoiding, or at least minimizing, any water intake into the stagnant sodium, each candle is provided with a plug characterized by the following features:

- it must eliminate or limit the water/steam flow from the volume above the candle itself (dome);
- it must prevent the candle pressurization, in case of internal SWR, so it has to operates a rupture disc;
- it must allow the differential thermal expansion of the hot and cold legs of the “U” tubes within the candle;
- it must provide a way to fill and drain the candle with sodium.

For this purpose, an idea has been developed (see Figure 13) where:

- the axial labyrinth seal provides a barrier against external steam/water inlet, but allows the differential thermal expansion of the U-tube legs;
- the central rupture disc will break in case of a limited candle pressurization, but it can be removed in order to allow access to the filling sodium (for purging/filling operations, as well as for ISI&R purposes)

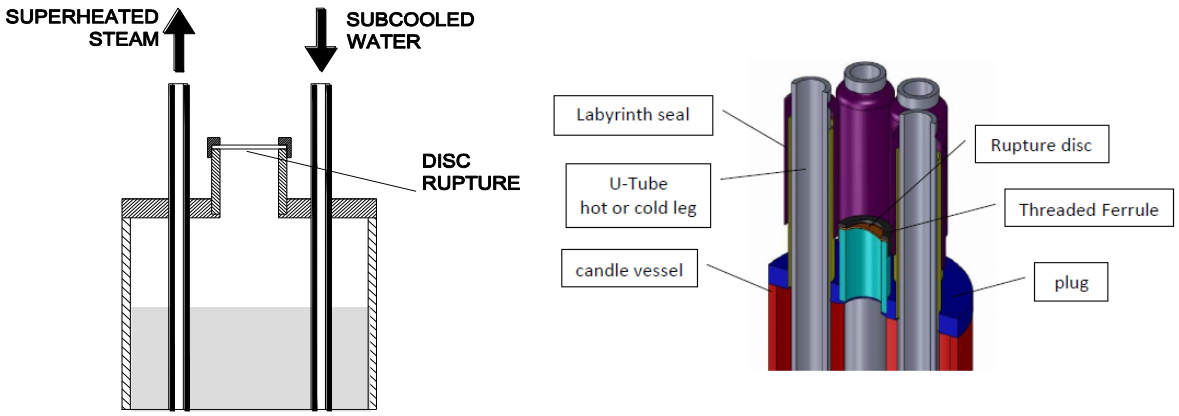

Figure 13. The candle vessel plug and scheme of the rupture disc

5. ENGINEERING OF THE TANKS HOSTING THE CANDLES

5.1 The support of piping in the candles

Important issues linked with thermal expansion phenomena must be taken into account. The cold leg of the "U" tube, the downcomer, is totally filled with subcooled water, while the hot leg, riser, is filled with saturated water and superheated steam at the same pressure. For this reason, the mean temperatures between the two sides of the "U" tube are very different. Due to the height of the water tube (more than 15 m), a significant length increase, due to thermal expansion of the steel, is expected. A rough calculation has been carried out, leading to the following results:

$$\Delta l = \alpha \cdot \left(T_{riser} - T_{downcomer}\right) \cdot h_{"U" tube} = 0.037\, m$$

$$where:$$

$$\alpha = steel\ thermal\ \exp ansion = 17.5 \cdot 10^{-6}\ \frac{m}{m}$$

$$T_{riser} = 420\,°C$$

$$T_{downcomer} = 280\,°C$$

$$h_{"U" tube} = 15\, m$$

The result shows a considerable differential thermal length increase, which should be taken into account in a further stage of design, for example, implementing a device based on a flexible support as that shown in Figure 14.

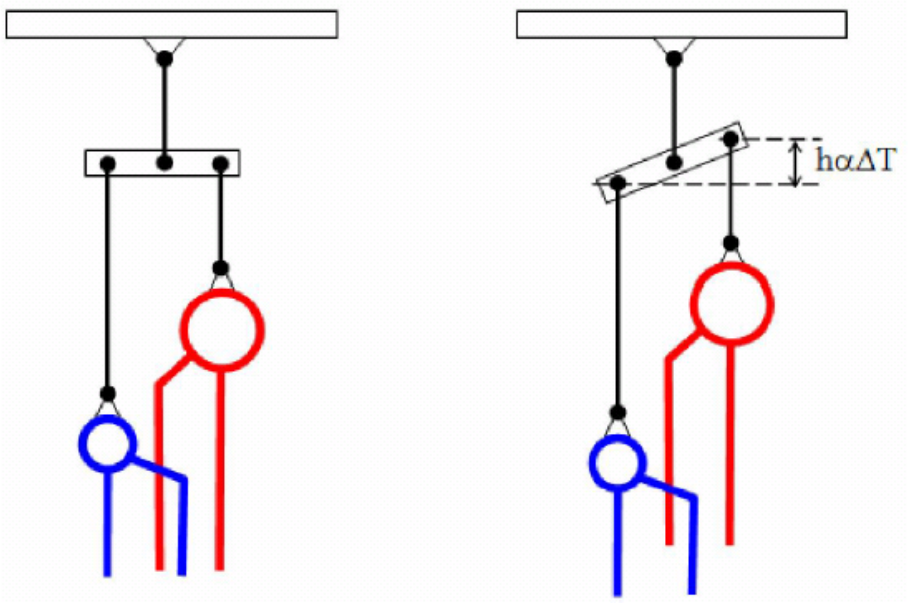

Figure 14. Schematic representation of the flexible support that allows free thermal expansion of the "U" tubes

5.2 The grouping of candles into modules

The whole steam supply system is made up of several candles and it is impossible to move each candle separately. Moreover, the very high aspect ratio (H/D) of the candle implies low structural strength. In order to take into account all these aspects and to make the construction easier, 36 candles are grouped within a single module (see Figure). This solution thus reduces time and costs required for manufacturing of the system, responding at the economic requirements for generation IV reactors.

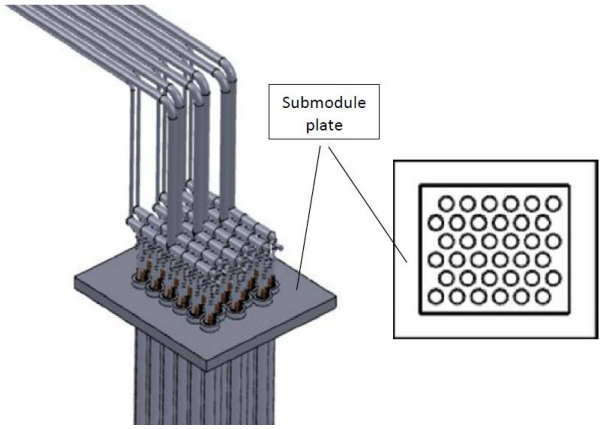

Figure 15. Single module made up of 36 candles

5.3 The dome

Since the required candles are a lot, they are arranged within special tanks outside the primary tank (the NPP configuration becomes a mixing between the "pool" and the "loop" concepts). Each SG tank will be enclosed, in the upper part, in a metallic dome, which has a double goal:

- it must contain sodium/water leakage from the circuits (avoiding any environment contamination), and it must be able to withstand the reference accidental conditions
- the pump supporting structure can be placed within such volume.

The volume within the dome must be filled with an inert gas, in order to prevent any air-sodium interactions (sodium fires). In this study, argon has been assumed as cover gas. The coupling of the dome with the cylindrical vessel can be realized, for example, with a flange along the full perimeter. Since the upper volume of the tank holds the sodium distribution piping, the inner diameter (15 m) is sized taking into account the dimensions of the tubes (in particular the hot ones).

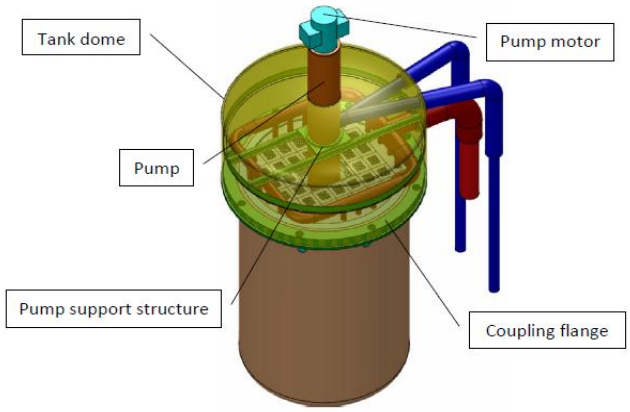

Figure 16. Representation of the dome above one of the candle tanks

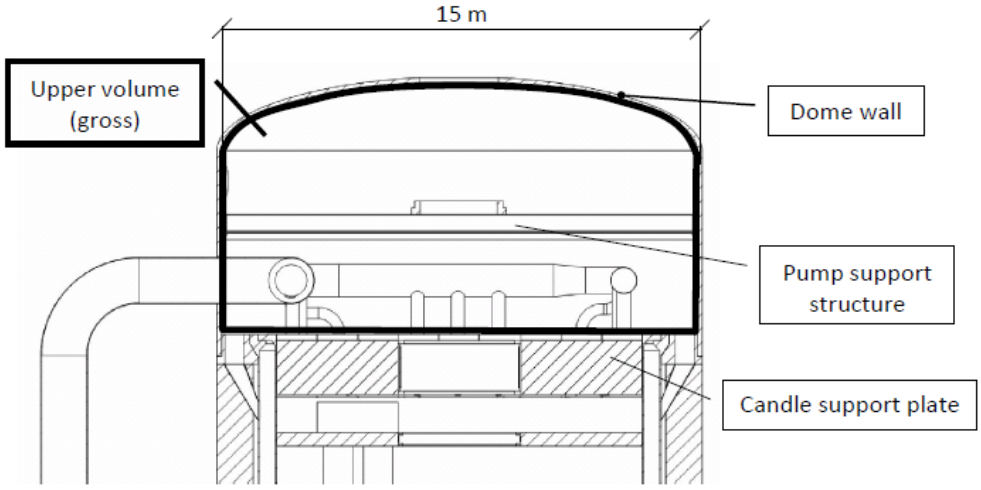

Figure17. Structural details of the dome and of sodium distribution piping within it

A preliminary evaluation of the necessary free volume within the dome has been carried out and later verified. Two independent evaluations of the dome pressurization due to the release of a high pressure water flow within candle have been carried out (1. RELAP5/mod3.3; 2. Computer code developed ad hoc). This preliminary evaluation did not take into account the thermal heat produced within the candle due to the sodium-water reaction. The simulation does not result conservative but it can give a rough indication of the pressure equilibrium value at

the end of the accident transient phase. Since the pressure transient has been evaluated to be very short (less than 1 second), the pressure value that affects the structural design of the dome is mainly due to the high pressure of the water/steam circuit; while concerning the structural design of the candle, it could be mainly influenced by the temperature and pressure values following the SWR.
The results of the simplified simulation concerning the failure a "U" tube within the candle, in terms of final pressure and temperature in the dome volume, are reported below:

Table 2. RELAP 5 DBA simulation results

Dome final conditions		
Vapor pressure	Total pressure	Temperature
0.535 bar	1.857 bar	280.1 °C

The main consequences of the reference accident condition on the structures are reported below:

- The temperature increase (+18 °C), within the dome, involves steel yield stress decreasing of about 2.4%, while the ultimate stress will remain almost constant (–0.15%);
- The dome volume pressure increment (+48.8%) causes an increase of the mechanical stress of the dome wall;
- The pressure rising within the dome volume causes a linear increase in the load carried by the plate itself.

Results show that the effects of this accident are acceptable. Nevertheless, should more than one candle be involved in the accident, the amount of released energy could be too high. Thinking to this case, it is advisable to provide a relief tank in order to increase the total volume available for gas expansion.

5.4 The mechanical support of candles and thermal protection

Due to the severe conditions in which the candle steam generators have to work, special solutions have to be provided in order to guarantee the integrity of all structures and not to reach extreme conditions (temperature and pressure values). In particular, in order to avoid any reduction of the mechanical resistance of the support plate, where the weight of the candle modules is borne, an intermediate plate, without any structural function, between the free sodium level and the support plate has been foreseen. In this way, the support plate operates at a lower temperature and higher mechanical performance is guaranteed.

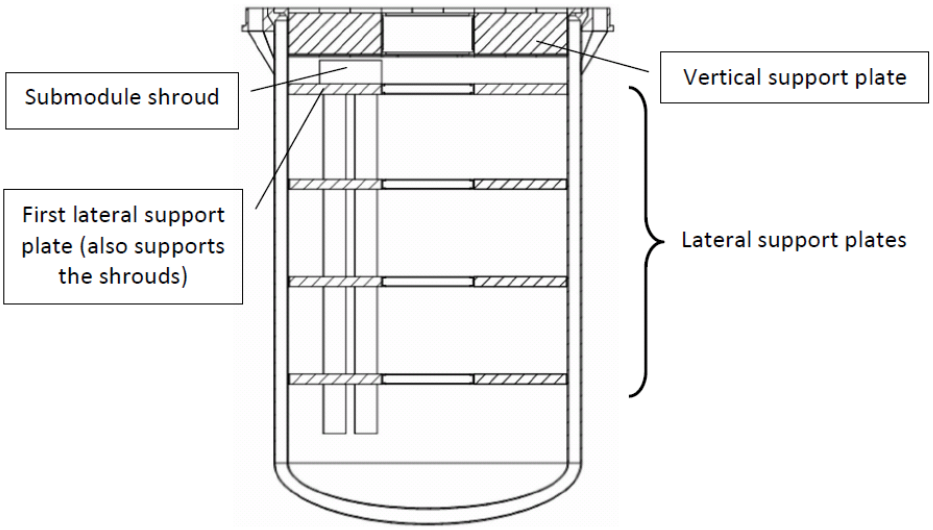

Figure18. Scheme of the internal support structure within a candle tank

5.5 Seismic candle protection

Due to the considerable length of the candles and to the presence of only upper mechanical constrains, in case of a seismic event candles could move horizontally causing possible candle vessel failure. In order to minimize the free horizontal movement of each candle, a series of lateral support plates has been foreseen, within the height of the candles, of the types shown below (see Figure19).

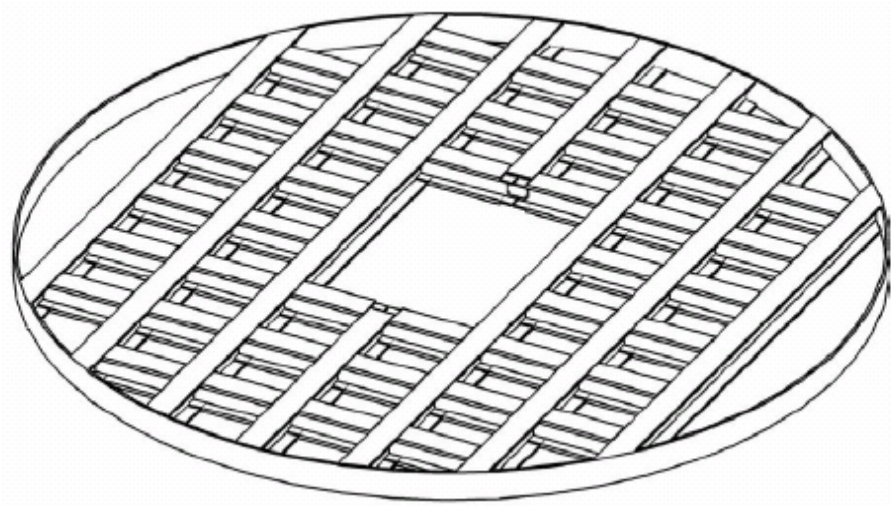

Figure19. Detail of a lateral support plate for the candle modules

6. THE BALANCE OF PLANT

6.1 Piping lay-out

In order to produce electricity, the steam has to be sent to a turbine and a suitable piping system is required. Due to the high number of candles and tubes (reminding that each candle is characterized by three feed water inlet and three steam line outlet), a complex system of

manifolds and pipes has been studied. During the development of the piping system of water and steam, a preliminary solution was selected; later, with the target of cost minimization, an alternative solution, based on standard components only, has been developed.
Since the first solution analyzed would require non-standard components, in spite of the possibility of lower diameter for the candle tank, an increase in costs would be experienced. Taking into account a solution described before (grouping several candles in a single module – see 0) and the use of standard components only, an alternative manifold solution has been identified. Each candle module is includes 36 candles arranged on 6 parallel rows; each row can have an independent manifold concerning both the feed water and the steam. This solution strongly simplifies the piping management since pipes with lower diameter can be used and also within a single module there are independent sub-systems made up of 6 candles that contribute to the complete modularization of the steam supply system.

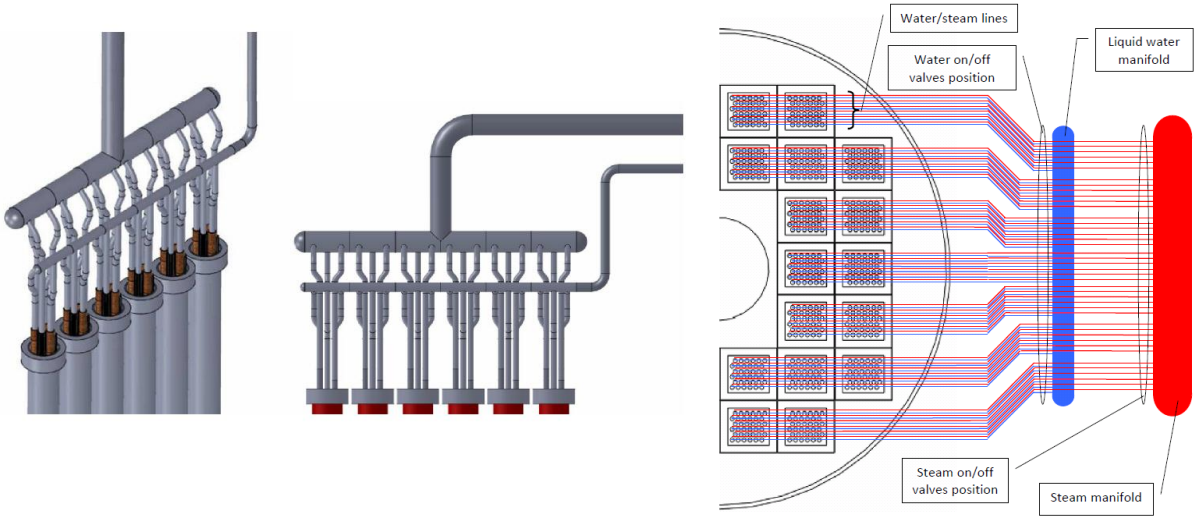

Figure 20. Schemes of a sub-system made up of 6 candles within a module of 36 candles and the schematic representation of piping connections to the main manifolds.

7. COST CONSIDERATIONS

7.1 Rough evaluation, based on weights of machined steel in SPX2 and on the Candle-based-SFR weights

The investment cost, duet the realization of the proposed Candle SG, is an essential parameter for its feasibility evaluation. At the present phase, detailed characteristics are not yet available, and no provision has been made yet on the realization phases of all the components necessary for a full integration in a nuclear power plant (i.e. concrete vault, instrumentation, safety cooling systems, dedicated radiological shielding for devices operating in radioactive environment, etc.). Therefore, at present only a very rough evaluation is possible for cost assessment, taking into account only the material cost. A preliminary whole evaluation of the steam generator system cost has been performed. As result of this evaluation, the comprehensive cost of a single tank including its internal components (candles, “U” tubes, piping, manifolds, valves, etc.), in a solution made up of three heat exchanger tanks, should be

in a range between 40 and 50 M€. Concerning the manufacturing costs, a percentage close to 50% of the whole cost could be assumed.

8. CONCLUSIONS

Studies carried out during the last years showed some very attractive features concerning the concept of the "Candle"-type steam generator for application in SFRs, especially in view at the elimination of the intermediate sodium circuit, through the "fusion" of the traditional IHX with the SG. The elimination of the intermediate sodium circuit, together with its components, results in a great saving in capital cost as well as in a reduction of component number and in ISI&R strategies simplification.
In spite of the great simplification due to the introduction of this system, the safety performance of the NPP are not compromised, but even improved.
In case of a possible double wall failure, of "U" tubes and of the candle vessel, since the SWR occurs outside the primary tank, only the reaction products can affect the operation of the reactor rather than the pressure transient too. Isolation valves on the sodium piping could, in any case, avoid also this remote problem.
Concerning the development of the innovative system to a more advanced stage, further studies should be performed in order to:

- Optimize the candle geometry according to results obtained in the safety analyses (possibility to increase the candle diameter to reduce the required draining time, evaluation of exact volume and other dimensions of the tank dome, etc.);
- Carefully evaluate the costs of the whole system manufacturing, in order to compare this solution with the alternative ones within the scope of GEN IV economics requirements.

9. NOMENCLATURE

GIF	Generation IV International Forum	NPP	Nuclear Power Plant
IHX	Intermediate Heat eXchanger	SFR	Sodium Fast Reactor
ISI&R	In Service Inspection and Repair	SWR	Sodium Water Reaction

REFERENCES

[1] *Generation IV Roadmap*, Generation IV International Forum.
[2] *SNE TP - Strategic Research Agenda* (http://www.snetp.eu/www/snetp/images/stories/Docs-AboutSNETP/sra2009.pdf).
[3] B. Farrar, J.C. Lefevre, S. Kubo, C.H. Mitchell, Y. Yoshinari, S. Itooka, *Fast reactor decay heat removal; approach to the safety system design in Japan and Europe*, Nuclear Engineering and design 193 (1999).
[4] A. Vasile & al., *The Collaborative Project for a European Sodium Fast Reactor CP ESFR*, ICAPP 2011.
[5] G.L.Fiorini, A.Vasile, *European Commission-7th Framework Programme: The Collaborative Project on European Sodium Fast Reactor (CP ESFR)*, Nuclear Engineering and Design, Volume 241, Issue 9, September 2011, Pages 3461-3469.
[6] L. Satish Kumar, K. Natesan, A. John Arul, V. Balasubramaniyan, S.C. Chetal, *Design and evaluation of Operation Grade Decay Heat Removal System of PFBR*, Nuclear Engineering and Design, Volume 241, Issue 12, December 2011, Pages 4953-4959.

PROBABILISTIC SAFETY ASSESSMENT FOR SPENT FUEL POOLS UNDER BLAST LOADING – PART ONE

Ennio Cortellini*

*Center of training and analysis in risk's engineering, "Al. I. Cuza" University, Iasi

ABSTRACT

Nuclear power plants are originally equipped with storage facilities for the wet storage of spent fuel assemblies. The nuclear fuel continues to produce heat from radioactive decay also after reactor's shut down. The superstructures and pools were not, however, specifically designed to resist terrorist attacks. Because this type of storage is located outside the reactor containment structure, particular concern has been raised about the vulnerability of spent fuel. If terrorists could breach a spent fuel pool's concrete walls and drain the cooling water, the spent fuel's zirconium cladding could overheat and ignite. In this paper we will discuss a methodology for PSA including the uncertainties associated with blast modeling and structural response. This approach can provide a rational and objective mean to assess risk and decide a protection from blast damage.

KEYWORDS

Probabilistic Safety Assessment, Spent Fuel pools, blast loading, risk, nuclear fuel, bulk modulus, damping, buried structure.

1. INTRODUCTION

After the Japan's nuclear crisis at Fukushima reactors it is obvious that, losing water, the spent fuel pools release highly radioactive material into the air, becoming an important hazard to people and the environment.

Nuclear power plants are originally equipped with storage facilities for the wet storage of spent fuel assemblies .The nuclear fuel continues to produce heat from radioactive decay also after reactor is shut down. During each refueling cycle, only one-third of the fuel in the reactor core is replaced. However, to facilitate the loading of fresh fuel or during the inspection and the repair of the reactor vessel and internals, the operators off-load the entire core into the pool during refueling. The spent fuel pools have a variety of designs. Almost all spent fuel pools are located outside the containment structure, but in some reactor designs, the spent fuel pools are contained inside the reactor building (see Figure 1).

In other designs, however, the spent fuel pool may be located into an auxiliary building that is located adjacent to the containment. Some pools are built underground, whereas others are located at the top of the reactor building. The structures enclosing the pool are typically made of steel. These buildings are designed to house cranes that are used to move reactor components and spent fuel. These superstructures are designed for seismic loads but not to resist tornados and missiles. In contrast, the typical spent fuel pool is robust and they are designed for seismic stability and to resist horizontal strikes of tornado missiles. The superstructures and pools were not, however, specifically designed to resist terrorist attacks.

The pool walls are constructed of reinforced concrete and the pools contain stainless steel liner attached to the walls and embedded in the concrete. Their dimensions are typically about :

- Deep = 12 ÷15 meters)
- Horizontal dimension = 12 ÷15x12 ÷15 meters.
- Walls thickness = 1.2 ÷2.4 meters
- Thick stainless steel liner = 6÷13 millimeters

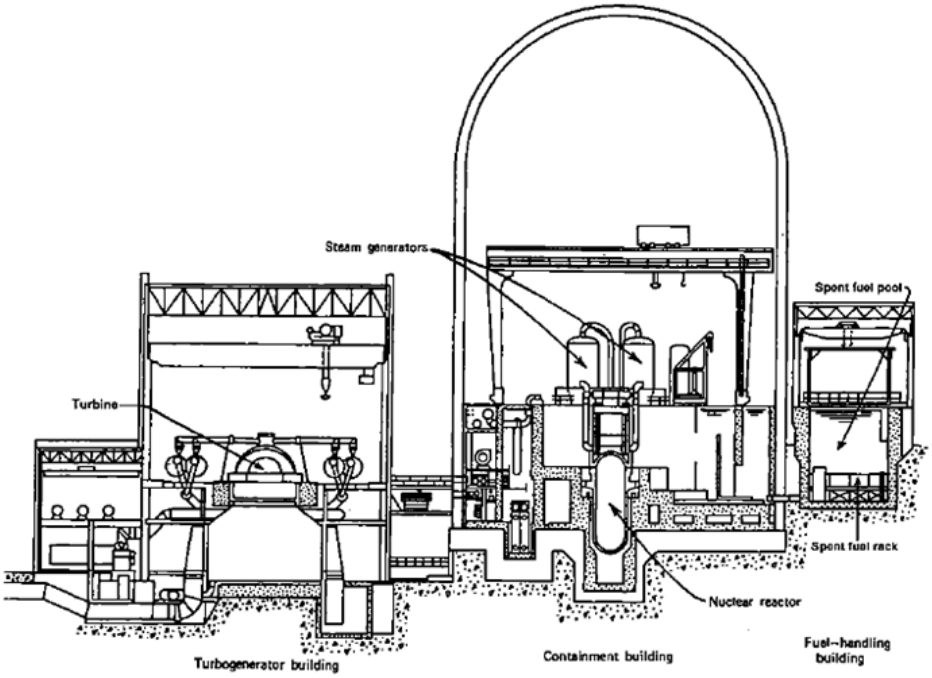

Figure 1 - Source [12]

There is another pool-type storage facility of a Soviet design (Figure 2). The facility consists of four storage pools interconnected by one transport corridor One storage pool is kept empty for emergency cases. Spent fuel is stored under water in open cylindrical baskets placed in steel lined concrete pools.

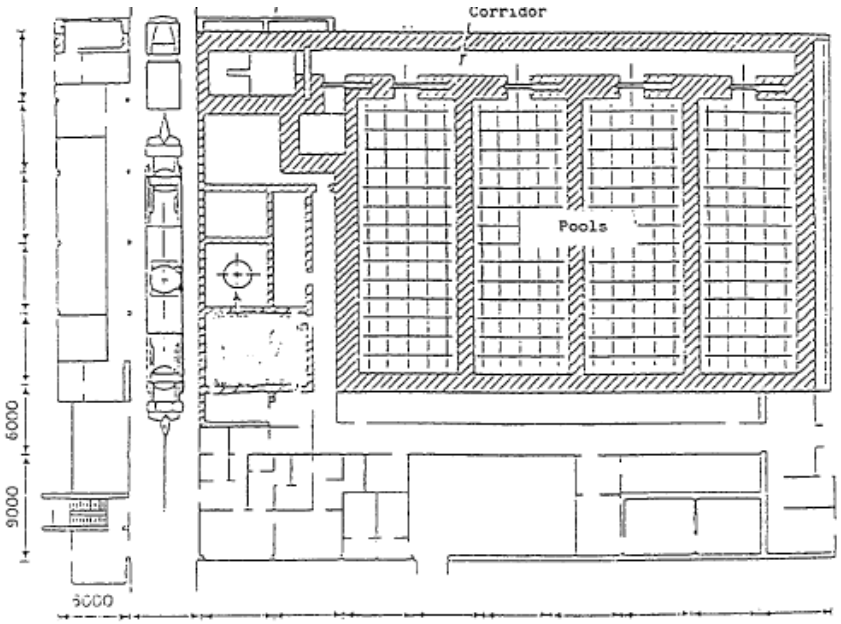

Figure 2 – Source: IAEA-TECDOC-1089

The pools also contain vertical storage racks for holding spent and fresh fuel assemblies and are installed near the bottom of the spent fuel pool. The storage racks have a height of about 4 meters and they have feet separators to provide space between their bottoms and the pool floor. There is also provided a space between the sides of the rack and the steel pool liners for circulation of water as in Figure 3. The spent fuel racks are covered by 8 meters of water to provide substantial radiation shielding even when an assembly is being moved above the rack.

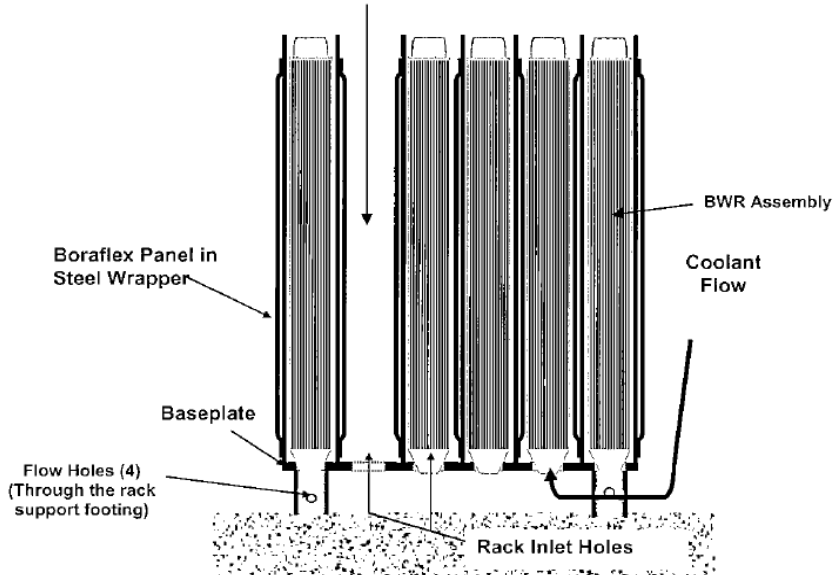

Figure 3 - Source [12]

The safety function of the spent fuel pool and storage racks is to cool the spent fuel assemblies and maintain them in a subcritical array during all credible storage conditions. Sub criticality is maintained using high density boron substituted storage racks. Borated water is used as an extra insurance against criticality. Sub criticality can be influenced by internal and external hazards which have the potential to reconfigure the pre-existing spent fuel assembly array in a manner to increase the potential for criticality.

Nearly all pools contain high-density spent fuel racks, which allow the storage of almost five times more quantities.

Equipment installed to make high-density pools safe actually exacerbates the danger of ignition, particularly with aged spent fuel. To compensate for the increased risks of a large-scale accident, pools have been retrofitted with enhanced water chemistry controls and neutron-absorbing panels between assemblies.

The new rack designs rely heavily on permanently installed neutron absorbers to maintain criticality requirements. Unfortunately, permanently installed neutron absorber has exhibited some degradation, namely, they have lost a significant portion of their neutron absorbing capability. Degradation is so extensive that these neutron absorbers can no longer be credited in the criticality analysis.

Also, the extra equipment restricts water and air circulation, making the pools more vulnerable to systemic failures. If the equipment collapses or fails, as might occur during a terrorist attack,

for example, air and water flow to exposed fuel assemblies would be obstructed to exposed fuel assemblies, causing a fire, according to the NRC's report.

The heat would turn the remaining water into steam, which would interact with the zirconium, making the problem even worse by yielding inflammable and explosive hydrogen. The NRC concluded that *"it is not feasible, without numerous constraints, to define a generic decay heat level (and therefore decay time) beyond which a zirconium fire is not physically possible."*

Typical design of the fuel pool arrangement for PWRs whit one reactor is shown in Figure 3. In Nuclear power plant sites that contain two reactors, they are usually arranged with two spent fuel pools or a shared pool located in a common area adjoining both reactor buildings.

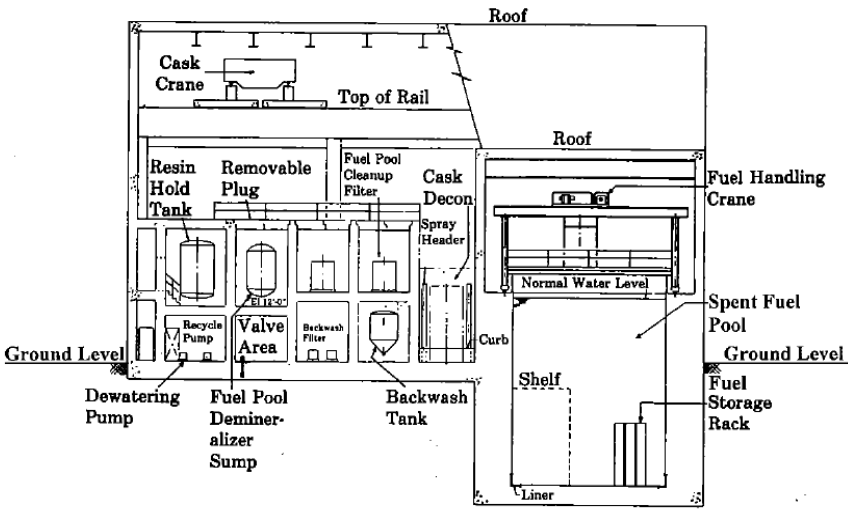

Figure 4- Source [12]

The BWR vessels, to accommodate control mechanisms that sit under the reactor and steam separation and drying equipment, are somewhat taller than PWR vessels. Consequently, BWRs have more elevated spent fuel pools, generally well above ground level. N.R.C – US Commission staff conducted a survey of the plants but, generally, a complete plant survey would be needed to establish the extent of pool exposure to attacks, because their vulnerability to terrorist attack depends in part on its location with respect to ground level as well as its construction .

2. RISKS OF TERRORIST ATTACKS ON SPENT FUEL STORAGE FACILITIES

The National Academy of Sciences (NAS) released a report in April 2005 that found that *"successful terrorist attacks on spent fuel pools, though difficult, are possible*," and that "*if an attack leads to a propagating zirconium cladding fire, it could result in the release of large amounts of radioactive material"*.

Indeed, if the fuel were exposed to air and steam, the zirconium cladding would react exothermically igniting at about 8000°C. In spent fuel pools there is the large amount of cesium-137 which contain from 20 to 50 million curies with half-life of 30 years. Cesium-137 gives off highly penetrating radiation and is absorbed in the food chain as if it were potassium

The nuclear industry and the Nuclear Regulatory Commission have also asserted that the robust construction and stringent security requirements at nuclear power plants make them less vulnerable to terrorist attack than softer targets such as chemical plants and refineries. Nuclear power plants (and their spent fuel facilities) are less desirable as terrorist targets because they are robust and well protected.

However, the committee commission judges that the plausibility of an attack on a spent fuel storage facility, coupled with the public fear associated with radioactivity, indicates that the possibility of attacks cannot be dismissed.

3. PROBABILISTIC SAFETY ANALYSIS

In safety analysis it's important that the spent fuel storage pool structures, systems, and components should be designed to accomplish the following:

- prevent loss of water from the fuel pool that would lead to water levels that are inadequate
  for cooling or shielding
- protect the fuel from mechanical damage
- provide the capability to limit potential offsite exposures in the event of a significant release
  of radioactivity from the fuel or significant leakage of pool coolant
- provide adequate cooling to the spent fuel to remove residual heat

The safety level cannot be determined from such a deterministic analysis. The reliability-based design and assessment techniques recognize that loads and capacities are variable in time and space and that these uncertainties need to be incorporated into any measure of safety.

In performing a safety analysis, a number of steps are basic to the analysis of the system being considered, but the PSA propagates these uncertainties through the computations to reveal an estimate of risk. A general description of probabilistic safety analysis and assessments for engineering systems is provided by (IAEA)

In blast loading and system response there is considerable uncertainty even if the explosive weight and stand-off distance are known precisely. Loading and system response models are subject to three sources of uncertainty may also be categorized as:

- stochastic (inherent variability)
- epistemic (parameter uncertainty and model error)

In first group of uncertainties, there is the irreducible variability of the phenomenon itself (weather, individual exposure to hazard, time of blast, etc) while in second group there is uncertainty of input parameters used in predictive models and uncertainty in the accuracy of predictive (computer models, threat scenarios, consequence models, etc. models).

These sources of uncertainty can be represented by probabilistic models. The variability and uncertainty of many system response parameters such as material properties and dimensions have been the subject of many studies.

Modeling the likelihood of explosive weight and stand-off distance is much more inexact, as this will be influenced by threat assessment. Nonetheless, scenarios can be hypothesized.

In these cases, the PSA is a reliabilities analysis that is summarized as:

- PSA step 1: Blast loading model
- PSA step 2: Probability of conditional failure on occurrence of a specific threat scenario.
- PSA step 3: Probability of failure obtained from aggregation of conditional risks.

In these circumstances, reliabilities need to be calculated from predictive models and probabilistic methods. The probability of failure can be generalized as

$$p_f = Pr[G(X) \leq 0] \qquad (1)$$

Where

- $G(\boldsymbol{X}) = R\text{-}S =$ limit state function;
- $\boldsymbol{X}$=vector of all relevant variables.

Note that $G(\boldsymbol{X}) = 0$ defines the boundary between the "*unsafe*" and "*safe*" domains.
Usually, predictive models of system loading and response are incorporated into the limit state function.

In the present case, the probability of failure conditional on the occurrence of a specific threat scenario is thus

$$p_f/\alpha_{ij} = \sum P_r[G(X) < 0 : S = s] Pr[S = s] \qquad (2)$$

Where

- α_{ij}=threat scenario for a specific explosive weight *I* and stand-off distance *j*
- $Pr[S = s]$ represents the probability distribution of blast loading for a specific threat scenario considering inherent model error and parameter uncertainties
- $\sum Pr[G(X) < 0 : S = s]$ represents the cumulative distribution function of resistance and is termed a *fragility curve.*

To assess the total value of safety, the threat probabilities are needed.
If the anticipated threat probability $Pr[\alpha_{ij}]$ is known for each threat scenario, then the probability of failure is an aggregate of conditional safety and we have

$$p_f = \sum_{i=1}^{N} \sum_{j=1}^{M} [p_f/\alpha_{ij} \times Pr(\alpha_{ij})] \qquad (3)$$

where

$$\sum_{i=1}^{N} \sum_{j=1}^{M} Pr(\alpha_{ij}) = 1 \qquad (4)$$

where

- N=number of possible explosive weights;
- M=number of stand-off distances;
- $Pr(\alpha_{attack}) = \sum_{i=1}^{N} \sum_{j=1}^{M} Pr(\alpha_{ij})$ is the probability of an attack occurring.

Clearly, the threat probability is very difficult to predict given the ever changing threat scenarios. However, for most infrastructures it should be possible to elicit expert judgments in order to obtain subjective appraisals of threat scenarios.

4. STRUCTURAL RESPONSE TO EXPLOSIVE BLAST LOADING

4.1 BLAST LOADING MODEL

This part briefly discusses the nature of explosions and the effects of explosions on structures. It will focus on the techniques for predicting the design blast loads that can be used to evaluate the structural of a building.

The following methods are available for prediction of blast effects on building structures:

- Empirical (or analytical) methods
- Semi-empirical methods
- Numerical (or first-principle) methods.

Empirical methods are essentially correlations with experimental data. Over the years a number of analytical methods for predicting blast loading were developed. These analytical procedures are presented in the following several technical design manuals and reports:

- TM 5-1300 (US Department of the Army, 1990)
- TM5-855-1 (US Department of the Army, 1986)

TM 5-1300 is one of the most widely used publications available to both military and civilian sectors for designing structures to provide protection against the blast effects of an explosion. It contains step-by-step analysis and design procedures, including information on

(i) blast loading;
(ii) principles of non-linear dynamic analysis;
(iii) reinforced concrete and structural steel design.

The blast wave parameters are a function of scaled distance for three burst environments:

(i) free air burst;
(ii) air burst;
(iii) surface burst.

When an explosion occurs adjacent to and above a building without the amplification of the initial shock wave between the explosive charge and the structure, then the blast loads are free-air blast pressures.

The air burst environment is produced by explosions that occur above the ground surface and away from the building structure so that the initial shock wave, propagating away from the explosion, impinges on the ground surface prior to arrival at the structure. The shock wave continues to propagate outward along the ground surface and a front (Mach front) is formed by the interaction of the incident wave and the reflected wave. The reflected wave is the incident wave that has been reinforced by the ground surface.

The blast environment is considered to be a *surface burst* when a charge is located on or very near the ground surface. The reflected wave merges with the initial wave at the point of detonation to form a single wave with a hemispherical ~~in~~ shape, similar to the Mach of the air burst.

The angle of incidence of a point on a surface is another important blast parameter. It is the angle between the outward normal and the direct vector from the explosive charge to the point. The impulse is generally increased from its free-field value if the angle of incidence is less than 90 degrees.

Impulse on the area of interest of the building surface with angles of incidence between zero and 45 degrees are well predicted with this simplified procedure (within 20% on the conservative side). For angles of incidence greater than 45 degrees, impulse on components can be underestimated by factors from 2.5 to 1.5 for angles of incidence between 45 and 70 degrees.

The step-by-step procedure for determining blast wave parameters for a surface blast:

- Step 1. Determine the explosive charge weight, *W*. Assume a hemispherical surface burst model. Select point of interest (centre of area) on the exterior vertical wall of a building at height *h* above ground.
- Step 2. For the point of interest, calculate standoff distance at height *h*, R_h, scaled standoff distance, Z_h, and angle of incidence :

$$\begin{aligned} \mathrm{R_h} &= (R_G^2 + h^2)^{1/2} \\ \mathrm{Z_h} &= \frac{\mathrm{R_h}}{W^{1/3}} \\ \alpha &= \mathrm{TAN}^{-1}\left(\frac{\mathrm{h}}{\mathrm{R_G}}\right) \end{aligned} \qquad (5)$$

- Step 3. Read peak reflected pressure *P*t and scaled positive reflected impulse $I_t/W1/3$.
- Step 4. To obtain the absolute values of the blast wave parameters, multiply the scaled values by a factor $W^{1/3}$

The manual TM5-855-1 provides procedures for the design and analysis of protective structures subjected to the effects of conventional weapons.

The manual also provides:

- Air blast effects,
- blast loads on structures, and auxiliary systems
- closed-form equations to generate the predicted air blast pressure – time histories

The basic steps are below:

- Divide a surface into sub-sections and evaluate a pressure – time history and impulse for each small zone.
- The total impulse applied to the surface is then obtained by summing up the impulses for each sub-section.
- The total load – time history is then defined to have an exponential form with a peak calculated assuming an average peak pressure applied over all the surfaces.

This simplified method has one limitation because it assumes the load – time history applied to all parts of the surface at the same time neglecting the true physics of the blast wave and of the interaction phenomena

Numerical methods are based on mathematical equations that describe the basic laws of physics governing a problem: conservation of mass, momentum, and energy and constitutive relationships. For the physical behavior of materials, these models are commonly termed computational fluid dynamics models.

The numerical methods used to simulate the blast effects problem typically are based upon a finite volume, finite difference, or finite element method with explicit time integration scheme.

.*Semi-empirical methods* are based on simplified models of physical phenomena. They attempt to model the underlying important physical processes in a simplified way.

The Air blast Loading Model, is been developed by [2], to provide equations to predict air blast parameters from spherical air bursts and from hemispherical surface bursts.

In TM5-855-1 it is proposed an approximate equivalent triangular pulse to represent the decay of the incident and reflected pressure, instead in Air blast Loading Model takes a more realistic approach and the decay of the pressure with time has exponential form (Figure 5).

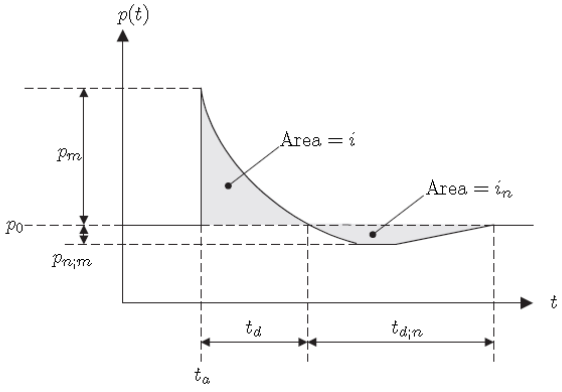

Figure 5

Form equation for Air blast Loading is:

$$P(t) = P_{so}\left[1 - \frac{t - t_a}{t_d}\right] exp\left[\frac{-A \times (t - t_a)}{t_d}\right] \qquad (6)$$

where

- $P(t)$ is the pressure at time t (kPa);
- t_a is the arrival time of the blast(msec);
- t_d is the positive (overpressure) phase duration of the blast(msec);

$$\frac{T_d}{W^{1/3}} = \frac{980\left[1+\left(\frac{Z}{0.54}\right)^{10}\right]}{\left[1+\left(\frac{Z}{0.02}\right)^{3}\right]\left[1+\left(\frac{Z}{0.74}\right)^{6}\right]\sqrt{1+\left(\frac{Z}{6.9}\right)^{2}}} \quad (7)$$

- $t_{d,n}$ is the negative (under-pressure i.e. negative overpressure) phase duration of the blast(msec);

$$t_{d,n} = 0.0104 \cdot W^{\frac{1}{3}}\ [s] \quad for\ Z < 0.3 \quad (8)$$

$$t_{d,n} = (0.003125 \cdot \log(Z) + 0.01201) \cdot W^{\frac{1}{3}}\ [s] \quad (9)$$
$$for\ Z \geq 0.3\ \wedge Z \leq 1.9$$

$$t_{d,n} = 0.0139 \cdot W^{\frac{1}{3}}\ [s] \quad for\ Z > 1.9 \quad (10)$$

- b is the parameter for decay of the curve:

$$ln\left(b\left|\frac{P_m}{P_{n,m}}\right|\right) + b + 1 = 0 \quad (11)$$

- p_0 is the ambient pressure (kPa);
- p_m is the peak static overpressure. First correlation between p_m and Z is developed by Brode, bat this correlation was subsequently reviewed by Smith. The model is considered valid within the range of z=0.2–2. For Kinney and Graham the peak static overpressure is

$$p_m = \frac{808P_0\left[1+\left(\frac{Z}{4.5}\right)^{2}\right]}{\sqrt{\left[1+\left(\frac{Z}{0.048}\right)^{2}\right]\left[1+\left(\frac{Z}{0.32}\right)^{2}\right]\left[1+\left(\frac{Z}{1.35}\right)^{2}\right]}} \quad (12)$$

- $p_{n,m}$ is the maximum value of under-pressure;
  - $p_{n,m} = \frac{0.35}{Z}10^5 P_a \quad for\ Z > 3.5 \quad (13)$
  - $p_{n,m} = 10^4 P_a \quad for\ Z < 3.5 \quad (14)$
- i is the impulse of the positive phase of the pressure-time curve;

$$i = \frac{0.067\sqrt{1+\left(\frac{Z}{0.23}\right)^{4}}}{Z^2\sqrt[3]{1+\left(\frac{Z}{1.55}\right)^{3}}} \cdot 100 \cdot \sqrt[3]{W} \quad (15)$$

with $I[P_a \cdot s]$, $Z\left[m/Kg^{1/3}\right]$, $W[Kg]$.

- i_n is the impulse of the negative phase of the pressure-time curve.

The reflected over-pressure Pr_{max} arising from the interaction of the blast waves with a flat-surface has been definite by Smith:

$$Pr_{max} = Cr \cdot Ps_{max} \quad (16)$$

where $Cr = 3\left(\sqrt[4]{Ps_{max}}\right)$ is the coefficient for the reflected over-pressure.

An amplification factor of 1.8 has been applied to account for the effects of waves reflecting from the ground surface in the common hemispherical blast scenarios.

An important parameter in the reflected over-pressure is the "clearing time", T', which defines the time taken for the reflected over-pressure to decay completely, and can be estimated by

$$T' = \frac{3S}{U} \qquad (17)$$

Where *S* is the minimum dimension on the frontal surface of the blast, and *U* is the blast front velocity which is given by

$$U = a_0 \sqrt{\frac{6P_m + 7P_0}{7P_0}}$$

with $a_0 = 335 \frac{m}{s}$ (speed of sound).

In this study, the tank walls were subject to linear elastic dynamic analyses based on the parameters blast pressure function defined in table 1 and table 2. The combined effect of both parameters is represented by scaled distance. We consider scaled distances ranging from 0,1- 3 m/kg$^{1/3}$ and W= 10 and 1000 kg TNT, which are equivalent to two realistic attack at Nuclear Power Plant, inside and outside the plant, respectively.

W [Kg]	**Z**	**Pm** [Pa]	**Pr,max** [Pa]	**T_d** [s]	**T_c** (ms)
10	0,20	2,89E+07	3,56E+08	2,09	0,81
10	0,30	1,67E+07	1,79E+08	0,62	0,93
10	0,40	1,06E+07	1,02E+08	0,27	1,04
10	0,50	7,21E+06	6,28E+07	0,18	1,15
10	0,60	5,14E+06	4,12E+07	0,23	1,25
10	0,70	3,81E+06	2,83E+07	0,41	1,35
10	0,80	2,91E+06	2,02E+07	0,65	1,44
	0,90	2,28E+06	1,49E+07	0,90	1,53
10	1,00	1,01E+06	5,38E+06	1,11	1,88
	1,50	7,31E+05	3,59E+06	1,89	2,03
10	2,00	3,74E+05	1,56E+06	2,50	2,40

Table 1

W [Kg]	**Z**	**Pm** [Pa]	**Pr,max** [Pa]	**T_d** [s]	**T_c** **(ms)**
1000	0,20	2,89E+07	3,56E+08	9,56	4,00
1000	0,30	1,67E+07	1,79E+08	2,83	5,26
1000	0,40	1,06E+07	1,02E+08	1,22	6,58
1000	0,50	7,21E+06	6,28E+07	0,82	7,96
1000	0,60	5,14E+06	4,12E+07	1,06	9,40
1000	0,70	3,81E+06	2,83E+07	1,86	10,87
1000	0,80	2,91E+06	2,02E+07	2,97	12,39
1000	0,90	2,28E+06	1,49E+07	4,09	13,93
1000	1,00	1,82E+06	1,12E+07	5,08	15,50
1000	1,50	7,31E+05	3,59E+06	8,62	23,39
1000	2,00	3,74E+05	1,56E+06	11,43	30,71

Table 2

Additional blast loading condition is stress soil induced by detonation. In fact, detonation of an explosive charge produces a radial expanding compressive wave which propagates through the soil medium. When the compressive wave comes in contact with a buried structure, a change in pressure occurs. On the basis of the TM 5-855-1 the following empirical formula is used to describe the decay of the free-field pressure with distance and time [10]

$$P(R,t) = p_a\left[e^{\frac{-t}{t_0}}\right] \quad (18) \quad \text{and} \quad p_a = f\beta\rho_C\left[\frac{R}{W^{\frac{1}{3}}}\right]^{-n} \quad (19)$$

where

- β =0.47 and f is the coupling factor of the explosive energy;
- ρ_C is the acoustic impedance of the soil;
- n is the attenuation coefficient usually taken to be 2.75;
- R and W are defined earlier.

4.2 THERMAL LOADING MODEL

Generally, the pools are designed for two working water levels, which must provide for radiation shielding in any operational mode as well as for sufficient spent fuel cooling. In this case we consider the operational level at 8 m in depth and the refueling level at 12 m in depth. Borated water is used as an extra protection against criticality. Fuel storage racks are located on the floor of the pool. Generally, the maximum operational pool temperature shall not exceed 45°C for normal operation and 58°C for fuel reloading and Regulatory Guide 1.13, specifies that pool water should be maintained below 60 °C for all heat load conditions, including full-core offloads during refueling. The temperature measurement in each section is provided by one thermocouple placed near the pool wall.

More sophisticated models, which involve clad ballooning and detailed thermal hydraulics, including radioactive heat transfer, have been developed for the analysis of severe in-core accidents. These models can be evaluated using more powerful computers. This paper considers a water thermal load T= 60°C.

4.3 POOL RESPONSE MODEL

In this case the Pool is a rectangular tank, whose geometry is given by the width a = 12 m, the length b = 12 m, the height h = 12 m and thickness s= 1,4m, as illustrated in the Figure 6.

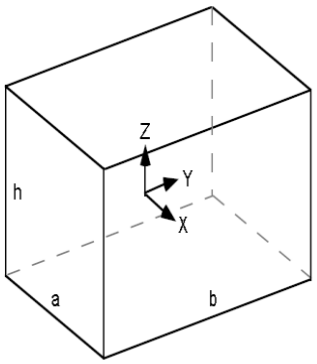

Figure 6

The tank is filled with water to a height of 11 m. The walls of the tank are modeled using a plate elements with 8 nodes and the water is modeled using brick elements whit 20 nodes. Figure 3 shows the analytical geometries and boundary conditions for pool explosion simulation.

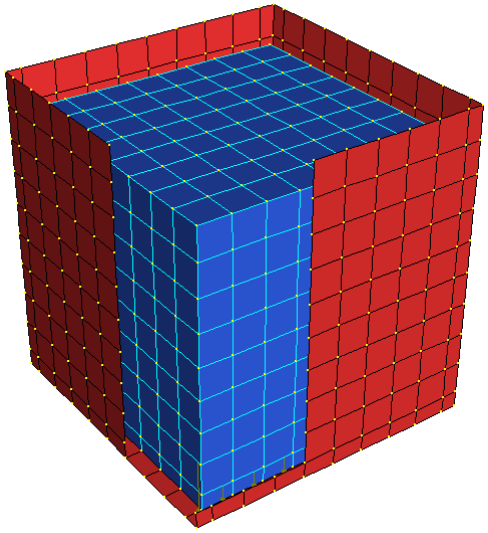

Figure 7

In the case of the liquid storage structure, it is very important to consider the fluid structure interaction. In the present study, for the fluid and its structure we have used the classical Lagrangian formulation, considering the liquid to be incompressible without any net in/out flow.

Small liquid displacement has been considered, i.e., there is no separation of liquid from structure at the interface. Displacement constraints between liquid and container have been imposed in the direction normal to interface. This model captures the sloshing modes of the liquid and effects of the liquid on the dynamics of the structure. However, energy dissipation in the viscous boundary layer at interface depends on racks number into the pool and boron concentration.

Let ϵ_V the volumetric component and the displacement vector. We have $\epsilon_V = div\,\mathrm{u}$ in V**.** Component of the associated stress with the condition of elasticity is $p = k\,\epsilon_V$ in V, where k is the volumetric modulus of elasticity. Assumption of linearity is true only for compressive strength for the well-known problems of cavitations. For a viscous fluid we have $\omega = \mathrm{rot\,u}$. For F.E.M. modeling this condition is not true in all points where spurious modes are. In a model of penalty the following are considered as micro-torques $\mathrm{m} = \beta\omega$, where β is the coefficient of penalty. If vectorial form of the kinematic and static components is as $\mathrm{s}^T = [p \quad m_x \quad m_y \quad m_z]$ and $\mathrm{e}^T = [\varepsilon_V \quad \omega_x \quad \omega_y \quad \omega_z]$ then equation of the elastic bond becomes $\mathrm{s} = \mathrm{C} \cdot e$, where $\mathrm{C} = \begin{bmatrix} k & & \\ & \beta & \\ & & \beta \end{bmatrix}$. If A is the free surface of the fluid, ρ density of the fluid u_z and vertical displacement of the fluid, then the deformation energy is $E_p = \int_A \rho g \mathrm{u}_z^2\, dA$, the strain energy is $E_D = (2\int_V e^T C\, dV)^{-1}$, and the kinetic energy is $E_C = (2\int_V \rho \dot{\mathrm{u}}^T \dot{\mathrm{u}}\ dV)^{-1}$.

For Hamilton's principle of and for a finite element discretization of the fluid, the discrete form equation of motion becomes:

$$\mathrm{M}\ddot{\mathrm{u}} + \mathrm{K}\mathrm{u} + \mathrm{K}_s\mathrm{u}_s = \mathrm{F} + \mathrm{M}\tau\ddot{\mathrm{u}}_g \qquad (20)$$

where

- u is the vector of displacements of the entire liquid system

- u_s and K_s are, respectively, the vector of vertical displacements and the stiffness matrix of the free surface

If $u_s \subseteq u$ then

$$M\ddot{u} + K_f u = F + M\tau\ddot{u}_g \qquad (21)$$

where K_f is the stiffness matrix containing the elastic component and the component surface.

Equation (21) is similar for the solid systems. The connection between the plates and bricks is captured using master-slave links, whith the active degrees of freedom set such that ~~the~~ they only act in the direction of plate normal. The proprieties of the brick elements are set to fluid material with a Bulk Modulus of 145 x 10^9 Pa and a estimated density of 480 kg/m^3. In addition, the fluid is analyzed for its sloshing modes separated from the rest of the model and the results are compared to those obtained from a theoretical approach. The analytical slosh frequencies f_{ij} for the rectangular tank are given by Equation (22).

$$f^2{}_{i,j} = \frac{g}{4\pi}\sqrt{\left(\frac{i}{a}\right)^2 + \left(\frac{j}{b}\right)^2}\ \tanh\left[h\pi\sqrt{\left(\frac{i}{a}\right)^2 + \left(\frac{j}{b}\right)^2}\right] \qquad (22)$$

where the gravity constant g = 10 m/sec^2 and i and j are the mode numbers in the X and Y directions, respectively Fig.2.

The foundation medium is considered to be uniform over a deep zone and the contact surface between the supported structure and the soil deposit is considered as a rigid plate and the soil is treated as elastic half space. The physical characteristics of soil adopted in the present analysis are given as per Table 3.

Dense sand	
modulus of subgrade reaction Ks, kN/m3	110000
Mass density, ρ (kg/m3)	1800
Seismic velocity, C (m/s)	600
Acoustic impedance, ρc (Pa/m/s)	8835
Attenuation coefficient, *n*	1.6
Poisson's ratio, υ	

Table 3

Tables 3 and 4 shows the Material properties for reinforced concrete and steel. Walls are supposed to resist at PGA=0,30g.

Property	**Concrete**	**Steel**
Modulus of elasticity (MPa)	30,000.0	200,000.0
Poisson's ratio	0.17	0.0
Ultimate compressive strain	0.0035	-
Compressive strength (MPa)	35.0	460.0
Area ratio of steel and concrete 0.026 (both directions)		

Table 4

Structural transient analysis determines the dynamic response of a structure corresponding to the action of any general time-dependent loads. This type of analysis can be used to obtain the

time-varying displacements, strains, stresses, and reaction forces in a structure as it responds to any combination of static, transient, and harmonic loads.
The time scale of the loading is such that the inertia or damping effects are considered to be essential in solving for the dynamic response. Initial conditions are assumed to be known:

$$[\mathrm{M}]\{\ddot{\mathrm{u}}\} + [\mathrm{C}]\{\dot{\mathrm{u}}\} + [\mathrm{K}]\{\mathrm{u}\} = \{\mathrm{F}_{ext}(t)\} \qquad (23)$$

where [M] is a mass matrix, [C] is a matrix, [K] is a stiffness matrix, {u} is a nodal displacement vector, and F_{ext} is an applied load vector.
Transient response of the linear problem requires the direct integration of the governing equations of motion (Equation (21)). In this study, the numerical integration is conducted using α-method or Hilbert-Hughes-Taylor method (7). This method has superior numerical characteristics over the widely used Newmark method. The type of damping used in these paper for incremental analysis is Rayleigh damping: damping matrix is proportional to the mass and stiffness matrices C = ηM+ δK, where the coefficients are determined to provide for two selected damping ratio of or two specific modes of vibration. In these case damping depends on the racks number into the pool, the boron concentration, the vertical speed flow of water cooling and the interaction soil-structure. The Analysis on a reactor tank with internal components has determined that the presence of internals (e.g. pumps) can significantly alter the dynamic characteristics of the sloshing motion. Notably, the fundamental frequency is considerably increased with the sloshing wave height reduced. The damping associated with the sloshing modes is usually quite low (approximately 0.5%). However, it should be noted that for higher viscosity fluids and tanks/vessels with internal baffles, the damping value is higher. For the impulsive components, the damping ratio is generally assumed to be approximately 2%. For this reason we consider two values of ζ (4% and 8%).

The dynamic linear analysis has been carried out to find the maximum bending moment *Ms*. Non linear analysis is not possible because the pool walls require a safe biological shield from the servicing staff: plastic deformation is not compatible whith radioprotection requirements. The structure has been subjected to surface blast of varying standoff distance and explosive magnitude. The finite element analysis is carried out using dedicated software. The principal measure of response performance obtained from the FEM model is the maximum dynamic bending moment of the plate following the impulsive blast load.

The total number of 24 blast load conditions were used to perform dynamic analyses. For W =10 [Kg] whit Z = 0,50 (see Figs. 8 and 9) and for W =1000 [Kg] whit Z = 2,5 (see Figs. 10 and 11) we have critical performance of the failure criteria, e.g. maximum stress, strain, displacement.

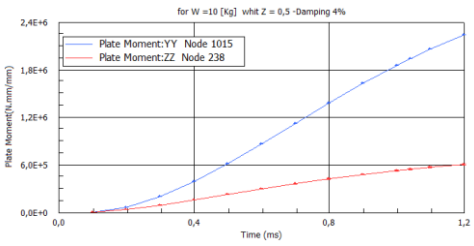

Fig.8

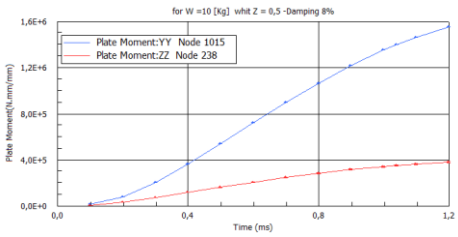

Fig.9

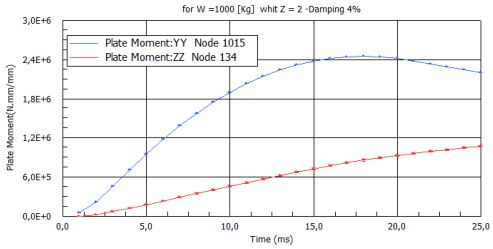

Fig.10

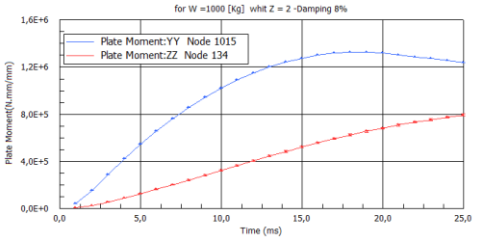

Fig.11

We substitute these values of maximum flexural moments into the following failure limit state function:

$$G(x) = h \cdot f_y \cdot A_S - \frac{\alpha \cdot f_y \cdot A_S}{b \cdot f_c} - M_S \qquad (22)$$

with the limitation $\varepsilon_{max} \leq \varepsilon_{elastic}$, and where $\alpha, M_S h, f_y, A_S, b$ and f_c are random variables.

5. PROBABILISTIC MODELS AND UNCERTAINTY MEASURES

The estimation of uncertainty measure is one of the most important tasks in reliability analysis. For a basic random variable, its uncertainty is generally represented by a probability distribution function determined by its statistical parameters, e.g., mean value and coefficient of variation (CoV). In general terms, the uncertainty measure of Y is conveniently expressed in a normalized form, Statistical properties of concrete are well documented and have been recently updated in the effort to calibrate the ACI design code for RC buildings. Table 5 summarizes the statistical properties of these random variables used in this study. The impulsive load is subject to inherent, parameter and model error uncertainties. An historical analysis of data suggests that the coefficient of variation (CoV) of measured impulses is approximately 0.12. For more complex blast environments the CoV is expected to increase. Max CoV of peak reflected pressure at various scaled distances is 0.31. This is an area for further research.

VARIABLE	DISTRIB.	bias	CoV
M_S	Normal	1	0.12 and 0,31
h	Normal	1	0.05
f_y	logNormal	1.105	0.10
A_S	Normal	1	0.05
α	Normal	1	0.1
b	Normal	1	0.05
f_c	logNormal	1.105	0.15

Table 5

In general terms, the uncertainty measure of Z is conveniently expressed in a normalized form. The stochastic variables are assumed to be independent. A transformation to normalized stochastic variables (with expected value 0 and standard deviation 1) is established by $X_z = U_z\sigma_z + \mu_z$ and $X_z = F_{Z_n}^{-1}[\Phi(u_z)]$. Define normalized random variables as:

$$M_S = u_{M_S}\sigma_{M_S} + \mu_{M_S}\ ; \quad f_y = e^{\left[\sqrt{\ln\left(\frac{\sigma_{f_y}^2}{\mu_{f_y}^2}+1\right)}\cdot \mu_{f_y} + \ln\mu_{f_y} - 0.5\ln\left(\frac{\sigma_{f_y}^2}{\mu_{f_y}^2}+1\right)\right]}\ ; \qquad h = \mu_h\sigma_h + \mu_h\ ;$$

$$A_S = \mu_{A_S}\sigma_{A_S} + \mu_{A_S}\ ;$$

$$\alpha = \mu_\alpha\sigma_\alpha + \mu_\alpha\ ; \qquad b = \mu_b\sigma_b + \mu_b\ ; \qquad f_c = e^{\left[\sqrt{\ln\left(\frac{\sigma_{f_c}^2}{\mu_{f_c}^2}+1\right)}\cdot \mu_{f_c} + \ln\mu_{f_c} - 0.5\ln\left(\frac{\sigma_{f_c}^2}{\mu_{f_c}^2}+1\right)\right]}\ ;$$

The limit state function is then written as:

$$G(x) = (\mu_h\sigma_h + \mu_h)\cdot e^{\left[\sqrt{\ln\left(\frac{\sigma_{f_y}^2}{\mu_{f_y}^2}+1\right)}\cdot \mu_{f_y} + \ln\mu_{f_y} - 0.5\ln\left(\frac{\sigma_{f_y}^2}{\mu_{f_y}^2}+1\right)\right]}\cdot(\mu_{A_S}\sigma_{A_S} + \mu_{A_S}) - \frac{(\mu_\alpha\sigma_\alpha + \mu_\alpha)\cdot e^{\left[\sqrt{\ln\left(\frac{\sigma_{f_y}^2}{\mu_{f_y}^2}+1\right)}\cdot \mu_{f_y} + \ln\mu_{f_y} - 0.5\ln\left(\frac{\sigma_{f_y}^2}{\mu_{f_y}^2}+1\right)\right]}\cdot(\mu_{A_S}\sigma_{A_S} + \mu_{A_S})}{(\mu_b\sigma_b + \mu_b)\cdot e^{\left[\sqrt{\ln\left(\frac{\sigma_{f_c}^2}{\mu_{f_c}^2}+1\right)}\cdot \mu_{f_c} + \ln\mu_{f_c} - 0.5\ln\left(\frac{\sigma_{f_c}^2}{\mu_{f_c}^2}+1\right)\right]}} - (u_{M_S}\sigma_{M_S} + \mu_{M_S}) \tag{23}$$

The conditional probabilities of failure are calculated from Equation (23), for scaled distances ranging from 0,1- 3 m/kg$^{1/3}$ and W= 10 and 1000 kg TNT, which are equivalent to two realistic attack at Nuclear Power Plant, inside and outside the plant, respectively. After this analysis, we have obtained the results given in the tables below:

W =10 [Kg] - **Z = 0,50**				
case	**ζ**	**Cov of Ms**	**Ms**	p_f/α_{ij}
1	4%	0,12	2,15e9 Nmm	3.977e-07
2	4%	0,35	2,19e9 Nmm	2.838 e-04
3	8%	0,12	1,32e9 Nmm	1.824e-14
4	8%	0,35	1,55e9 Nmm	1.874e-09

Table 6

W =1000 [Kg] - **Z = 2,5**				
case	**ζ**	**Cov of Ms**	**Ms**	p_f/α_{ij}
5	4%	0,12	2,47e9 Nmm	2.972e-05
6	4%	0,35	2,47e9 Nmm	1.507 e-02
7	8%	0,12	2,15e9 Nmm	3.977e-07
8	8%	0,35	2,15e9 Nmm	2.807 e-03

Table 7

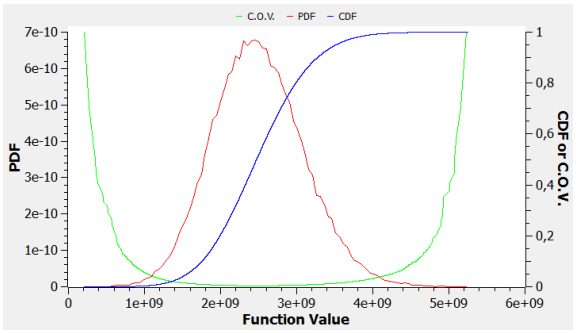

Figure 12. Case 2

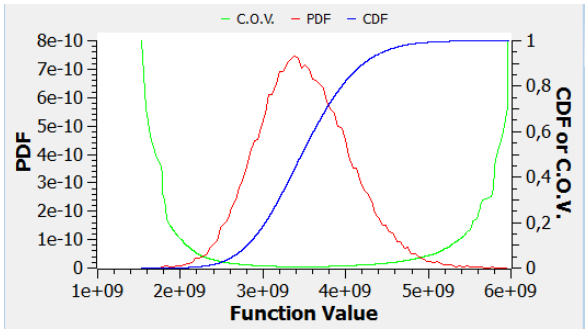

Figure 13. Case 1

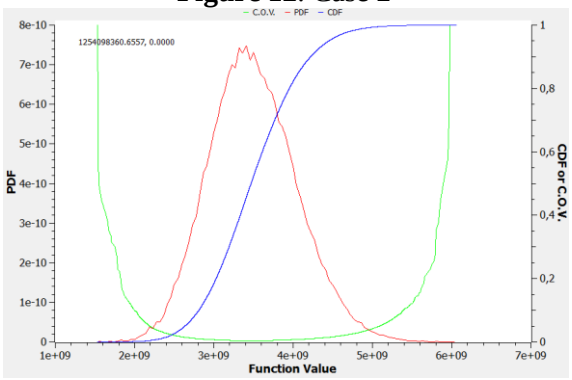

Figure 14. Case 3

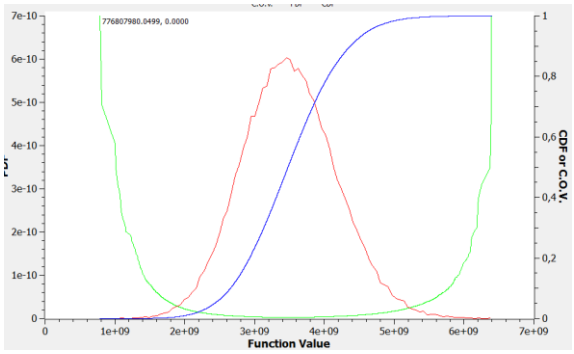

Figure 15. Case 4

Fragility curves

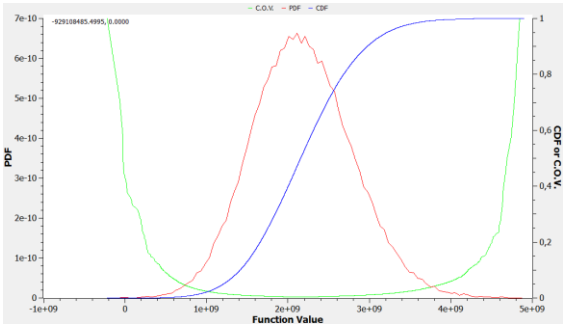

Figure 16. Case 5

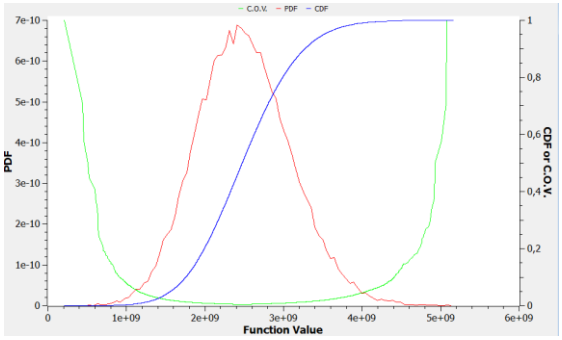

Figure 17. Case 6

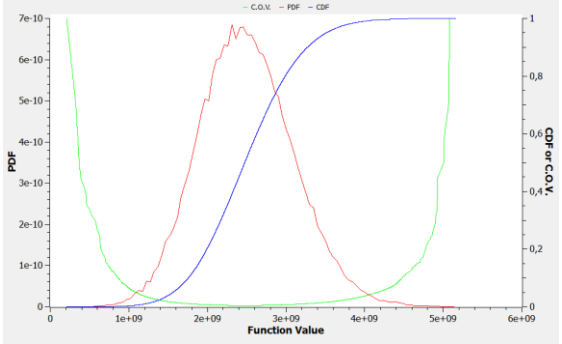

Figure 18. Case 7

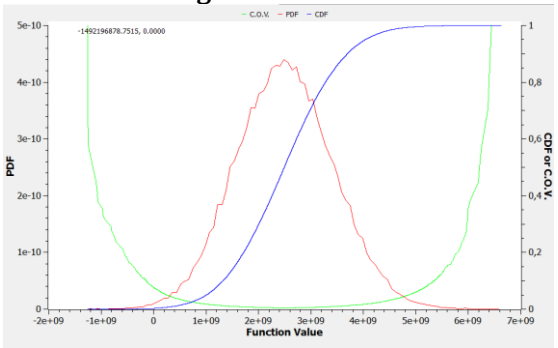

Figure 19. Case 8

Fragility curves

Since there is not generally 100% certainty about a potential threat, it is necessary to include uncertainty of various threat scenarios. The probability of Failure is calculated from the aggregation of conditional probability from various threat scenarios weighted by their relative

threat probabilities. It is assumed that the likelihood of attack by 10 kg TNT is as likely as by 1000 kg TNT is 50%. For each previous case the results are:

Threat Scenario	Explosive Weight (kg TNT)	Z	Relative Threat Probability $p_f(\alpha_{ij})$	Conditional Probability of Failure p_f/α_{ij}
α_1	10	0,5	0,5	3,977e-07
α_2	1000	2,5	0,5	2,972e-05
	Probability of Failure		$p_f(\alpha_{ij})$**=1,50589E-05**	

Table 7: Damping 4% and Cov $_{Ms}$ =0.12

Threat Scenario	Explosive Weight (kg TNT)	Z	Relative Threat Probability $p_f(\alpha_{ij})$	Conditional Probability of Failure p_f/α_{ij}
α_1	10	0,5	0,5	2,838 e-04
α_2	1000	2,5	0,5	1,507 e-02
	Probability of Failure		$p_f(\alpha_{ij})$ = **0,0076769**	

Table 8: Damping 4% and Cov $_{Ms}$ =0.35

Threat Scenario	Explosive Weight (kg TNT)	Z	Relative Threat Probability $p_f(\alpha_{ij})$	Conditional Probability of Failure p_f/α_{ij}
α_1	10	0,5	0,5	1,824e-14
α_2	1000	2,5	0,5	3,977e-07
	Probability of Failure		$p_f(\alpha_{ij})$ =**1,9885E-07**	

Table 9: Damping 8% and Cov $_{Ms}$ =0.12

Threat Scenario	Explosive Weight (kg TNT)	Z	Relative Threat Probability $p_f(\alpha_{ij})$	Conditional Probability of Failure p_f/α_{ij}
α_1	**10**	**0,5**	**0,5**	**1,874e-09**
α_2	**1000**	**2,5**	**0,5**	**2,807 e-03**
	Probability of Failure		$p_f(\alpha_{ij})$**=0,001403501**	

Table 10: Damping 8% and Cov $_{Ms}$ =0.35

6. CONCLUSIONS

The present paper has described how a probabilistic safety analysis can be used to assess and mitigate the risk of blast damage to Spent Fuel pools under blast loading. Tank walls were

subject to linear elastic dynamic analyses based on two attacks at Nuclear Power Plant, i.e. inside and outside the plant. Influence of damping on conditional probability of failure is investigated to value the probability of failure and exact measure of damping is essential for PSA. Numerical results showed the importance of assignment of property COV to blast loading. In this work we have an high variation of probability. These results are preliminary only and subject to further refinement. Further work will focus on other exact fuel configurations inside the pool, as well as refining inherent, parameter and model error uncertainties for response and blast loading uncertainty and other threat scenarios. It is necessary to investigate probabilistic response of fuel cladding under blast loading and to define a equivalent single degree of freedom system modeling of tank wall which is not defined in [19].

REFERENCES

[1] *Structures to Resist the Effects of Accidental Explosions*, U.S. Department of the Army, Technical Manual 5-1300, Nov. 1990.
[2] *Report ARBL-TR-02555*, U.S. Army BRL, Aberdeen Proving Ground, MD, 1984.
[3] *Fundamentals of Protective Design for Conventional Weapons*, U.S. Department of the Army, Technical Manual 5-855-1, 1986.
[4] H.L. Brode, *Numerical solution of spherical blast waves*, Journal of Applied Physics, June 1955, No.6.
[5] G.F. Kinney, K.J. Graham, *Explosive Shocks*, Air. Springer-Verlag, New York, NY, second edition, 1985.
[6] C.N. Kingery, G. Bulmash, *Air blast parameters from TNT Spherical Air Blast and Hemispherical Surface Blast*, Technical Report ARBRL-TR-02555. US Armament Research and Development Centre, Ballistic Research Laboratory, Aberdeen Proving Ground, MD, April 1984.
[7] P.D. Smith. J.G. Hetherington, *Blast and Ballistic Loading of Structures*, Butterowrth-Heinemann, Oxford 1994.
[8] *Spent fuel storage facility design basis U.S. Nuclear*, Regulatory Guide 1.13.
[9] D.C. Lamb, *Hydrodynamics*, Regulatory Commission, Washington, Dover Publication, Sixth Edition, 1932.
[10] Z. Yang, *Finite element simulation of response of buried shelters to blast loadings*, International Journal of Finite Element in Analysis and Design, Vol. 24, pp 113-132, 1997.
[11] R.W. Clough, J. Penzien, *Dynamics of structures*, McGraw-Hill, New York, U.S.A., 1975.
[12] *Safety and security of commercial spent nuclear fuel storage*, Public Report, National Academy of Sciences, 2005.
[13] A.S. Benjamin et al., *Spent Fuel Heat up Following Loss of Water During Storage*, Sandia National Laboratory, NUREG/CR-0649.
[14] *Nuclear Power Plant Security and Vulnerabilities*, US-CRS Report for Congress, Congressional Research Service 7-5700, 2010, www.crs.gov.
[15] *Design of Spent Fuel Storage Facilities*, International Atomic Energy Agency, SAFETY SERIES No 116, VIENNA, 1994.
[16] *Technical Study of Spent Fuel Pool Accident Risk at Decommissioning Nuclear Power Plants*, Nuclear Regulatory Commission, Draft Final, 2000.
[17] NUREG/CR-6683 ORNL/TM-2000/230.
[18] *Standard Review Plan for Spent Fuel Dry Storage Systems at a General License Facility*, Draft Report.

[19] *STRUCTURES TO RESIST THE EFFECTS OF ACCIDENTALEXPLOSIONS*, UFC 3-340-02, Departments of the Defense USA.
[20] *Storage of spent fuel from power reactors*, IAEA-TECDOC-1089, Vienna, 1998.
[21] *Design of Spent Fuel Storage Facilities*, INTERNATIONAL ATOMIC ENERGY AGENCY, Safety Series No. 116, IAEA, Vienna (1994).
[22] *Implementation of Burnup Credit in Spent Fuel Management Systems*, INTERNATIONAL ATOMIC ENERGY AGENCY, IAEA-TECDOC-1013, Vienna (1998).
[23] E. Cortellini, *Nuclear decommissioning Course*, CEFAIR, Iasi, 2011.
[24] E. Cortellini, *About random and pseudo-random sequences*, FUZZY SYSTEMS & A.I. – Romanian Academy, vol. 11 n.3-4, 2005.
[25] E. Cortellini, *Some Epistemological Aspects of Mathematical Statistics*, in Current Topics in COMPUTER SCIENCE, Iasi 2004, and in FUZZY SYSTEMS & A.I. – Romanian Academy, vol. 11 n.3-4, 2004.
[26] E. Cortellini, *Una metodologia ed uno strumento operativo per di analisi di rischio*, Rivista ISPESL, n.3/97, Fogli di informazione, 1997.

RISK ASSESSMENT OF IN-VITRO CELL EXPOSURE TO LOW-LET RADIATIONS

C. Borcia[1,3], M. C. Teodor[2], L. Gorgan[2,3], Mihaela Dulcescu[4] and D. Mihailescu[1,3]

[1]*Faculty of Physics, "Al. I. Cuza" University, Iasi*
[2] *Faculty of Biology, "Al. I. Cuza" University, Iasi*
[3] *Center of training and analysis in risk's engineering, "Al. I. Cuza" University, Iasi*
[4]*Spitalul Universitar*

ABSTRACT

The biological effects induced by low level-dose irradiations are still a subject of debate. The last report "Biological Effects of Ionizing Radiation" (BEIR VII), focusing on low linear energy transfer radiations, suggests the use of linear approximation in assessing the risk of exposure at low-level doses. The present work presents a study of the effects on normal and modified cells of low-LET radiations (electrons) delivered at low-doses. The risk of radiation-induced effects is estimate using the COMET-assay, a tool to identify the DNA fragmentation. The results show a hormesis-like effect in the case of normal cells, while modified cells are more sensible to exposure and follow the linear-no-threshold model suggested by BEIR VII.

KEYWORDS

cell exposure, low-LET radiation, COMET assay, DNA fragmentation, radiation risk assessment

1. INTRODUCTION

Biological Effects of Ionizing Radiation (BEIR) VII Report [1] develops the most up-to-date and comprehensive risk estimates for cancer and other health effects from exposure to low-level ionizing radiation. This document supports previously reported risk estimates for cancer and leukemia and focuses on the health effects of low levels of low linear energy transfer (low-LET) ionizing radiation such as electrons (beta rays and accelerated beams), x-rays and gamma rays.

It is knows that ionizing radiations induce damages to living cells and, consequently, biological effects occurs following an exposure [2]. Injury to living cells results from the transfer of energy to atoms and molecules in the cellular structure. Ionizing radiation causes atoms and molecules to become ionized or excited, which can produce free radicals and break chemical bonds. New chemical bonds are created and cross-linkage develops between macromolecules. It is obvious that damages to molecules that regulate vital cell processes (e.g. DNA, RNA, proteins) are more important that damages to other molecules.

Linear energy transfer (LET) describes the rate at which a type of radiation deposits energy as it passes through tissue [3]. Higher levels of deposited energy on the path length cause more DNA breaks. Therefore, it is expected that more cells to be killed by a given dose of ionizing radiation. Low- LET radiation deposits less energy in the cell along the radiation path

and is considered less destructive per radiation track. For low-LET radiation, the number of ionizations per path length unit is low and DNA damages are mostly isolated, single break lesions. Different types of radiation have different levels of LET. For example, x-rays, gamma rays, and electrons are known as low-LET radiation. Neutrons, heavy ions, and pions are classified as high-LET radiation. Generally, radiation sources have a mixture of high- and low-LET radiation.

When damaged, the DNA molecule can repair itself, lead to the cell death or mutate [4,5]. The most likely outcome for low doses is repair, while the probably events as mutations can lead to cancer [6]. Cancer caused by radiation is no different than that caused by other carcinogens. Radiation is not the only agent that can cause mutations in DNA. Some other mutagens are chemicals, heat, and ultraviolet light.

The BEIR VII report concludes that the current scientific evidence is consistent with the hypothesis that, at the low doses of interest in this report, there is a linear dose-response relationship between exposure to ionizing radiation and the development of solid cancers in humans. It is unlikely that there is a threshold below which cancers are not induced, but at low doses the number of radiation induced cancers will be small [1].

An important task of the BEIR VII committee was to develop "risk models" for estimating the risk that an exposed individual will develop cancer. This task requires expressing the dependence of risk on radiation dose and also on sex and age at exposure. Data from epidemiologic studies were used to accomplish this task.

On average, the BEIR VII lifetime risk model predicts that approximately one individual in 100 persons would be expected to develop cancer (solid cancer or leukemia) from a dose of 100 mSv. Approximately 42 of the 100 individuals would be expected to develop solid cancer or leukemia from other causes. Lower doses would produce proportionally lower risks. For example, it is predicted that approximately one individual in 1000 would develop cancer from an exposure to 10 mSv [1].

At doses of 100 mSv or less, statistical limitations make it difficult to evaluate cancer risk in humans. A comprehensive review of available biological and biophysical data led the committee to conclude that the risk would continue in a linear fashion at lower doses without a threshold and that the smallest dose has the potential to cause a small increase in risk to humans. This assumption is termed the "linear-no-threshold" (LNT) model [6].

There are two competing hypotheses to the linear no-threshold model. One is that low doses of radiation are more harmful than a linear no-threshold model of effects would suggest. The other hypothesis suggests that risks are smaller than predicted by the linear no-threshold model. The BEIR VII report concludes that the preponderance of information indicates that there will be some risk, even at low doses, although the risk is small [1]

According to some epidemiological data, low exposures to radiation are beneficial to health, even if larger doses may be harmful [7,8]. Hormesis model is based on two arguments. Firstly come epidemiologic studies, where there is a lack of proof for the LNT model combined with a number of studies indicating beneficial effects of radiation [9]. Secondly, cells irradiated in vitro with low absorbed doses, a few tens of mGy, show less damage as a result of a subsequent exposure within hours than do unirradiated cells.

Under these circumstances, we propose to determine the level of various molecular markers of DNA damage as a function of low dose ionizing radiation. We are also interested in

assessing the DNA repair fidelity, especially double and multiple strand breaks at low doses, and whether repair capacity is independent of dose. Finally, we aim to evaluate of the relevance of adaptation, low-dose hypersensitivity, bystander effect, hormesis, and genomic instability for radiation carcinogenesis.

2. IN VITRO ESTIMATION OF THE RISK OF BIOLOGICAL EFFECTS

In order to fulfill our aims, we propose to identify the effects of low-level dose from low-LET radiations on normal and modified cells. In this respect, we intend to implement the COMET test in assessing the effects of ionizing radiations. The results will allow the study of the relationships between dose and cellular DNA damages.

A. Materials and methods

Cellular cultures of normal renal monkey (RM) cells were grown in a culture medium (Dulbecco's Modified Eagle Medium - DMEM), supplemented with 2% fetal bovine serum. Cellular cultures of neoplastic HeLa cells were also grown in a DMEM culture medium, supplemented with 10% fetal bovine serum.

Both culture cells were maintained on dedicated plates with a surface of 25 cm^2. The initial density of cells was of about $5x10^5$ cells/plate (25 cm^2). After 24 h from initiating the cultures, when the cells are in the log phase of their development, the plates were exposed to a flux of electrons. After the treatment, the exposed and unexposed (control) cells were kept in an incubator to grow for another 48 h, in order to complete several cellular cycles. At the end of this interval, the cellular film was detached using trypsin and the cellular suspension was subjected to the COMET test.

Cells exposure was done using an electron beam generated by a radiotherapy linear accelerator Varian. The maximum value of the beam energy was 8 MeV. The cells were exposed to single doses between 1 and 20 Gy, calculated by the accelerator treatment planning system.

B. DNA damage assessment

The COMET test is an uncomplicated and sensitive technique for the detection of DNA damage (single stranded breaks) at the level of the individual eukaryotic cell. The test can be applied to *in vitro*, *ex vivo* and *invivo* systems. The methodology was developed by Singh et. al. in the mid-1980s [10], and was modified later [11] it by including unwinding under alkaline conditions The COMET assay is a standard technique for evaluation of DNA damage/repair, biomonitoring and genotoxicity testing. As a working method, it consists in including the studied cells into a low gelling point agarose, followed by the lysis of cells with a specific buffer on neutral or alkaline medium, unwinding of DNA and the electrophoresis of the cell lysed suspension. Electrophoresis is followed by a visual analysis of the DNA after staining with a specific fluorochrome. The DNA damage assessment is done by fluorescence intensity measurements. A cell with migrating DNA resembles a comet with a concentration of DNA at the "head" and a diffused trailing migration of DNA referred to as the ""tail". Studies using this assay have largely included those involving radiation and radiomimetic chemicals [12,13].

In our experimental conditions, the COMET test was performed in alkaline condition.

Images for DNA breaks assessment were taken with a epifluorescence microscope and a digital camera. The analysis software was CometScore v1.5. To quantify the level of DNA damage, the extent of DNA migration was defined using the 'Olive Tail Moment' (OTM), which is the relative amount of DNA in the tail of the comet multiplied by the median migration distance [14]. The statistical analysis of data was done using the *Student's t* test [15]. The minimum signification threshold was $p<0,0$.

3. RESULTS AND DISCUSSIONS

The exposure of normal renal cells to different doses of low-LET radiations determined the variation of the number of registered comets. In the first case, when cells were exposed to 1Gy, the number of comets decreases by respect to the control (unexposed) cells. Greater doses (5, 10 and 20 Gy) lead to a gradual increase of the number of comets, as presented in Table 1.

The decrease of the number of comets, evidenced for low-dose exposures (1Gy), may be determined by minor modification at DNA macromolecule level, followed by the activation of DNA repair mechanism. These mechanisms ensure a more efficient monitoring and error repairing activities of DNA. This behavior is similar to hormesis phenomena described in the introductory part.

Higher doses determine an increase of DNA breaks in the macromolecule, as evidenced by the increase of the amount of DNA fragmented comet tails. We note a gradual increase in dose-proportional number of comets used. Even if the number of experimental data in small, the increase seems to follow a linear dependence, suggesting that the linear model is suitable to describe this behavior.

Another cell line used was the HeLa neoplastic (cancer) cells. Their main characteristic is a high rate of proliferation, favoring a certain fragility of the DNA macromolecule.

Compared with control cells (Table 2), cultures exposed to electron beam with different doses lead to a progressive increase in the frequency and quantity of DNA comets expelled from exposed cells.

Table 1 Values of "Olive tail moments" obtained after COMET assay of normal monkey renal cells, for control and low-LET radiation exposed cultures.

Exposure (Gy)	X±ES	p	variation (%)
Control (unexposed)	1.08±0.20	-	100
1 Gy (RM1)	0.45±0.09	<0.01	41.28
10 Gy (RM10)	3.12±0.63	<0.01	288.92
20 Gy (RM20)	6.96±1.52	<0.001	645.07

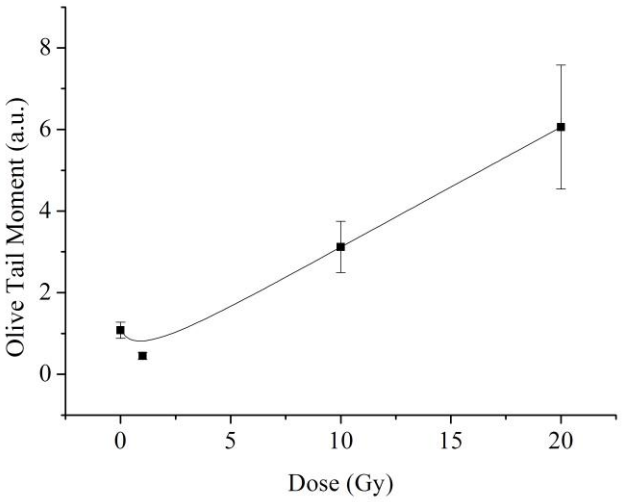

Figure 1 Variations of the OTM for RM normal cells for control and low-LET radiation exposed cultures.

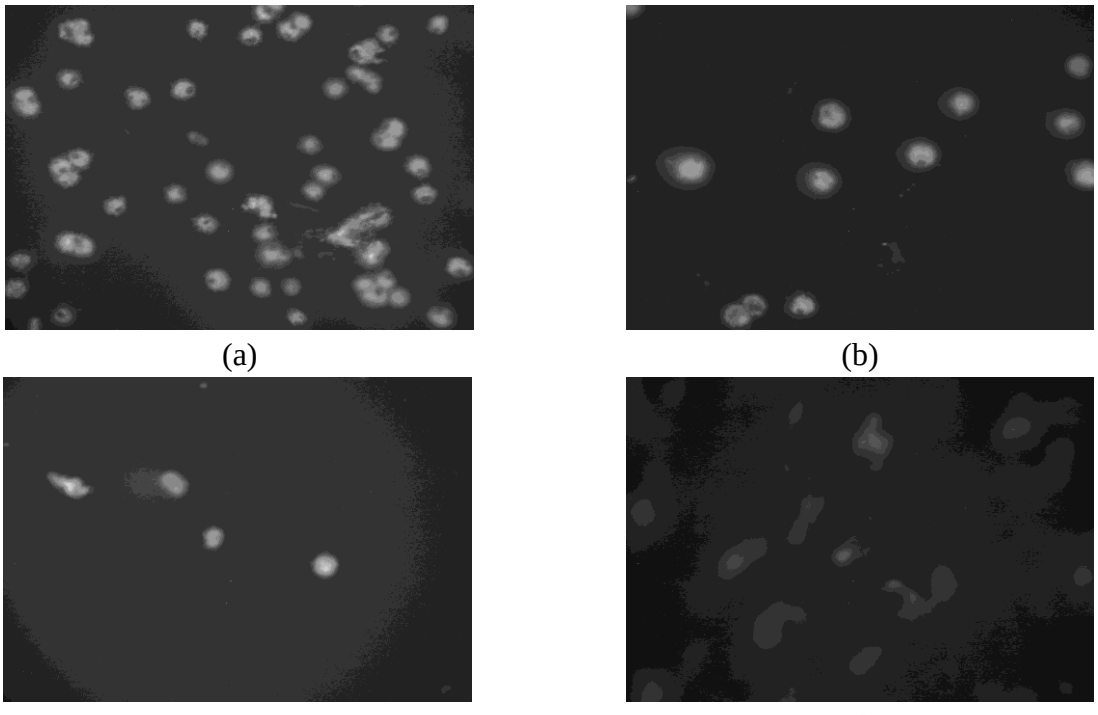

Figure 2 Aspect of comets corresponding to control (a) and exposed RM normal cell cultures to low-LET radiation doses: 1Gy (b), 10 Gy (c) and 20 Gy (d).

Table 2 Values of "Olive tail moments" obtained after COMET assay of HeLa neoplastic cells, for control and low-LET radiation exposed cultures.

Exposure (Gy)	OTM (a.u.)	p	variation (%)
Control (unexposed)	1.21±0.34	-	100
1 Gy (RM1)	2.03±0.35	NS	167.94
10 Gy (RM10)	31.19±2.40	<0.001	2,583.05
20 Gy (RM20)	51.87±4.54	<0.001	4,294.97

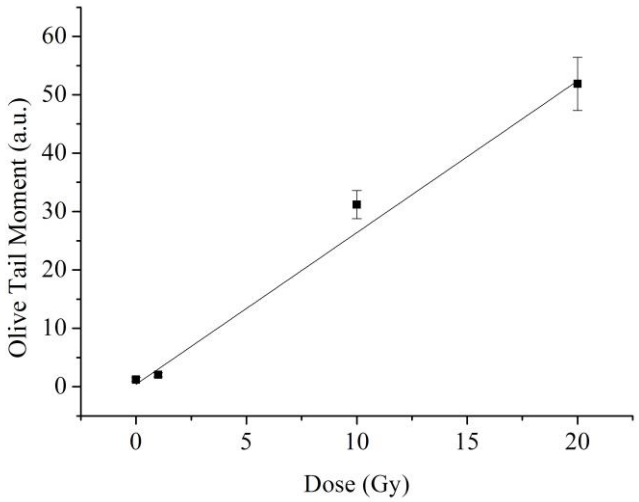

Figure 3 Variations of the OTM for neoplastic HeLa cells for control and low-LET radiation exposed cultures.

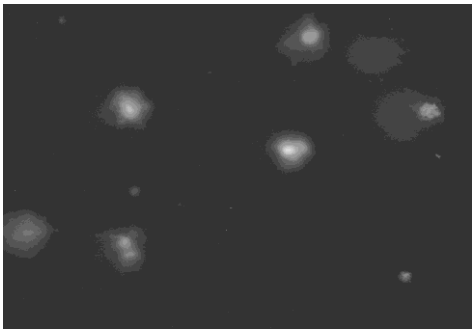

(a)

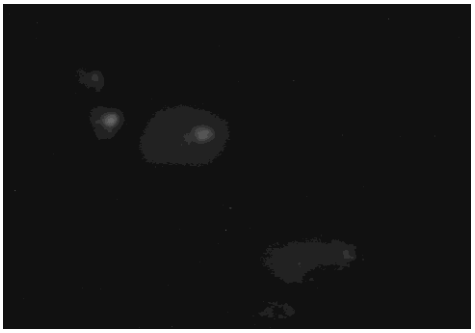

(b)

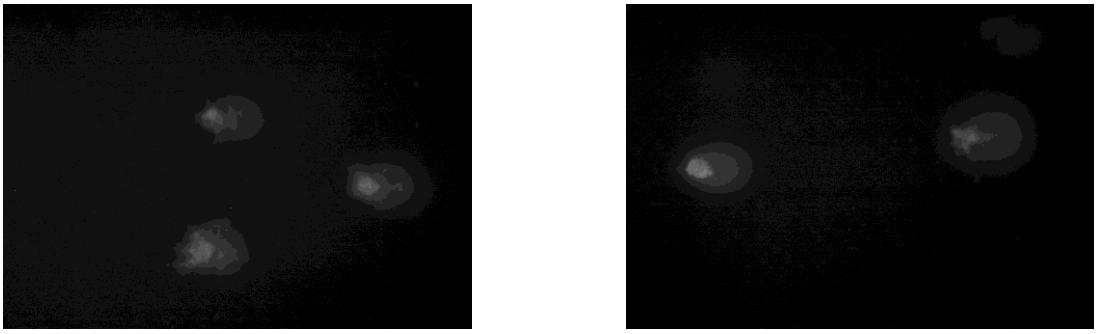

(c) (d)

Figure 4 Aspect of comets corresponding to control (a) and exposed neoplastic HeLa cell cultures to low-LET radiation doses: 1Gy (b), 10 Gy (c) and 20 Gy (d).

This increase in the number of comets for HeLa cells (Figure 3) can be attributed to a combination of three factors: the breaks generated by the electrons, the malfunction of DNA repair mechanisms in cancer cells and the high rate of proliferation. The result is a more pronounced response of these cells to the exposure.

The graphs presented in Figure 2 and Figure 4 support the statement that a dose-risk relationship could be determined. In the case of normal cells, a hormesis effect is evidenced, followed by a linear dependence of the dose-effect. Neoplastic cells show a linear-non-threshold like behavior.

4. CONCLUSIONS

Exposure to low-LET radiations of normal and neoplastic cells shows that DNA damages occur. The evaluation of DNA breaks was assessed using the COMET test and Olive Tail Momentum. For normal renal cells, a hormesis effect seems to be activated at low doses. For higher doses, the dose-effect relationship seems to be linear. In the case of neoplastic HeLa cells, a dose-effect relationship can also be established. The genetic material fragility of neoplastic cells is increased compared with normal cells.

At this stage of research, we conclude that the effect of electron beam is more pronounced on cancer cells compared with normal. The confirmation of dose-effect relationships allows more investigation in order to establish a dose-risk model.

ACKNOWLEDGEMENTS

This work was supported by IUCN grants 04-9-1077-2009/2011 and by the European Social Fund, Sectoral Operational Programme Human Resources Development 2007 - 2013, project "*Center of Training and Analysis in Risk's Engineering*", *POSDRU/18/1.2/G/34597* (sponsor and financial support acknowledgment goes here). One of the authors (M.C. Teodor) also acknowledges the financial support from the Sectorial Operational Programme for Human Resources Development, project "*Developing the innovation capacity and improving the impact*

of research through post-doctoral programmes", POSDRU/89/1.5/S/49944.

REFERENCES

[1] *Health risks from exposure to low levels of ionizing radiation*: BEIR VII phase 2, The National Academies Press, Washigton D.C.(2006).
[2] S. Loft, H.E. Poulsen, *Cancer risk and oxidative DNA damage in man*, Journal of Molecular Medicine 74(6) (1996) 297-312.
[3] J.P. Pouget, S.J. Mather, *General aspects of the cellular response to low- and high-LET radiation*, European Journal of Nuclear Medicine 28(4) (2001) 541-561.
[4] M. Christmann, M.T. Tomicic, W.P. Roos et al., *Mechanisms of human DNA repair: an update* , Toxicology 193(1-2) (2003) 3-34.
[5] P. Ross Wynand, Kaina Bernd, *DNA damage-induced cell death by apoptosis*, Trends in Molecular Medicine 12(9) (2006), 440-450.
[6] E. Ron, *Ionizing radiation and cancer risk: Evidence from epidemiology*, Radiation Research 150 (5): S (1998) S30-S41.
[7] R. Cook, J.E. Calabrese, *The importance of hormesis to public health*, Environmental Health Perspectives 114(11) (2006) 1631-1635.
[8] L.E. Feinendegen, *Evidence for beneficial low level radiation effects and radiation hormesis* , Conference: UK Radiological Congress Location: Manchester, ENGLAND (2004), British Journal of Radiology 78(925) (2005) Pages: 3-7.
[9] K.E. Vanwyngaarden, E.K.J. Pauwels, *Hormesis - are low-doses of ionizing-radiation harmful or beneficial*, European Journal of Nuclear Medicine 22(5) (1995) 481-486.
[10] O. Ostling, K.J.Johanson, *Microelectrophoretic study of radiation-induced DNA damages in individual mammalian cells*, Biochem. Biophys. Res. Commun. 123 (1984) 291–298.
[11] N.P. Singh, M.T. McCoy, R.R. Tice, E.L. Schneider, *A simple technique for quantitation of low levels of DNA damage in individual cells*, Exp. Cell Res. 175 (1988) 184–191.
[12] R.R. Tice, P.W. Andrews, O. Hirai, N.P. Singh, *The single cell gel (SCG) assay: an electrophoretic technique for the detection of DNA damage in individual cells*, C.R. Witner, R.R. Snyder, D.J. Jollow, J.F. Kalf, I.J. Kocsis, I.G. Sipes, Editors, *Biological Reactive Intermediates, Molecular and Cellular Effects and their impact on Human Health*, Plenum Press, New York (1991) 157–164.
[13] M. Klaude, S. Eriksson, J. Nygren, G. Ahnstrom, *The Comet assay: mechanisms and technical considerations*, Mutat. Res.363 (1996) 89–96.
[14] P.L. Oliv, J.P. Banath, *Multicell spheroid response to drugs predicted with the comet assay*, Cancer Research 57 (1997) 5528-5533.
[15] R.C. Blair, J.J. Higgins, *A comparison of the power of Wilcoxon's rank-sum statistic to that of Student's t statistic under various nonnormal distributions*, Journal of Educational Statistics 5(4) (1980) 309–334.

RANDOM PRICES AND RISK IN ELECTRICITY MARKETS

Carlo Mari[1], Lucianna Cananà[2]

[1]*Dipartimento di Metodi Quantitativi e Teoria Economica, Universita "G. d'Annunzio" di Chieti-Pescara, Viale Pindaro 42, 65127 Pescara, Italy.*
Tel. +39 085 4537530; Fax: +39 085 4537096; E-mail: c.mari@unich.it

[2]*Dipartimento di Scienze Economiche e Matematico-Statistiche, Universita del Salento, Via per Monteroni, 73010 Lecce, Italy.*
Tel. +39 0832 298774; E-mail: lucianna.canana@unisalento.it

ABSTRACT

Hedging power price risk is a crucial task in competitive electricity markets. The definition of risk management strategies as well as the pricing process of power derivatives require that the fine behavior of power prices is well understood. Suitable models must reproduce therefore the main features of market prices, such as the alternance of stable and turbulent periods in which jumps and spikes can be observed. From this point of view, regime-switching models seem to be good candidates.
In this paper we propose an equilibrium methodology to derive electricity prices dynamics from the interplay between supply and demand in a stochastic environment. Assuming that the supply function is described by an exponential function where the argument is a two-state Markov process, we derive a regime switching dynamics of power prices in which regime switches are induced by transitions between Markov states. The empirical analysis, performed on the Victoria power market and on the ERCOT market, confirms that the proposed approach seems quite flexible and capable of incorporating the main features of power prices time-series, thus reproducing the first four moments of log-returns empirical distributions in a satisfactory way.

KEYWORDS

electricity prices, stochastic processes, regime-switches, spikes

1. INTRODUCTION

At the beginning of the nineties several countries all around the world decided to undertake a liberalization process of the electricity sector in order to bring competition to the existing monopolistic market. In all those countries electricity is now a traded commodity and its price is determined according to the rule of supply and demand. In competitive markets power prices exhibit a very erratic dynamics: prices are variable and unpredictable with stochastic volatility, frequent jumps and short-lived spikes of very high magnitude. The interaction between demand and supply has dramatically increased the volatility of price returns, and this fact has introduced a new source of risk related to the randomness of observed market prices. Understanding the fine structure of power prices is therefore a crucial task in order to hedge the exposure to power price risk. Good models of electricity prices must reproduce the main features observed in real

markets, and this is a fundamental step to value power derivatives as well as to define risk management strategies.

Figure 1 shows the historical behavior of daily base-load power prices, calculated as arithmetic averages of the 24 hourly market prices, at the Victoria power market in Australia, and at the ERCOT market (the Electric Reliability Council of Texas).

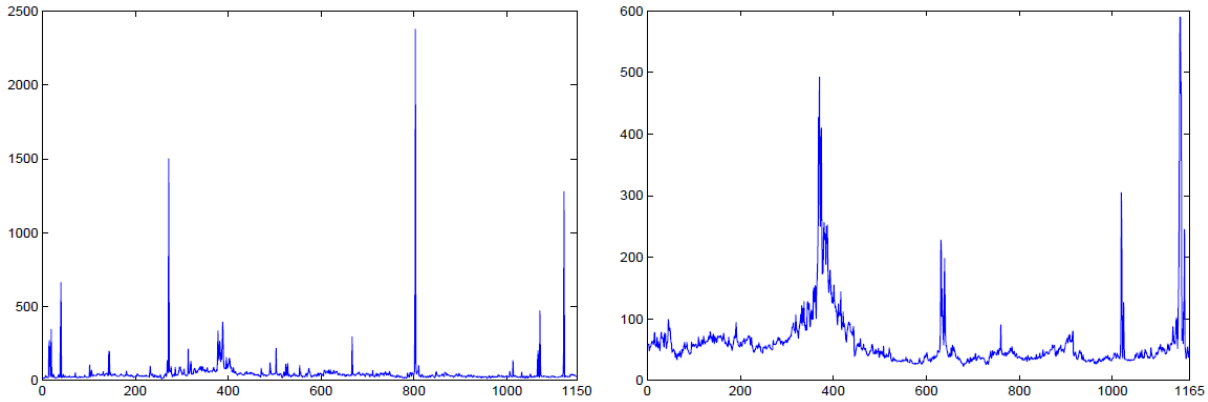

Figure 1: Historical behavior of power prices at the Victoria power market (left) since January 1,2006 until May 31, 2010, and at ERCOT (right) since January 4, 2006 until September 16, 2011. Prices are expressed in (Au/US) dollars per MWh

The resulting time series exhibit multi-regime dynamics where stable periods can be distinguished by turbulent periods in which unanticipated, short-lived extreme price changes may occur. After a jump, power prices are forced back to their normal level by some mean-reversion mechanism that induces them to fluctuate around the long-run average. Regime-switching models are widely used in literature to describe the random character of power prices. They offer the possibility to introduce various mean-reversion rates and volatilities in order to distinguish the dynamics in different regimes, and they seem good candidates to capture the most important observed features of historical data. From the pioneeristic work by Huisman and Mahieu [1], several studies have been proposed on the use of regime-switching models to describe the dynamics of power prices (see [2]-[5] and references therein for a comprehensive overview of the topics). In their seminal paper, Huisman and Mahieu presented a three-regime approach in which one regime is used to model the stable dynamics, the second regime is devoted to capture the spiking phenomenon, and the third one describes the return to the stable state. In this model multiple jumps are not allowed thus limiting the duration of the spikes to be of one day. To relax this assumption, two-regime switching models have been proposed in literature to distinguish the normal stable motion from the turbulent dynamics in which spikes of random duration may occur (see e.g., Weron et al. [6]; de Jong [7]; Mari [8]). In all the above quoted models the switching mechanism is driven by an unobservable Markov process.

In this paper we show that regime-switching dynamics arises in a quite natural way by modelling the stochastic movements of demand and supply. In an equilibrium context where the functional form of the supply curve is described by an exponential function in which the argument is a two-state Markov process, we propose a general methodology to model the spiking mechanism and the dynamics of power prices. In the hybrid approach we follow, the regime-switching dynamics can be obtained in a straightforward way as a consequence of transitions between Markov states in the supply curve. We also show that, in this context, the Markov

process governing the switching mechanism is observable and can be estimated from market data. To test the adaptability of the approach, an empirical analysis is performed on the Victoria power market and on the ERCOT market. In the period under investigation both markets are characterized by a very erratic behavior: prices exhibit evidence of stable periods and turbulent periods in which jumps and spikes of very high magnitude can be observed. The analysis reveals that the followed methodology is quite flexible and capable of incorporating the main features of observed prices time-series, thus reproducing the first four moments of empirical distributions of log-returns in a satisfactory way. Empirical distributions play a central role in defining risk management strategies as well as in the pricing process of power derivatives. In particular fitting the first moments of empirical distributions is very important for pricing purposes in which the calculus of expectations values is a crucial task [9].

This paper completes the work presented in [10], and it is organized as follows: Section 2 is devoted to a complete description of the methodology; Section 3 provides the empirical analysis; some comments conclude the paper.

2. THE MODEL

To introduce the methodology let us recall some basic facts. It is well known that electricity is a very special commodity: with the exception of hydroelectric power, it cannot be stored and must be generated at the instant it is consumed. In general the generation process is assured by generators with low marginal costs to cover the base load, as hydroelectric plants, nuclear power plants, and coal units. The demand is highly inelastic and very sensitive to the temperature and weather conditions. To meet peaks in the demand, emergency units (oil and gas fired plants) with high marginal costs are to be put on operation [11]. The supply curve (stack function) exhibits therefore, in the continuous approximation, a time variable kink after which offer prices start rising almost exponentially [12], as depicted in Figure 2 in which we approximated the demand curve by a vertical line.

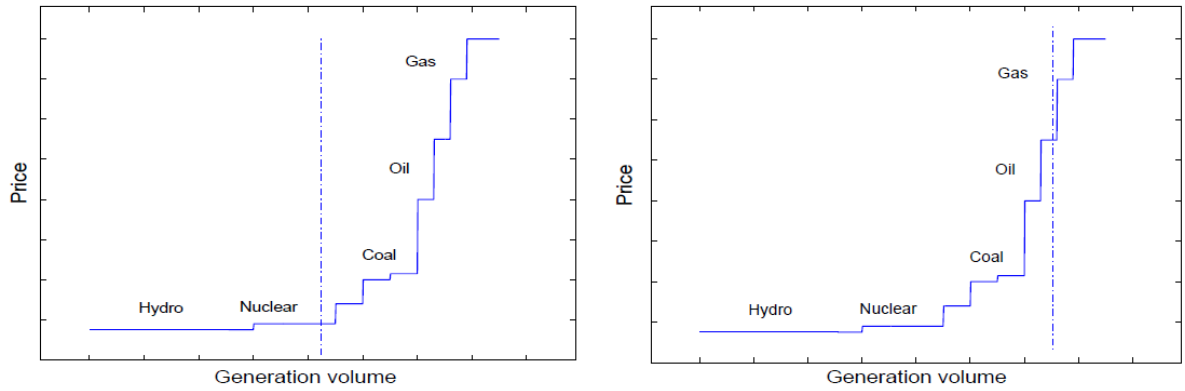

Figure 2: Understanding the spike phenomenon in electricity markets: a schematic supply stack with a hypothetical demand curve superimposed in the flat part of the supply (left) and in the almost vertical part of the supply (right)

The position of the kink in the supply curve is variable and unpredictable as a consequence, for example, of random outages of power plants, shortages in electricity generation due to

unpredictable fluctuations of fuel prices, or random fluctuations of renewable resources (mainly water and wind). Horizontal and vertical shifts of the supply curve, including unpredictable changes in the slope, may be very frequent. Whenever the load (demand) crosses the offer curve in the rapidly raising part of the curve, electricity prices may assume very high values: a spike occurs when the load intersects the offer curve in the almost vertical part. This may be due to unpredictable peaks in electricity demand, and/or random movements of the supply curve reducing the power offer in a significant way [13].

In order to incorporate all the above quoted features, we assume that the supply function can be cast in the following form:

$$P(t) = h_0(t)\exp\left[\beta(t)\left(\frac{q(t)-k(t)}{h_1}\right)\right], \quad (1)$$

where $q(t)$ represents the market volume at time *t*, $k(t)$ defines the kink position in the offer curve, $h_0(t)$ is a deterministic function of time and h_1 a normalization parameter. $\beta(t)$ is a discrete, strictly positive Markov process assuming two values, β_0 and β_1, with $\beta_0 < \beta_1$. In this approach, the process $k(t)$ is responsible for horizontal shifts of the supply curve, and $\beta(t)$ accounts for the varying slope of the curve. Since the demand is fairly inelastic, it can be represented by a quasi-vertical line. We assume that the following approximation of the load at time *t* holds:

$$q(t) = D(t), \quad (2)$$

for some stochastic process $D(t)$ which is independent of the power price [14]. The equilibrium between demand and supply is assured if

$$P(t) = h_0(t)\exp\left[\beta(t)\left(\frac{D(t)-k(t)}{h_1}\right)\right] \equiv h_0(t)\exp(\beta(t)z(t)), \quad (3)$$

where

$$z(t) = \frac{D(t)-k(t)}{h_1} \quad (4)$$

measures the (normalized) power margin level at time *t*, that is the (normalized) difference between the demand level and the kink position in the offer curve at time *t*. The above characterization can capture random movements of the offer curve due to unpredictable changes in the generation process as outages and grid congestions as well as random power generation from renewable sources. In the adopted parametrization, $z(t)$ is negative during normal periods: a spike occurs when $z(t)$ becomes positive and the demand intersects the supply function in the rapidly increasing part of the curve. Typical movements of the supply function and of the related load are shown in Figure 3, where we simulated a situation in which at the same level of the market volume the switching mechanism of the offer curve can produces very high prices. This may happen, for example, whenever unpredictable outages reduce the offer in a significant way thus determining price spikes also in the case of normal market volumes. In the following we will prove that transitions between Markov states in the offer curve induce regime-switching dynamics on power prices.

Without loss of generality, we assume that $h_0(t)$ describes the seasonality of power

prices. In such a case, $z(t)$ represents the deseasonalized power margin at time t. By posing $\log P(t) = \log h_0(t) + p(t)$, where $p(t)$ is the stochastic component of log-prices, we get:

$$p(t) = \beta(t) z(t). \quad (5)$$

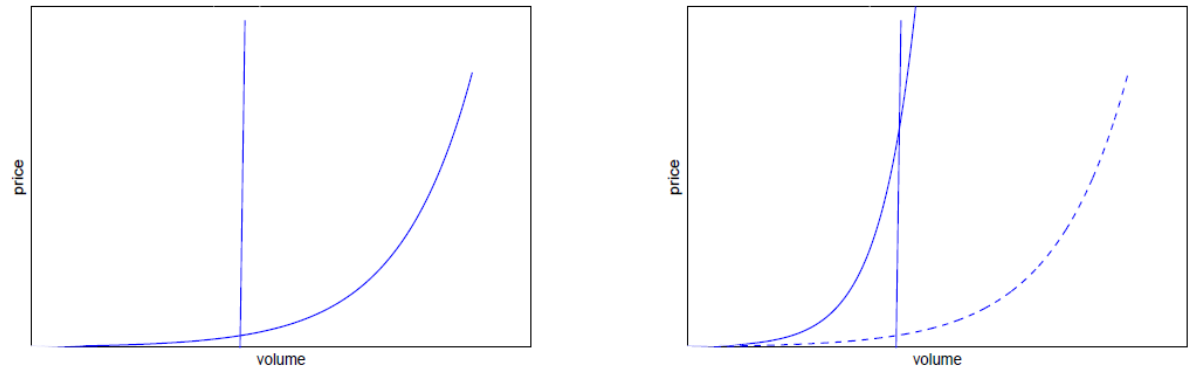

Figure 3: Understanding the spike phenomenon as a consequence of the switching mechanism in the offer curve

The dynamics of power prices is then obtained from the time evolution of $z(t)$, and from the dynamics of the Markov process $\beta(t)$. We assume the transition probability matrix can be cast in the following form:

$$\pi = \begin{pmatrix} 1-\gamma dt & \eta dt \\ \gamma dt & 1-\eta dt \end{pmatrix}, \quad (6)$$

where γdt denotes the transition probability for the switching from the base state β_0 to β_1 in the infinitesimal time interval $[t, t+dt]$ and ηdt is the probability for the opposite transition. As shown in [10], if the supply curve makes a transition from state i to state j in the infinitesimal time interval $[t, t+dt]$, that is if $\beta(t)$ switches from state i to state j $(i, j = 0,1)$, we obtain:

$$dp(t) = \beta_j dz(t) + \frac{\beta_j - \beta_i}{\beta_i} p(t), \quad (7)$$

where β_i is the value assumed by the Markov process in the state i and β_j is the value in the state j. Apart from the dynamics of $z(t)$, the switching mechanism in the supply curve introduces a non-Brownian component of the motion which is given by the last term in equation (7). Further non-Brownian components can be introduced in the dynamics to account for jumps in the power margin. To do this we assume that, during the transition from state i to state j in the infinitesimal time interval $[t, t+dt]$, the dynamics of $z(t)$ is described by a mean-reverting jump-diffusion process of the form

$$dz(t) = \left(\tilde{\mu}_{ij} - \tilde{\alpha}_{ij} z(t)\right) dt + \tilde{\sigma}_{ij} dW_{ij}(t) + \tilde{\theta}_{ij} dN_{ij}(t), \quad (8)$$

where $W_{ij}(t)$ are one-dimensional Brownian motions and N_{ij} are Poisson processes. By substituting equation (8) into equation (7) we easily get:

$$dp(t) = \left(\mu_{ij} - \alpha_{ij}\, p(t)\right)dt + \sigma_{ij} dW_{ij}(t) + \theta_{ij} dN_{ij}(t) + \frac{\beta_j - \beta_i}{\beta_i}\, p(t), \qquad (9)$$

where

$$\mu_{ij} = \beta_j \tilde{\mu}_{ij}, \quad \alpha_{ij} = \frac{\beta_j}{\beta_i}\tilde{\alpha}_{ij}, \qquad (10)$$

and

$$\sigma_{ij} = \beta_j \tilde{\sigma}_{ij}, \quad \theta_{ij} = \beta_j \tilde{\theta}_{ij}. \qquad (11)$$

Equation (9) clearly shows that the ratio between β_j and β_i is observable in the dynamics of power prices and that it can be estimated from market data. In the next Section we provide an empirical analysis in order to test the flexibility and the adaptability of the model to market prices.

3. THE EMPIRICAL ANALYSIS

According to the presented methodology, we provide in this Section a parsimonious dynamical model in order to capture the random behavior of power prices observed in real markets. We notice that the dynamics of transitions between Markov states (transitions $i \to j$ and $j \to i$) can be modelled independently from the dynamics of the stable regime (transition $i \to i$) and of the turbulent regime (transition $j \to j$). It is only during transitions $i \to j$ and $j \to i$ that the Markov parameters β_i and β_j become observable, specifically in the ratio β_i / β_j. The following parametrization is therefore adopted:

$$dp = \begin{cases} -\alpha_0 p dt + \sigma_0 dW_0 \\ \sigma_{01} dW_{01} + \frac{\beta_1 - \beta_0}{\beta_0}\, p \\ \sigma_1 dW_1 + \theta dN \\ \mu_{10} dt + \sigma_{10} dW_{10} + \frac{\beta_0 - \beta_1}{\beta_1}\, p. \end{cases} \qquad (12)$$

The random jump amplitude θ is assumed to be distributed according to a normal random variable, $\theta \sim N(0, \sigma_\theta)$, with mean 0 and standard deviation σ_θ. We also assume that the Brownian motions $W_0(t)$, $W_{01}(t)$, $W_1(t)$, and $W_{10}(t)$, the Poisson process $N(t)$, and the jump amplitude are mutually independent. Even if the process $\beta(t)$ is a two-state Markov process, the dynamics of power prices can be described in terms of four distinct processes: the first one governs the dynamics in the base state and it is described by a mean-reverting diffusion process responsible for stable motion; the second describes the dynamics of transitions from state 0 to

state 1; the third accounts for the dynamics in the excited state and it contains a jump component to model the spiking phenomenon; the fourth is responsible for transitions from state 1 to the base state 0. In this dynamical representation the transition probability matrix is described by the following 4×4 matrix, directly obtained by the two-state matrix (6):

$$\pi = \begin{pmatrix} 1-\gamma & 0 & 0 & 1-\gamma \\ \gamma & 0 & 0 & \gamma \\ 0 & 1-\eta & 1-\eta & 0 \\ 0 & \eta & \eta & 0 \end{pmatrix}. \quad (13)$$

We estimate the model on the Victoria power market and on the ERCOT market. We will show that the proposed approach seems capable of incorporating the main features of observed power prices thus reproducing the first four moments of the empirical distributions of log-returns.

The data set consists of day-ahead base-load prices since January 1, 2006 until May 31, 2010 for the Victoria market, and since January 4, 2006 until September 16, 2011 for the ERCOT market. Market prices are available respectively at www.aemo.com.au and at www.eia.doe.gov; they are provided as average daily prices without weekend days. The behavior of electricity prices time-series is depicted in Figure 1. In the period under investigation both markets are characterized by a very erratic behavior: prices are variable and unpredictable with high volatility, frequent jumps and short-lived spikes of very high magnitude.

To account for seasonal effects we can adopt the following decomposition:

$$\log P(t) = f_p(t) + p(t), \quad (14)$$

where $f_p(t) \equiv \log h_0(t)$ is a deterministic function of time. In general, power prices are higher in winter time and in summer time, and we assume that the seasonality component of the motion is given by:

$$f_p(t) = b_0 + b_1 \frac{t}{261} + b_2 \cos\left(b_3 + \frac{2\pi t}{261}\right) + b_4 \cos\left(b_5 + \frac{4\pi t}{261}\right), \quad (15)$$

in which a linear trend has been included. We estimated the parameters of the deterministic component by fitting $f_p(t)$ to market data using ordinary least-squares (OLS) techniques. The results are reported in Table 1. The estimated seasonal component has been superimposed on the historical path of market log-prices in Figure 4.

	Victoria	Ercot
b_0	3.7417	4.2261
b_1	-0.0686	-0.1239
b_2	-0.1486	-0.2299
b_3	0.3841	0.3566
b_4	0.0836	0.1765
b_5	0.0975	0.8459

Table 1: Estimated parameters of the seasonal component

Figure 5 shows the historical behavior of deseasonalized log-returns. The rule of demand and supply has strongly increased the volatility of price returns: deregulated markets exhibit, in general, large price fluctuations, and the presence of jumps and spikes is revealed by non-normal empirical distributions with very high values of the kurtosis. The descriptive statistics of log-returns observed in the markets under investigation is displayed in Table 2.

Both markets show negative skewness. Such a statistical parameter is related to the properties of upward versus downward jumps. Negative skewness indicates that price drops (downward jumps) have on average a greater weight than upward jumps. To account for this feature, an independent parameter, μ_{10}, has been introduced in the fourth equation of the dynamics. Furthermore, we assumed that the volatility coefficients in transient regimes are equal, that is $\sigma_{01} = \sigma_{10}$.

The model has been estimated by maximum-likelihood using the Hamilton filtering technique [15]-[16]. Following this approach, the likelihood function in multi-regime dynamics can be expressed as a linear combination of likelihoods of the single regimes. The estimation results are summarized in Table 3.

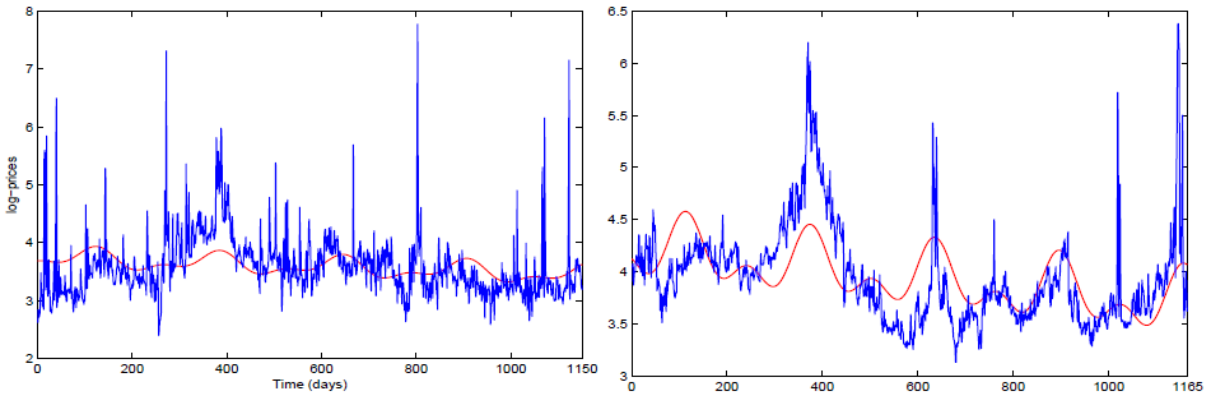

Figure 4: Daily log-prices and their seasonal components (thick red lines) at the Victoria market (left), and at ERCOT (right) in the period under investigation

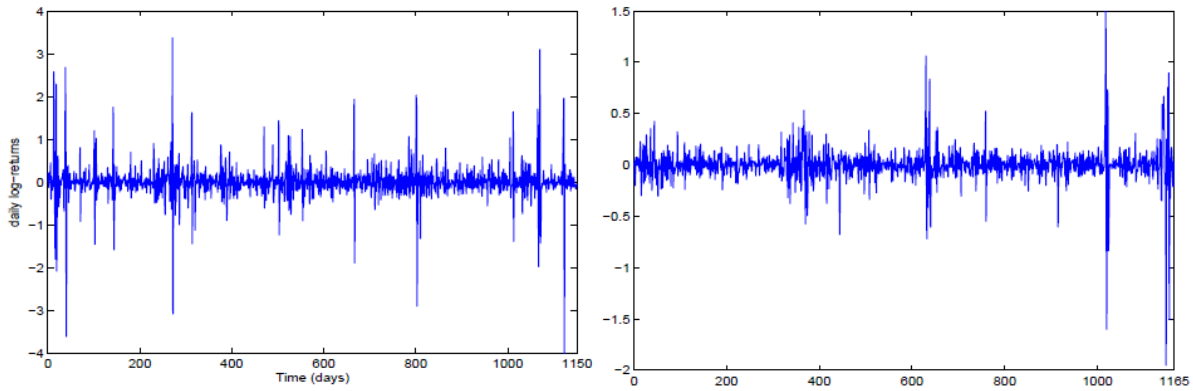

Figure 5: Deseasonalized log-returns at the Victoria market (left), and at ERCOT (right)

	Victoria	Ercot
Start	Jan 1, 06	Jan 4, 06
End	May 31, 10	Sep 16, 11
Mean	0.0006	-0.0003
Std.Dev.	0.4426	0.1704
Skewness	-0.3666	-1.5963
Kurtosis	26.0731	37.9016

Table 2: Descriptive statistics

	Victoria	Ercot		Victoria	Ercot
α_0	0.1491	0.0390	σ_θ	1.7146	0.7988
	(0.0184)	(0.0089)		(0.2424)	(0.1724)
σ_0	0.1791	0.0769	μ_{10}	-0.2083	-0.1265
	(0.0092)	(0.0033)		(0.1025)	(0.0501)
$\sigma_{01} = \sigma_{10}$	0.6035	0.1469	β_1/β_0	1.6181	1.2367
	(0.1444)	(0.0436)		(0.1891)	(0.0808)
σ_1	0.4163	0.2382	$1-\gamma$	0.9440	0.9533
	(0.0969)	(0.0410)		(0.0147)	(0.0156)
λ	0.5492	0.1782	$1-\eta$	0.5526	0.7596
	(0.1673)	(0.0748)		(0.0809)	(0.0679)
			LL	-90.4260	921.3793

Table 3: Estimation results. Standard errors are between parentheses

The proposed model seems to well capture the main features of power prices dynamics observed in real markets. In particular, the model distinguishes the stable regime from the turbulent one in the sense that the value of the volatility parameter is lower in the stable regime with respect to the value of the excited one. Furthermore the ratio β_1/β_0 is greater than one, thus revealing that the switching mechanism in the supply curve works well to capture transitions from the base state to the excited state. Table 4 displays the first four moments of the model distribution of log-returns, obtained by averaging over 5000 simulated paths randomly generated using estimated

parameters. The statistical analysis of simulated trajectories reveals a very interesting agreement with experimental data: the first four moments of log-returns distributions are very close to the empirical ones.

	Victoria	Ercot
Mean	0.0009	-0.0001
	(0.0008)	(0.0006)
Std.Dev.	0.4609	0.1733
	(0.0504)	(0.0207)
Skewness	-0.2247	-0.1622
	(0.9522)	(1.6233)
Kurtosis	24.6421	33.5292
	(6.5642)	(12.8252)

Table 4: Simulated moments. Standards errors are between parentheses

4. CONCLUDING REMARKS

Within the context of an equilibrium methodology where the supply curve follows an exponential law in which the argument is a two-state Markov process, we proposed a regime-switching model to capture the main features of power prices observed in deregulated markets. Switches in the dynamics are induced by transitions of the offer curve between Markov states. The model is flexible enough to account for non-zero skewness and very high values of the kurtosis. The empirical analysis reveals that the proposed dynamics reproduces market data in a satisfactory way: the first four moments of the model distributions of log-returns are very close to the empirical ones. It is worth notice that a good representation of observed price movements is crucial to value power derivatives, to design supply contracts, and to define risk management strategies. In particular fitting the first four moments of the empirical distributions is very important for pricing purposes in which the calculus of expectations values is a crucial task. Regime-switching models offer a good compromise between physical description of electricity prices dynamics and mathematical tractability. Their use may be very helpful for financial applications and for energy risk management: option prices, as well as forward and futures prices, can be obtained as solutions of well defined partial differential equations and are smooth functions of the spot price [17].

REFERENCES

[1] R. Huisman, R. Mahieu, *Regime jumps in electricity prices*, Energy Economics 25, (2003) 423-434.
[2] R. Huisman, M. Kilic, *A history of European electricity day-ahead prices*, Erasmus School of Economics, Technical Report (2011).
[3] J. Janczura, R. Weron, *An empirical comparison of alternate regime-switching model for*

electricity spot prices, Energy Economics 32, (2010) 1059-1073.
[4] H. Geman, A. Roncoroni, *Understanding the fine structure of electricity prices*, J. of Business 79, (2006).
[5] A. Cartea, M.G. Figueroa, *Pricing in electricity markets: a mean reverting jump diffusion model with seasonality*, Applied Mathematical Finance 12, (2005) 313-335.
[6] R. Weron, M. Bierbrauer, S. Trck, *Modeling electricity prices: jump-diffusion and regime switching*, Physica A 336, (2004) 39-48.
[7] C. de Jong, *The Nature of power spikes: a regime switch approach*, Studies in Nonlinear Dynamics & Econometrics 10, (2006).
[8] C. Mari, *Regime-switching characterization of electricity prices dynamics*, Physica A 371, (2006) 552-564.
[9] H. Geman, *Commodities and Commodity Derivatives*, Wiley, 2005.
[10] C. Mari, D. Tondini, *Regime switches induced by supply-demand equilibrium: a model for power-prices dynamics*, Physica A 389, (2010) 4819-4827.
[11] R. Weron, *Modeling and Forecasting Electricity Loads and Prices*, John Wiley & Sons Ltd., 2006.
[12] T.D. Mount, Y. Ning, X. Cai, *Predicting price spikes in electricity markets using a regime-switching model with time-varying parameters*, Energy Economics 28, (2006) 62-80.
[13] C. Mari, *Random movements of power prices in competitive markets: a hybrid model approach*, Journal of Energy Markets 1, (2008) 87-103.
[14] M.T. Barlow, *A diffusion model for electricity prices*, Mathematical Finance 12, (2002) 287-298.
[15] J.D. Hamilton, *A new approach to the economic analysis of nonstationary time series and the business cycle*, Econometrica 57, (1989) 357-384.
[16] J.D. Hamilton, *Time Series Analysis*, Princeton University Press, 1994.
[17] S. Deng, *Stochastic models of energy commodity prices and their applications: mean-reversion with jumps and spikes*, Working paper (1999).

SOME REMARKS ABOUT FUZZY NUMBERS

I. Tofan*

*Faculty of Mathematics, "Al. I. Cuza" University, Iasi

ABSTRACT

In this paper new operations on the set of triangular fuzzy numbers are investigated and the derived algebraic structures, based on proposed arithmetic operations, are inspected. The interest for fuzzy numbers is given by the fact that these numbers are really suitable to represent (many) perceptional informations which can be involved in the mathematical modelling of the reality.

1. INTRODUCTION

Let $\mathbb{R}$ be the field of real numbers.

We remember that by fuzzy number on intend a fuzzy subset, $\mu : \mathbb{R} \to [0,1]$, of $\mathbb{R}$ satisfying the following properties:

i) $\exists x_0 \in \mathbb{R} : \mu(x_0) = 1$;

ii) $\mu(\lambda x + (1-\lambda)y) \geq \min\{\mu(x), \mu(y)\}$, for any $x, y \in \mathbb{R}$, and $\lambda \in [0,1]$.

iii) μ is upper semicontinuous (for any $\varepsilon > 0$ and any $x_0 \in \mathbb{R}$ there is a neighborhood V of x_0 such that $\mu(x) \leq \mu(x_0) + \varepsilon$, for any $x \in V$).

iv) the support of μ (the closure of $\{x \in \mathbb{R} \backslash \mu(x) > 0\}$) is compact.

A class of fuzzy numbers covering many applications is given by $\mu : \mathbb{R} \to [0,1]$

$$\mu(x) = \begin{cases} 0, & x \leq a; \\ \pi_1(x), & x \in (a,b); \\ 1, & x \in [b,c]; \\ \pi_2(x), & x \in (c,d); \\ 0, & x \geq d \end{cases}$$

where $a \leq b \leq c \leq d$ are real numbers and $\pi_1 : [a,b] \to [0,1]$, $\pi_2 : [c,d] \to [0,1]$ are continuous functions such that π_1 is increasing, π_2 is decreasing, $\pi_1(a) = 0 = \pi_2(d)$, $\pi_1(b) = 1 = \pi_2(c)$.

If $b = c$ and π_1, π_2 are linear functions, the triangular fuzzy numbers are obtained.

It is clear that a triangular fuzzy number is determined by a triple $(a, b, c) \in \mathbb{R}^3$ with $a \leq b \leq c$.

We denote by $\mathbb{R}_t$ the set of triangular fuzzy numbers. The interest for fuzzy numbers is given by the fact that these numbers are really suitable for representing and modelling the vague, ambiguous, imprecise informations. In this context $\mathbb{R}_t$ is sufficiently fine from the above point of view and, in the same time, is sufficiently easy to work in it.

The standard operations on $\mathbb{R}_t$ are typically defined using Zadeh's extension principle and the concept of level subset of a fuzzy set, but they do not have, for example, the property of distributivity, among other lacking desirable properties.

Comprehensive early works covering fuzzy numbers are representing by [1, 3, 4]. An interesting overview and a consistent bibliography are contained in [2].

2. NEW OPERATIONS

A triangular fuzzy number $(x, y, z) \in \mathbb{R}_t$ is uniquely determined by a triple (λ, y, ρ) where $\lambda = y - x$, $\rho = z - y$ are positive reals, called the left, respectively right tolerance. The form is (λ, y, ρ) is known as the LR notation for $\mathbb{R}_t$.

Throughout this paper we will use the notation with the central value on the first place. So,

$$\mathbb{R}_t = \{(a, \lambda, \rho) | a \in \mathbb{R}; \lambda, \rho \in \mathbb{R}_+\}, \quad \mathbb{R}_+ = \{x \in \mathbb{R}, x \geq 0\}.$$

Let be $a \in \mathbb{R}$. We denote by $\mathbb{R}_t(a) = \{(a, \lambda, \rho) | \lambda, \rho \in \mathbb{R}_+\}$.

Define $d : \mathbb{R}_t(a) \times \mathbb{R}_t(a) \to \mathbb{R}$, $d((a, \lambda, \rho), (a, \lambda', \rho')) = \max\{|\lambda - \lambda'|, |\rho - \rho'|\}$.

Remark 2.1 The following conditions hold:

i) $d(x, x) = 0$;

ii) $d(x, y) = d(y, x)$;

iii) $d(x, z) \leq d(x, y) + d(y, z)$

for any $x, y, z \in \mathbb{R}_t(a)$.

Let $(a,\lambda,\rho),(b,\lambda',\rho')\in\mathbb{R}_t$. We consider the operations

$$(a,\lambda,\rho)\oplus(b,\lambda',\rho')=(a+b,f(\lambda,\lambda'),f(\rho,\rho')),$$

$$(a,\lambda,\rho)\odot(b,\lambda',\rho')=(a\cdot b,f(\lambda,\lambda'),f(\rho,\rho')),$$

where $f:\mathbb{R}_+\times\mathbb{R}_+\to\mathbb{R}_+$.

Denote by $*$ either $\oplus$ or $\odot$ on $\mathbb{R}_t$ (and respectively $+$ or $\cdot$ on $\mathbb{R}$).

In the following a,b,c are arbitrary in $\mathbb{R}$.

Proposition 2.1 *i) The following conditions are equivalent:*

1) $*$ *(on* $\mathbb{R}_t$*) is commutative;*

2) $d(x*y,y*x)=0$*, for any* $x\in\mathbb{R}_t(a)$*,* $y\in\mathbb{R}_t(b)$*;*

3) $d(x*y,u)=d(y*x,u)$*, for any* $u\in\mathbb{R}_t(a*b)$*,* $x\in\mathbb{R}_t(a)$*,* $y\in\mathbb{R}_t(b)$*;*

4) $f(\alpha,\beta)=f(\beta,\alpha)$*, for any* $\alpha,\beta\in\mathbb{R}_+$*;*

ii) the following conditions are equivalent:

1) $*$ *(on* $\mathbb{R}_t$*) is associative;*

2) $d(x*(y*z),(x*y)*z)=0$*, for any* $x\in\mathbb{R}_t(a)$*,* $y\in\mathbb{R}_t(b)$*,* $z\in\mathbb{R}_t(c)$*;*

3) $d(x*(y*z),u)=d((x*y)*z,u)$*, for any* $u\in\mathbb{R}_t(a*b*c)$*,* $x\in\mathbb{R}_t(a)$*,* $y\in\mathbb{R}_t(b)$*,* $z\in\mathbb{R}_t(c)$*;*

4) $f(\alpha,f(\beta,\gamma))=f(f(\alpha,\beta),\gamma)$*, for any* $\alpha,\beta,\gamma\in\mathbb{R}_+$*;*

iii) the following conditions are equivalent:

1) $\odot$ *is distributive with respect to* $\oplus$*;*

2) $d(x\odot(y\oplus z),x\odot y\oplus x\odot z)=0$*, for any* $x\in\mathbb{R}_t(a)$*,* $y\in\mathbb{R}_t(b)$*,* $z\in\mathbb{R}_t(c)$*;*

3) $d(x\odot(y\oplus z),u)=d(x\odot y\oplus x\odot z,u)$*, for any* $u\in\mathbb{R}_t(a(b+c))$*,* $x\in\mathbb{R}_t(a)$*,* $y\in\mathbb{R}_t(b)$*,* $z\in\mathbb{R}_t(c)$*;*

4) $f(f(\alpha,\beta),f(\alpha,\gamma))=f(\alpha,f(\beta,\gamma))$*, for any* $\alpha,\beta,\gamma\in\mathbb{R}_+$*;*

iv) the following conditions are equivalent:

1) $(0,0,0)$ *is neutral element for* $\oplus$*;*

2) $d(x\oplus(0,0,0),u)=d(x,u)=d((0,0,0)\oplus x,u)$*, for any* $u,x\in\mathbb{R}_t(a)$*;*

3) $f(\alpha,0)=\alpha=f(0,\alpha)$*, for any* $\alpha\in\mathbb{R}_+$*;*

v) the following conditions are equivalent:

1) $(1,0,0)$ *is unity element for* $\odot$*;*

2) $d(x \odot (1,0,0), u) = d(x,u) = d((1,0,0) \odot x, u)$*, for any* $u, x \in \mathbb{R}_t(a)$*;*

3) $f(\alpha, 0) = \alpha = f(0, \alpha)$*, for any* $\alpha \in \mathbb{R}_+$.

One can remark that $(0,0,0)$ is neutral element for $\oplus$ if and only if $(1,0,0)$ is units element for $\odot$.

We define, also, a relation "$\sim$" on $\mathbb{R}_t$, by:

$$(a,\lambda,\rho) \sim (b,\lambda',\rho') \text{ if } \begin{cases} a = b; \\ \lambda - \lambda' = \rho - \rho'. \end{cases}$$

Remark 2.2 The relation "$\sim$" is an equivalence relation on $\mathbb{R}_t$.

One obtains:

Proposition 2.2 *The function* $\max : \mathbb{R}_+ \times \mathbb{R}_+ \to \mathbb{R}_+$, $\max(x,y) = \begin{cases} x, & x \geq y \\ y, & x \leq y \end{cases}$ *is the unique function such that*

i) $\oplus, \odot$ *are associative;*

ii) $\oplus, \odot$ *are commutative;*

iii) $\odot$ *is distributive with respect to* $\oplus$*;*

iv) $(0,0,0)$ *is neutral element for* $\oplus$*, and* $(1,0,0)$ *is neutral element for* $\odot$.

v) $(a,\lambda,\rho) \oplus (-a,\rho,\lambda) \sim (0,0,0)$*; if* $a \neq 0$*,* $(a,\lambda,\rho) \odot (\frac{1}{a},\rho,\lambda) \sim (1,0,0)$*;*

vi) $f(x,y) \leq f(x,z)$ *whenever* $y \leq z$*;*

vii) $f(x,y) \leq \max\{x,y\}$ *(the uncertainty of the result is not less than the uncertainty of any of operands);*

viii) $f(0,0) = 0$ *(the operations with crisp numbers produce the same results as the arithmetic operations real line).*

Remark 2.3 i) The above operations has some very productive properties such as: – the structure of "$\sim$" field (in view of i)-v) proposition 2.1) which can permit the development of a theory of divisibility in $\mathbb{R}_t$; – and – the fact that the uncertainty of the result is not less than the uncertainty of any of opperands (so it is possible to work with series of triangular fuzzy numbers). For the unicity involved in Proposition 2.2 an elegantly proof is comunicated by Prof.Dr. m.c. H.N.Teodorescu.

ii) In a future work we shall investigate the case in which the left and the right tolerances will be obtained in different ways and proper form for any of the operations $\oplus$ respectively $\odot$.

REFERENCES

[1] D. Dubois, H. Prade, *Fuzzy Sets and Systems*, Academic Press, New York, 1980.

[2] R.E. Giachetti, R.E. Young, *A parametric representation of fuzzy numbers and their arithmetic operators*, Fuzzy Sets and Systems, 91, 2, p. 185-202, 1997.

[3] E.E. Kerre, J.N. Mordesson, *A historical overview of fuzzy mathematics*, New Math. and Natural Computations, 1, n.1, p. 1-26, 2005.

[4] M. Ma, F. Friedman, A. Kandel, *A new fuzzy arithmetic*, Fuzzy Sets and Systems, 108, pp. 83-90, 1999.

AUTHOR GUIDELINES

JOURNAL TOPICS

- Technological Risk
- Economic and Financial Risk
- Chemistry and Physics of Undesired Events
- Mathematics and Informatics for Risk Theory
- Natural Risk

PAPER FORMAT

Content will be in English, in *doc* format (for Microsoft Word), and the following format of paragraph will be used: Paper size: B5; Identation: left 0, right 0; Spacing: before 0, after 0; Line spacing: Multiple At 1.15.

Paper Title

Paper title will be written in 12-point bold type, Times New Roman in uppercase and will be centered across the top of the page.

Paper Authors

Author's names will be written under the paper title, centered across the page, in 12 point type, Times New Roman in lowercase.

Author's Affiliation

Author's affiliation will be written under the author's names, centered across the page, in 12 point type italic, Times New Roman in lowercase, specifying: title, university affiliation, country and e-mail address.

Paper Abstract

The abstract must include sufficient information for readers to judge the nature and significance of the topic, the adequacy of the investigative strategy, the nature of the results and the conclusions. An abstract is not an introduction, it summarizes the substantive results of the work, not merely list topics that are discussed in the paper.
The abstract will be written in 10 point type italic, Times New Roman. It must have 200 to 300 words, single spaced type.

Keywords

Select four to eight keywords (words or expressions) that capture the essence of your paper. List the words in decreasing order of importance.

Introduction

The function of the Introduction is to establish the context of the paper. This is accomplished by discussing the relevant primary research literature (with quotations) and summarizing current understanding of the problem you are investigating. State the purpose of the work in the form of the hypothesis, questions or problems you investigate and, briefly explain your approach and the necessary arguments. Whenever possible, present the possible outcomes your study can reveal.

Paper Body

Organize the body of the paper using titles and subtitles to emphasize both content and clarity. Consider the following: use the accepted terminology of the field to describe any subjects or experimental procedures used to gather and analyze data; include detailed methods, so readers could be able to follow the investigation; state the results clearly and succinctly; thoroughly discuss, interpret and analyze the implications of the findings and minutely discuss the impact of the results, both globally and specifically.

The section titles will be written in 12-point bold type, Times New Roman in uppercase and will be aligned to left. Typeface must be 12-point Times New Roman type single spaced. Tables and figures should be sized and placed in the body of the paper just as the authors want them printed in the journal. Care should be taken so that tables and figures could be on one page. The tables contents will be written in 10 point type, Times New Roman and the heading of the tables will be in 10 point type bold, Times New Roman. The titles and numbers will be positioned above the table and the title and number of the figures bellow. When it is needed, the source will be mentioned. The number of the tables and figures are to be positioned in the body of the text, in a parenthesis, wherever they are mentioned, for example: (fig. nr.1), (table nr. 1). The graphs must be executed clearly so as to give clear black and white copies. Number all the equations and formulas used positioning the numbers in parenthesis on their right side. Define abbreviations and acronyms the first time they are used in the text, even after they had already been defined in the abstract. Avoid the use of footnotes or endnotes.

Conclusions

A conclusion section is required. Conclusions may review the main points of the paper, do not replicate the abstract as the conclusion. A conclusion might elaborate on the importance of the work or suggest applications and extensions and extensions of the research.

References

References will be written in the format of the following model:

[1] A. Edalat, M.B. Smyth, *Information categories*, Applied Categorical Structures, 1, 1993, p. 197–232.

Also, references in the articles will be numbered with [1] and if there are more than one reference with, [1,3] or [1-5]. Sources should be in alphabetical order by author's last name. When certain studies, research, articles are published in a volume, the volume numbers and pages will be specified.

Acest periodic informativ a fost realizat prin:

Titlul programului: "Programul Operaţional Sectorial Dezvoltarea Resurselor Umane 2007 – 2013"
Titlul proiectului: "Centrul de formare şi analiză în ingineria riscurilor (CeFAIR)"
Editorul materialului: Universitatea "Alexandru Ioan Cuza" din Iaşi
Data publicării: decembrie 2011

„Conţinutul acestui material nu reprezintă în mod obligatoriu poziţia oficială a Uniunii Europene sau a Guvernului României"